Subcytoplasmic location of translation controls protein output

Ellen L. Horste[1,2], Gang Zhen[2], Mervin M. Fansler[2,3], Xiuzhen Chen[2], Flora C. Y. Lee[4,5], Jernej Ule[4,5], and Christine Mayr[1,2,3†]

[1]Gerstner Sloan Kettering Graduate School of Biomedical Sciences, New York, NY 10065, USA
[2]Cancer Biology and Genetics Program, Sloan Kettering Institute, New York, NY 10065, USA
[3]Tri-Institutional Training Program in Computational Biology and Medicine, Weill-Cornell Graduate College, New York, NY 10021, USA
[4]UK Dementia Research Institute, King's College London, London, SE5 9NU, UK
[5]The Francis Crick Institute, 1 Midland Road, London NW1 1AT, UK

[†]Correspondence: mayrc@mskcc.org

Summary

The cytoplasm is highly compartmentalized, but the extent of subcytoplasmic mRNA localization in non-polarized cells is largely unknown. We used fluorescent particle sorting to determine mRNA enrichment in three unenclosed cytoplasmic compartments: the canonical rough endoplasmic reticulum (CRER), the TIS granule-associated rough endoplasmic reticulum (TGER), and the cytosol. Focusing our analysis on non-membrane protein-encoding mRNAs, we observed that 52% have a biased subcytoplasmic localization pattern which is determined by a combinatorial code of 3′UTR-bound RNA-binding proteins. Compartment-biased mRNAs differed in the functional classes of their encoded proteins. TGER-enriched mRNAs encode low-abundance proteins such as transcription factors, whereas CRER-enriched mRNAs encode highly expressed proteins. TGER/CRER-enriched mRNAs are more stable than cytosolic mRNAs, thus influencing protein output in a compartment-dependent manner. We observed that redirecting cytosolic mRNAs to the ER increases their protein expression by two-fold, independently of the bound RNA-binding proteins. In summary, the cytoplasm is functionally compartmentalized by local translation environments.

Keywords

Cytoplasmic organization; spatial regulation; mRNA localization; unenclosed cytoplasmic compartments; functional compartmentalization, translation environment; regulation of protein expression; condensates; rough endoplasmic reticulum membrane; 3′UTRs; RNA-binding proteins; CLIP analysis; TIS11B; TIAL1; LARP4B

Introduction

In polarized cells such as neurons, intestinal epithelial cells, or cells of the early fly embryo, the majority of mRNAs have a distinct spatial localization pattern (Huttelmaier et al., 2005; Lecuyer et al., 2007; Moor et al., 2017; Tushev et al., 2018; Glock et al., 2021), which enables the local control of protein production and activity (Moretti et al., 2015; Buxbaum et al., 2015; Biever et al., 2019). In non-polarized cells, local protein synthesis has primarily been studied for membrane and secretory proteins, which are predominantly translated on the endoplasmic reticulum (ER) (Reid and Nicchitta, 2012; Jan et al., 2014; Fazal et al., 2019). However, the cytoplasm is compartmentalized by additional membrane-bound and membraneless organelles (Banani et al., 2017; Shin and Brangwynne, 2017; Ma and Mayr, 2018). Compartmentalization allows reactions to occur in parallel and may enable the generation of unique biochemical

translation environments (Ma and Mayr, 2018; Peeples and Rosen, 2021). Subcellular localization within the cytoplasm was observed for specific mRNAs enriched on the mitochondrial surface (Fazal et al., 2019; Qin et al., 2021). However, it is currently largely unknown to what extent mRNAs that encode non-membrane proteins differentially localize to the ER or the cytosol or if the amount of protein synthesis differs depending on the subcytoplasmic location of an mRNA.

We recently discovered a cytoplasmic condensate, called TIS granule network, that is generated through assembly of the RNA-binding protein (RBP) TIS11B together with its bound mRNAs (Ma and Mayr, 2018). According to single cell RNA-seq data, *TIS11B* mRNA is expressed in more than 100 human cell types and was detected in all cell types analyzed, suggesting that TIS granules are widespread (Han et al., 2020). TIS granules are present under steady-state cultivation conditions and form a network-like structure that is associated with the surface of the rough ER (Ma and Mayr, 2018; Ma et al., 2021). With respect to their functions, it was shown that translation of specific mRNAs in TIS granules allows assembly of protein complexes that cannot be established when the mRNAs are translated on the ER but outside of TIS granules (Ma and Mayr, 2018). These results suggested that in addition to the canonical rough ER (CRER), the ER contains another region that is associated with TIS granules, called TIS granule ER (TGER).

To investigate the broader biological significance of TIS granules, we set out to determine the mRNAs enriched in TGER, CRER, and the surrounding cytosol. Several methods were developed to investigate subcellular transcriptomics. They include RNA sequencing (RNA-seq) after biochemical fractionation, APEX-seq, MERFISH, and fluorescent particle sorting (Mili et al., 2008; Hubstenberger et al., 2017; Khong et al., 2017; Moor et al., 2017; Xia et al., 2019; Fazal et al., 2019). Application of these methods identified mRNAs that localize to cellular protrusions of migrating fibroblasts and distinguished between mRNAs that localize to the apical or basal sides of gut epithelial cells (Mili et al., 2008; Moor et al., 2017). These methods also determined the transcriptomes of cytoplasmic condensates such as P bodies or stress granules (Hubstenberger et al., 2017; Khong et al., 2017) and identified mRNAs associated with membrane-bound organelles such as the ER or mitochondria (Fazal et al., 2019; Qin et al., 2021). To identify mRNAs enriched in TIS granules, we used fluorescent particle sorting (Hubstenberger et al., 2017). This decision was based on the observation that TIS11B protein (also called ZFP36L1) is present in cells in two assembly states. It exists in an unassembled state in the cytosol and assembles together with its bound mRNAs into TIS granules (Fig. 1A) (Ma and Mayr, 2018; Ma et al., 2021).

We applied fluorescent particle sorting to isolate TGER and CRER-associated mRNAs and compared them with digitonin-extracted cytosolic mRNAs. In addition to ~1,700 mRNAs that encode membrane proteins, we detected more than 2,100 mRNAs that encode non-membrane proteins with a biased localization to TGER or CRER, indicating that the ER membrane is a general translation compartment and is not restricted to membrane and secretory proteins. We focused our analysis on mRNAs that encode non-membrane proteins. For more than half of them, we observed a biased localization to one of the three subcytoplasmic compartments. The localization pattern was largely controlled by a combinatorial code of the 3′UTR-bound RBPs TIS11B, TIA1/L1, and LARP4B. Compartment-enriched mRNAs differed substantially in their production and degradation rates as well as in the functional classes and expression levels of their encoded proteins. In addition to RBPs, we found that the location of translation has an independent effect on protein expression. We observed that redirecting cytosolic mRNAs to the rough ER membrane increased their steady-state protein expression levels by two-fold, indicating that the ER environment promotes protein expression.

Results

Approach to determine subcytoplasmic mRNA localization

We set out to study differential mRNA localization across three major unenclosed cytoplasmic compartments in non-polarized human HEK293T cells under steady-state cultivation conditions. We determined the mRNAs enriched at the cytosolic surface of the ER – the largest cytoplasmic organelle, and TIS granules, an ER-associated condensate network, as well as the cytosol (Fig. 1B). For simplicity, we consider here the sum of the three compartments as the universe of cytoplasmic mRNAs.

To identify TIS granule-localized mRNAs, we used fluorescent particle sorting followed by RNA-seq. After transfecting cells with fluorescently tagged TIS11B to label TIS granules, we used mechanical lysis and differential centrifugation to isolate the cytoplasmic membrane fraction which was followed by flow cytometry-based sorting of TIS11B-positive particles (Fig. S1A, S1B). DAPI staining allowed us to identify and discard nuclei that were still associated with the ER and TIS granules and to isolate TIS11B-positive particles free of nuclei. To investigate if the obtained particles were pure TIS granules or if they contained ER membrane, we double-labeled TIS granules and the rough ER membrane, followed by particle sorting and confocal microscopy. This revealed that the TIS11B-positive particles cannot be separated from the rough ER membrane and therefore, we call them TIS granule ER (TGER) particles (Fig. 1C).

To isolate the canonical rough ER (CRER), we labeled the rough ER membrane with fluorescently tagged SEC61B and isolated CRER particles with the same strategy. We obtained particles similar in size to TGER particles (Fig. 1C, Fig. S1C). To isolate cytosolic mRNAs, we used digitonin extraction (Liu and Fagotto, 2011). The extracted cytosol was not contaminated by nuclei or the ER, but it contained cytosolic proteins, including unassembled TIS11B protein and GAPDH which was used as positive control (Fig. S1D).

We performed RNA-seq to determine the mRNA composition in the three fractions. The biological replicates of the compartment samples were highly reproducible (Fig. S1E). We focused our analysis on protein-coding mRNAs. Previous analyses showed that most mRNAs that encode membrane or secretory proteins are translated on the ER, whereas mRNAs that encode non-membrane proteins are translated in the cytosol (Jan et al., 2014; Fazal et al., 2019). Consistent with this, we observed distinct partitioning patterns between the two groups across the three compartments (Fig. S1F).

mRNAs that encode membrane and secretory proteins are strongly enriched on the CRER membrane

Based on the different partitioning patterns, we analyzed the mRNAs that encode membrane or secretory proteins separately from the mRNAs that encode non-membrane proteins. Proteins that contain either a signal sequence or transmembrane domain are defined as secretory or membrane proteins and are encoded by 23% of mRNAs expressed in HEK293T cells, whereas the remaining 77% encode non-membrane proteins. We determined the compartment-specific partition coefficients in each group: For each gene, we calculated the fraction of mRNA transcripts that localize to TGER, the CRER, or the cytosol and observed the expected baseline distributions across the three compartments (Fig. S1F).

For mRNAs that encode membrane/secretory proteins, we observed 69% (N = 1,476) to be enriched at the CRER (Fig. S1G). When comparing the CRER membrane-enriched mRNAs with analyses from alternative isolation methods, we detected approximately 80% overlap among the ER membrane-enriched mRNAs, supporting the validity of our purification strategy (Fig. S1H) (Reid and Nicchitta, 2012; Fazal et al., 2019).

A third of mRNAs that encode non-membrane proteins have an ER-biased localization

For mRNAs that encode non-membrane proteins, the baseline partitioning across the three compartments was more even. For a typical mRNA, we observed that roughly a third of transcripts localizes to TGER, CRER or to the cytosol (Fig. S1F). Next, we identified mRNAs whose transcript localization was biased towards a single compartment. We considered an mRNA to be compartment-enriched if the fraction of transcripts that localize to one compartment is 1.25-fold higher than the median fraction observed in the compartment. With this strategy, we identified 1246 mRNAs enriched in TGER, 919 non-overlapping mRNAs enriched on the CRER, and 1481 mRNAs enriched in the cytosol (Fig. 1D, S1I). The remaining 3369 mRNAs were not enriched in a single compartment and are considered to have an unbiased localization pattern (Fig. 1D, Table S1). To illustrate the compartment-biased localization, for individual mRNAs, we depicted the fraction of transcripts observed in the three compartments (Fig. 1E). Presented are examples obtained from the top 10%, bottom 10% and the median fraction of compartment-enriched transcripts, showing that the transcript enrichment is relative (Fig. 1E). Overall, we found that 52% of mRNAs that encode non-membrane proteins have a biased localization pattern to a single subcytoplasmic compartment in steady-state conditions of non-polarized cells.

Taken together, for the two ER-associated compartments (TGER and CRER), we found enrichment of mRNAs that encode membrane or secretory proteins, but we detected even more mRNAs that encode non-membrane proteins enriched (Fig. 1F). Dozens of these mRNAs have been found previously by several other groups (Lerner et al., 2003; Diehn et al., 2006; Chen et al., 2011; Reid and Nicchitta, 2012; Cui et al., 2012; Voigt et al., 2017) but the extent of localization of mRNAs that encode non-membrane proteins to TGER or CRER was previously unknown. This suggests that the rough ER membrane is a general translation compartment not restricted to membrane or secretory proteins. All remaining analyses were performed on mRNAs that encode non-membrane proteins.

Validation of subcytoplasmic mRNA localization patterns by single-molecule RNA-FISH

To validate mRNA localization across the three compartments, we performed single-molecule (sm) RNA-FISH on endogenous mRNAs predicted to localize to TGER or to the cytosol (Boraas et al., 2021). The TGER domain was visualized using fluorescently tagged TIS11B. To quantify compartment localization for individual mRNAs, we determined the area occupied by TGER or the cytosol in each cell and calculated the expected distribution of mRNA foci across the two compartments. We determined the fold-change between the foci observed in each compartment and the foci expected to be in each compartment. Our smRNA-FISH experiment confirmed enrichment of all candidates predicted to be overrepresented in the TGER domain. mRNAs predicted to be biased to the cytosol were not enriched in the TGER domain and were even excluded from the TGER domain in some samples (Fig. 1G, 1H, S1J, S1K, Table S2).

The fine reticulated structure of the ER membrane makes it challenging to perform a similar colocalization analysis for the CRER. ER-localized mRNAs are tethered to the ER and are relatively resistant to digitonin extraction compared to cytosolic mRNAs (Lerner et al., 2003; Cui et al., 2012). To validate the enrichment of mRNAs on the CRER, we performed smRNA-FISH before and after digitonin extraction and calculated the fraction of retained mRNAs. We observed significantly higher retention rates for mRNAs predicted to be CRER-localized compared to mRNAs predicted to be cytosolic (Fig. 1I, 1J, S1L, S1M, Table S2). Based on our high validation rates for mRNAs that localize to the three investigated cytoplasmic compartments, we conclude that about half (52%) of mRNAs that encode non-membrane proteins have a biased subcytoplasmic localization pattern.

mRNA and protein levels strongly correlate with the location of translation

Next, we characterized the features of compartment-enriched mRNAs and found substantial differences in their steady-state mRNA and protein levels (Fig. 2A, 2B). We observed that TGER-enriched mRNAs have the lowest steady-state expression levels and encode proteins with the lowest expression levels (Fig. 2A, 2B). To examine if the low mRNA levels are caused by mRNA degradation, we estimated mRNA half-lives by analyzing Precision Run-On sequencing (Pro-seq) and RNA-seq data (Fig. 2C, 2D, Fig. S2A) (Patel et al., 2020; Blumberg et al., 2021). Pro-seq values can be treated as transcription rates and RNA-seq data can be viewed as a measure of RNA concentration to estimate RNA decay rates required for a steady-state equilibrium (Blumberg et al., 2021). For TGER-enriched mRNAs, we observed that the low steady-state mRNA levels were not primarily caused by a low mRNA stability. Instead, these mRNAs had the lowest transcription rates which suggests that these mRNAs are either produced at a low rate or have high cotranscriptional degradation rates (Fig. 2C, 2D) (Smalec et al., 2022).

Cytosol-enriched mRNAs showed the highest degree of mRNA regulation with high production and high degradation rates (Fig. 2C, 2D). CRER-enriched mRNAs encode proteins with the highest expression levels, particularly when considering their intermediate steady-state mRNA levels (Fig. 2A, 2B). The compartment-enriched mRNAs also showed differences in their gene architectures. Cytosolic mRNAs have shorter 3′UTRs that are GC-rich and contain fewer AU-rich elements (Fig. S2B-D). Furthermore, CRER-enriched mRNAs encode the largest proteins which are more than twice as large as proteins encoded by cytosol-enriched mRNAs (Fig. S2E).

Consistent with the observed differences in steady-state protein expression levels, compartment-enriched mRNAs encode substantially different functional gene classes (Huang da et al., 2009). TGER-biased mRNAs are strongly enriched in zinc fingers and transcription factors (Fig. 2E). CRER-biased mRNAs are enriched in helicases, cytoskeleton-binding proteins and chromatin regulators which represent large proteins that are highly expressed in cells (Fig. 2F). Cytosol-enriched mRNAs often encode smaller proteins involved in the regulation of translation or splicing (Fig. 2G).

The TGER region supports active translation

Transcription factors are known to be expressed at lower abundance levels than non-transcription factors (Vaquerizas et al., 2009). Our analysis suggests that proteins that need to be expressed at low levels, such as transcription factors, are translated in the TGER domain (Fig. 2A, 2B, 2E). To obtain direct evidence for translation in the TGER domain, we applied the SunTag system to simultaneously visualize mRNAs and their nascent proteins in TGER and in the cytosol (Fig. S2F, S2G) (Yan et al., 2016). We confirmed that the TGER domain represents a translation environment for mRNAs (Ma and Mayr, 2018). We observed that the number of mRNA foci in TGER was five-fold lower compared to the cytosol. However, the proportion of mRNA translated was similar in TGER and the cytosol (Fig. S2H, S2I). Taken together, our data show that the TGER translation environment is not repressive and that the low expression level of TGER-translated proteins is predominantly a result of their low nuclear gene expression (Fig. 2A, 2C).

Lack of 3′UTRs in expression constructs causes default mRNA localization to the cytosol

Our next goal was to identify the RBPs responsible for mRNA enrichment in the three compartments (Fig. 1D, 1E). As TIS11B is the scaffold protein of TIS granules, we performed iCLIP of TIS11B in HEK293T cells (Fig. S3A, S3B). We confirmed that the top binding motif of TIS11B in 3′UTRs of mRNAs is the canonical AU-rich element (UAUUUA) (Fig. S3C). To perform a comprehensive analysis on localization regulators, we analyzed additional CLIP datasets (Küspert et al., 2015; Zhao et al., 2021). Altogether, we correlated the 3′UTR binding pattern of 170 RBPs with mRNA enrichment in the three subcytoplasmic compartments. Among

them, we found that the 3′UTR CLIP peak distributions of 25 RBPs were biased towards one of the three compartments (Table S4). We applied logistic regression and identified seven RBPs whose binding contributed significantly to mRNA localization to the three compartments. They include TIS11B, HuR, PUM2, HNRNPC, TIA1/L1, LARP4B and METAP2 (Fig. 3A). As a previous CLIP analysis showed that peaks for TIA1 and TIAL1 cannot be distinguished (Wang et al., 2010), we used the sum of peaks from TIA1 and TIAL1 to obtain the values for TIA1/L1.

Among all mRNAs that encode non-membrane proteins, we observed 2154 without binding sites for any of the seven RBPs. Comparing mRNAs with CLIP peaks for the seven RBPs with mRNAs lacking the RBPs, we observed increased cytosolic localization for the latter group (Fig. S3D, S3E). This suggests that they either contain binding sites for RBPs that were not studied by us or that these mRNAs localize to the cytosol by default. Two candidates (*LHPP, PTP4A3*) whose subcytoplasmic mRNA localization was experimentally verified by us did not contain binding sites for any of the seven RBPs. As these mRNAs localized to the cytosol in the presence or absence of their 3′UTRs, our data support a model of default cytosolic localization (Fig. 3B-D, S4A).

AU-RBPs promote mRNA localization to TGER or CRER, whereas LARP4B promotes cytosolic localization

Next, we focused on RBPs that differentially localize mRNAs to the ER-associated TGER or CRER regions versus the cytosol. Our CLIP analysis suggested that presence of LARP4B or METAP2 enhanced cytosolic mRNA localization. In contrast, the presence of all other RBPs, including TIS11B, HuR, PUM2, HNRNPC, and TIA1/L1, which bind to U-rich or AU-rich sequences (called here AU-RBPs) enhanced localization to either TGER or CRER (Fig. 3A, 3E-H)(Wang et al., 2010; Hafner et al., 2010; Lebedeva et al., 2011; Mukherjee et al., 2011; Meyer et al., 2018; Yugami et al., 2020). Although both LARP4B and METAP2 binding were correlated with cytosolic mRNA localization, few mRNAs (N = 90) were exclusively bound by METAP2, whereas 740 were exclusively bound by LARP4B (Fig. S3F, S3G). We experimentally validated the localization pattern of three mRNAs (*SF3A2, MAP2K2, MLST8*) that were only bound by LARP4B or METAP2 and confirmed their cytosolic localization (Fig. 3B, Fig. 1H).

In contrast, all validated candidates with predominant binding of AU-RBPs (*DNAJB1, BAG3, DUSP1, ALDH18A1, TES, IQGAP1, FOS, THAP1, FBXL3,* and *HSPA1B*) localized to TGER or CRER (Fig. 3B, Fig. 1H, 1J, Fig. 3I-K, S4B). For a selection of candidates, those expressed with and without their 3′UTRs, we observed that TGER enrichment was dependent on presence of their 3′UTRs, suggesting AU-RBP binding is required for mRNA localization to these compartments (Fig. 3I-K, S4B). In total, we experimentally confirmed differential mRNA localization to TGER/CRER versus the cytosol for all 15 tested candidates.

These experiments demonstrate that the presence of AU-RBPs strongly determines mRNA localization to TGER/CRER, whereas their absence promotes localization to the cytosol. Taken together with the observations that TGER/CRER mRNAs have very high AU content and are strongly enriched in AU-rich elements in their 3′UTRs (Fig. 3L, 3M), this region can be considered an AU compartment. mRNAs with a high AU content have a higher mRNA stability than the non-enriched (Fig. 3N), as was reported previously (Courel et al., 2019; Litterman et al., 2019). They also have longer 3′UTRs and lower pre-mRNA production rates (Fig. S3H, S3I).

The ratio of 3′UTR-bound TIS11B versus TIA1/L1 differentiates between TGER and CRER

Next, we set out to identify the RBP drivers that distinguish between different regions of the AU compartment. 3′UTRs bound by either TIS11B, HuR or PUM2 significantly promoted mRNA localization to TGER (Fig. S5A). However, few mRNAs were exclusively bound by HuR (N = 124), PUM2 (N = 38) or HNRNPC (N = 2) (Fig. S5B). While 441 mRNAs were exclusively bound

by TIS11B, 230 mRNAs were only bound by TIA1/L1 and most mRNAs were cobound by TIS11B and TIA1/L1 (Fig. 4A, *N* = 862). Whereas presence of TIS11B positively correlated with TGER localization, presence of TIA1/L1 negatively correlated with it (Fig. 4B, 4C). For the cobound mRNAs, the ratio of 3′UTR-bound TIS11B over TIA1/L1 was strongly associated with TGER localization (Fig. 4B). In contrast, mRNAs predominantly bound by TIA1/L1 correlated best with localization to CRER (Fig. 4C).

mRNAs with 3′UTR-bound TIS11B had the highest number of AU-rich elements and the lowest pre-mRNA production rates (Fig. 4D, 4E). As all mRNAs in the AU compartment had generally high mRNA stability rates, the low production rates of TIS11B-bound mRNAs were associated with low steady-state mRNA and protein levels (Fig. 4F-H). In contrast, mRNAs predominantly bound by TIA1/L1 had significantly higher pre-mRNA production rates, and higher steady-state mRNA and protein levels (Fig. 4E-H). TIS11B or TIA1/L1-bound mRNAs also differed in the length and AU content of their 3′UTRs (Fig. S5C, S5D). Our analysis showed that although the presence of AU-RBPs is associated with high mRNA stability, different AU-RBPs, such as TIS11B or TIA1/L1 have a differential influence on subcytoplasmic mRNA localization and are associated with vastly different abundance levels.

3′UTR-bound TIAL1 localizes non-membrane protein-encoding mRNAs to the ER

Our CLIP data analysis suggested that TIA1/L1-bound mRNAs are enriched on the CRER, which has never been reported (Fig. 4A, 4C). To validate TIA1/L1-dependent mRNA localization to the ER, we used the MS2 tethering system to mimic 3′UTR-binding of TIA1/L1 (Fig. 5A). We generated a GFP-tagged reporter mRNA that contains MS2-binding sites as 3′UTR (Bertrand et al., 1998; Berkovits and Mayr, 2015; Lee and Mayr, 2019). Coexpression of mCherry-tagged MS2 coat protein (MCP) fused to TIAL1 tethers TIAL1 to the 3′UTR of the reporter mRNA (Fig. 5A). As control, mCherry-tagged MCP was tethered to the GFP reporter mRNA.

Coexpression of the reporter mRNA and MCP resulted in evenly distributed cytosolic expression of both MCP protein and reporter mRNA, due to the absence of a specific RBPs (Fig. 5C-E). In contrast, coexpression of the reporter mRNA and MCP-TIAL1 resulted in perinuclear, reticulated expression of MCP-TIAL1 with the mRNA reporter predominantly localized to the rough ER (Fig. 5B-E). Colocalization was assessed by RNA-FISH of the GFP-tagged reporter mRNA and simultaneous visualization of the rough ER through fluorescently tagged SEC61B. Using line diagrams of the fluorescence intensities, we quantified the overlap between the reporter mRNAs and the ER (Fig. 5C-E). In the presence of MCP-TIAL1, we observed higher correlation coefficients between the reporter mRNA and the ER (Fig. 5E). This result indicates that 3′UTR-bound TIAL1 causes localization of non-membrane protein encoding mRNAs to the rough ER surface.

3′UTR-bound TIAL1 increases protein expression

For endogenous mRNAs, our analysis suggested that TIA1/L1-bound mRNAs are highly abundant at steady-state and encode highly expressed proteins (Fig. 4G, 4H). Using the mRNA reporter, we investigated the contribution of TIAL1 to steady-state protein expression. We used FACS to measure GFP protein expression of the mRNA reporter with and without tethering of TIAL1 to the 3′UTR (Fig. 5A, Fig. S6A-C). We observed a 3.5-fold increase in protein expression upon 3′UTR-tethering of TIAL1 compared to tethering of MCP alone (Fig. 5F, 5G). We confirmed the TIA1/L1-dependent increase in protein expression using a second GFP reporter (Fig. S6D-F). As TIAL1 promotes translation of mRNAs on the ER membrane, it was unclear if increased protein expression was caused by TIAL1 or by a potentially unique translation environment provided by the rough ER membrane. For example, it was reported that mRNAs that encode non-membrane proteins contain 1.4-fold more ribosomes when translated on the ER membrane than when translated in the cytosol (Voigt et al., 2017).

TIAL1 cooperates with the rough ER environment to promote protein expression

To disentangle the effects of TIAL1 and the ER membrane on protein expression, we tethered the reporter mRNA directly to the ER surface by fusing MCP to SEC61B, a subunit of the translocon complex in the rough ER (Fig. 6A). MCP-SEC61B perfectly colocalized with the ER and recruited reporter mRNAs to the ER (Fig. 6B, S6G-I). However, reporter protein expression only increased by 1.25-fold compared to the tethering of MCP alone (Fig. 6B-D). We used a second ER localization reporter by fusing MCP to TRAPα, which represents a different subunit of the translocon complex and obtained a similar result. We observed an increase in protein expression by 1.5-fold when the reporter mRNA was tethered to TRAPα (Fig. S6J-M). These results suggested that the ER membrane environment has a significant but small stimulatory effect on protein expression.

Next, we investigated if the TIAL1-dependent increase in protein expression is intrinsic to TIAL1 or if it depends on its localization to the ER membrane. We added a CAAX motif to TIAL1 to localize the TIAL1-bound mRNA reporter to the plasma membrane instead of the ER membrane (Fig. 6E). The CAAX signal is a prenylation motif that efficiently localized MCP and MCP-TIAL1 to the plasma membrane (Fig. 6F)(Yan et al., 2016). Translation of the TIAL1-bound mRNA reporter at the plasma membrane increased protein expression by 1.8-fold (Fig. 6G, 6H). As translation of the TIAL1-bound reporter at the ER membrane resulted in two-fold higher protein expression than its translation at the plasma membrane (Fig. 6H), our result suggested that TIAL1 cooperates with the environment on the rough ER membrane to promote protein expression. As the RBPs bound to the reporter mRNA were identical in these experiments, our results demonstrate that the subcytoplasmic location of translation controls steady-state protein expression levels by two-fold when comparing plasma and ER membranes.

The repressive effect of unassembled TIS11B on protein expression is overcome by its localization to rough ER membrane

Next, we examined if the environment on the rough ER membrane also promotes protein expression of mRNAs bound by other RBPs, including TIS11B (Fig. 7A, 7B). In cells expressing GFP- or mCherry-TIS11B fusion constructs, about 30% form TIS granules at steady state (Fig. S7A, S7B) (Ma and Mayr, 2018). However, we noticed that addition of MCP to TIS11B fusion constructs resulted in limited TIS granule formation and predominant expression of unassembled TIS11B in the cytosol (Fig. S7A, S7B). In the unassembled state, binding of MCP-TIS11B to reporter mRNA repressed reporter protein expression by two-fold, compared to tethering of MCP alone (Fig. 7C, 7D). This result is consistent with previous reports that suggested that unassembled TIS11B represses the expression of certain cytokine mRNAs and cell cycle regulators (Stoecklin et al., 2002; Lykke-Andersen and Wagner, 2005; Galloway et al., 2016). In contrast, fusing TIS11B to MCP-SEC61B localizes TIS11B and the bound reporter mRNA to the rough ER, and this overcomes the repressive effect of unassembled TIS11B, increasing protein expression by two-fold (Fig. 7A-D). The two-fold increase in protein expression was recapitulated with a second reporter and indicates that the repressive effect on protein expression mediated by cytosolic, unassembled TIS11B is overcome by translation of the TIS11B-bound mRNA in the TGER region (Fig. 7D, Fig. S7C-E).

Taken together, we observed that 3′UTR-bound TIAL1 has a promoting effect on protein expression, whereas the binding of TIS11B is repressive. These results confirm the primary regulatory impact of RBPs on steady-state protein expression (Fig. 6H, 7D). Moreover, protein expression is additionally regulated by the subcytoplasmic location of translation in a manner that is independent of the bound RBP (Fig. 6H, 7D). Our findings show that relocalization of mRNAs that encode non-membrane proteins to the rough ER membrane stimulates their protein expression by two-fold, regardless of the bound RBPs (Fig. 7E).

Discussion

Using fluorescent particle sorting and digitonin extraction, we determined differential mRNA localization under steady-state cultivation conditions for TGER, CRER and cytosol. We confirmed that the rough ER membrane is the predominant site of protein synthesis for membrane and secretory proteins as 79% of these mRNAs (*N* = 1688) are strongly enriched there (Jan et al., 2014; Fazal et al., 2019). However, we detected even more mRNAs that encode non-membrane proteins with a biased localization to ER (*N* = 2165), representing 31% of mRNAs encoding non-membrane proteins in our dataset (Fig. 1F). Our findings indicate that the ER membrane is a general site of translation for both membrane and non-membrane proteins. We confirm previous reports (Lerner et al., 2003; Diehn et al., 2006; Chen et al., 2011; Reid and Nicchitta, 2012; Cui et al., 2012; Voigt et al., 2017), but we expand substantially the number of mRNAs that encode non-membrane proteins on the rough ER. As this group of mRNAs has not been characterized, we focused our analysis on these mRNAs.

Compartment-specific translation of functionally related genes

We observed that 52% of mRNAs that encode non-membrane proteins have a biased mRNA transcript localization pattern towards a single cytoplasmic compartment. We used RNA-FISH on endogenous and transfected mRNAs to validate the results of our subcytoplasmic mRNA localization dataset and confirmed the predicted mRNA enrichment in their respective compartments (Fig. 1, 3, and 4). One of our most striking findings was that within each cytoplasmic compartment a different group of functionally related mRNAs is translated (Fig. 2). Moreover, the compartment-enriched mRNAs are characterized by substantially different production and degradation rates as well as expression levels of their encoded proteins (Fig. 2). These features are consistent with the compartment-enriched gene groups, indicating that the cytoplasm is strongly partitioned into different functional and regulatory compartments that are not enclosed by membranes.

For example, we observed that low-abundance proteins are translated in the TGER region. mRNAs encoding zinc finger proteins and transcription factors were substantially enriched (Fig. 2E), likely because these gene classes are usually expressed at lower levels than other gene classes (Vaquerizas et al., 2009). Transcription factors may also take advantage of other, so far unknown, features of the TGER environment that may allow for regulation of protein complex assembly. This idea is based on the previous observation that membrane proteins that are translated in the TGER domain are able to establish protein complexes that cannot be formed when the proteins are translated on the ER membrane outside of TIS granules (Ma and Mayr, 2018).

In contrast, mRNAs that are the most stable and encode the most highly expressed proteins are enriched on the CRER and include helicases, cytoskeleton-bound proteins, and chromatin regulators (Fig. 2). It was previously shown that global translation is inhibited during stress, including hypoxia, but local translation on the ER is sustained. Active translation of hypoxia-induced genes was accomplished through their increased ER localization during stress (Staudacher et al., 2015). Our findings show that the rough ER membrane is not only a privileged site of protein synthesis during stress, but also promotes high protein expression for a selected group of genes in steady-state cultivation conditions.

It was previously assumed that the majority of non-membrane protein-encoding mRNAs are translated in the cytosol (Jan et al., 2014; Fazal et al., 2019). Although for nearly all mRNAs some transcripts localize to the cytosol, we show that for only ~21% of these mRNAs the majority of transcripts localizes there. The group of mRNAs overrepresented in the cytosol had

the highest production and degradation rates (Fig. 2). They are enriched in proteins involved in mRNA processing and translation factors, whose abundance levels require tight control. Taken together, despite not being separated by membranes, we observed strong evidence for the functional compartmentalization of the subcytoplasmic space.

A combinatorial code of 3′UTR-bound RBPs controls subcytoplasmic mRNA localization

According to the RNA regulon hypothesis, functionally related mRNAs are coregulated by specific RBPs that orchestrate the different regulatory steps during their lifetime (Keene, 2007). As compartment-enriched mRNAs differed substantially in their mRNA features, we determined the RBPs responsible for subcytoplasmic localization. In polarized cells, differential mRNA localization has been described between soma and neurites or between apical and basal compartments (Miller et al., 2002; Huttelmaier et al., 2005; Moor et al., 2017). Although HEK293T cells lack such polarity, we identified a hierarchy in subcytoplasmic mRNA localization. Differential mRNA localization between the perinuclear region, containing the TGER/CRER, and the cytosol was largely determined by the antagonistic effects of 3′UTR-bound AU-RBPs and LARP4B. mRNAs bound by AU-RBPs tend to localize to the perinuclear region, TGER/CRER, whereas lack of AU-RBPs or the presence of LARP4B promotes cytosolic localization (Fig. 3E-H).

However, not all mRNAs bound by AU-RBPs behave similarly. TIS11B-bound mRNAs are biased towards TGER, whereas TIA1/L1-bound mRNAs are biased towards the CRER. For mRNAs that are cobound by both RBPs, the ratio of TIS11B to TIA1/L1 is the best discriminator for biased mRNA localization between TGER and CRER (Fig. 4). Early mRNA localization studies performed in fibroblasts and neurons detected unique localization signals (Lawrence and Singer, 1986; Miller et al., 2002; Chao et al., 2010). Our study did not identify such signals, but instead, we found that 3′UTR-bound RBPs had cumulative effects on mRNA localization. For example, we observed that increasing levels of a 3′UTR-bound RBP enhanced its respective effect on mRNA localization, but when two RBPs with opposing effects were bound to the same mRNA, they neutralized each other’s contribution (Fig. 4).

TIA1/L1 localizes mRNAs to the CRER and promotes protein expression

We discovered a previously undescribed role for 3′UTR-bound TIA1/L1 in mRNA localization to CRER and identified TIAL1 as a strong positive regulator of mRNA and protein expression (Fig. 4G, 4H). So far, TIA1 and TIAL1 have mostly been described as regulators of pre-mRNA splicing and as translational repressors in the context of cellular stress where they assemble into stress granules (Kedersha et al., 1999; Gilks et al., 2004). However, in the absence of stress, TIA1/L1 has been reported to promote polysome association which supports our findings (Mazan-Mamczarz et al., 2006; Meyer et al., 2018).

We generated a reporter system to investigate mRNA localization-dependent regulation of protein expression. By using this new experimental system, we observed a 3.5 to 4-fold increase in protein expression caused by TIAL1 (Fig. 5G, 6H). This increase is partially achieved by the intrinsic activity of TIAL1 but the full increase in protein expression was only accomplished through cooperative action between TIAL1 and the rough ER membrane environment (Fig. 6H). Taken together, our data suggest that highly expressed non-membrane proteins take advantage of the translation-promoting environment of the rough ER through recruitment of TIA1/L1. The mechanistic nature of the translation-promoting environment is not yet understood and may be a combination of direct effects on translation and indirect effects, such as protection of mRNAs from degradation.

mRNA localization to the rough ER membrane promotes protein expression

Surprisingly, we observed that mRNA localization to the rough ER membrane also promoted protein expression for TIS11B-bound mRNAs. Unassembled TIS11B localizes to the cytosol and was previously found to repress expression of specific mRNAs (Stoecklin et al., 2002; Lykke-Andersen and Wagner, 2005; Galloway et al., 2016). We confirmed this result by showing that cytosolic unassembled TIS11B represses reporter protein expression. However, translation of a TIS11B-bound mRNA on the rough ER membrane overrode the intrinsically repressive effects of cytosolic, unassembled TIS11B (Fig. 7D).

Taken together with the results obtained from endogenous mRNAs, our findings strongly suggest that the rough ER membrane represents a privileged site for protein expression. Translation of highly abundant mRNAs results in highly expressed proteins. Notably, the TGER seems to ensure that low-abundance mRNAs are effectively translated into low-abundance proteins, effectuating control over the protein synthesis of a class of proteins strongly enriched in transcription factors.

The mechanism by which the rough ER membrane generates a stimulating environment for protein expression is currently unknown. It was shown previously that mRNAs are bound by more ribosomes when translated on the ER instead of the cytosol (Voigt et al., 2017). Furthermore, ER-resident enzymes may modulate the translation machinery or the 3′UTR-bound RBPs to boost translation (Bertolotti, 2018). We speculate that the environment on the rough ER, which is generated in part by the enriched mRNAs and their bound RBPs, may exclude repressive factors that seem to be active in the cytosol. This idea is supported by our observation that cytosolic mRNAs have the highest degradation rates (Fig. 2D, 3N).

In our dataset, cytosolically-enriched mRNAs have a higher GC-content and the lowest mRNA stability values, which is consistent with previous reports showing that GC-rich 3′UTRs are destabilizing, whereas mRNAs with AU-rich 3′UTRs are more stable (Courel et al., 2019; Litterman et al., 2019). There are currently two models that are consistent with the observed data. According to the prevailing model, mRNA stability is regulated by the mRNA-bound RBPs (Gebauer et al., 2021), meaning the RBPs that bind to AU-rich mRNAs would stabilize them. However, our data also support an alternative model that takes into account subcellular localization. In this model, mRNAs with AU-rich 3′UTRs use RBPs to preferentially localize to the rough ER, a region that might be inherently protected from degradation. This latter model is supported by our reporter experiments. Although we did not measure mRNA stability rates, we observed that redirecting mRNAs to the rough ER membrane increased their protein levels independently of 3′UTR sequence, which was kept constant in the relocalization experiments (Fig. 6H, 7D).

Our study revealed a surprisingly high degree of cytoplasmic compartmentalization. This is the basis for the translation of functionally related proteins in defined environments that strongly affect mRNA stability and protein expression (Fig. 7E). Our results highlight the contribution of spatial regulation whose consequences go beyond the effects mediated by the mRNA-bound proteins. In the future, our findings may provide the basis for biotechnology applications that make use of engineered 3′UTR sequences to boost protein expression in experimental settings or to increase protein production of mRNA vaccines.

Limitations of our study

To obtain sufficient material for TGER and CRER particle sorting, we used transfected, fluorescently labeled proteins instead of endogenous proteins. As TGER and the CRER are tightly associated (Fig. 1C), for some mRNAs that encode membrane proteins, differential mRNA localization to TGER or the CRER could not be resolved. However, despite their tight association, TGER- and CRER-enriched mRNAs that encode non-membrane proteins differed

substantially in their functional gene classes and in their mRNA and protein features, suggesting that our purification method was successful.

The reporter relocalization experiments showed that the subcytoplasmic location of translation strongly influences steady-state protein expression. It is thought that both mRNA stability and translation cause this effect, but the extent by which the two regulatory mechanisms contribute to protein expression was not examined.

Acknowledgements

This work was funded by the NIH Director′s Pioneer Award (DP1-GM123454), the R35GM144046 NIH grant, a grant from the Pershing Square Sohn Cancer Research Alliance, a grant from the G. Harold and Leila Y. Mathers Foundation, and the MSK Core Grant (P30 CA008748) to CM. J.U. received funding from the ERC under the European Union Horizon 2020 Research and Innovation Program (835300-RNPdynamics) and The Francis Crick Institute receives its core funding from Cancer Research UK (CC0102), the UK Medical Research Council (CC0102), and the Wellcome Trust (CC0102). An NIH F31 (CA254335-01) fellowship was awarded to E.L.H.

We thank Yevgeniy Romin and Eric Chan from the Molecular Cytology Core Facility for help with microscopy and image analysis. We thank Kathleen Daniels from the Flow Cytometry Core Facility (now Sana Biotechnologies) for help with particle sorting and Liana Boraas at Yale University School of Medicine for help with endogenous RNA-FISH. We thank Weirui Ma and Sibylle Mitschka for experimental guidance and mentorship and Alban Ordureau for analysis of the TMT mass spectrometry data. We thank Yang Luo and Sibylle Mitschka for helpful discussions and critical reading of the manuscript.

Author contributions

E.L.H. performed all experiments, except the mass spectrometry analysis whose samples were prepared by X.C. F.C.Y.L. and J.U. performed and analyzed the TIS11B iCLIP experiment. G.Z. analyzed the CLIP, and RNA-seq data with input from C.M. and integrated all datasets. M.M.F performed the logistic regression on the RBPs. E.L.H. and C.M. conceived the project, designed the experiments, and wrote the manuscript with input from all other authors.

Declaration of Interests

The authors declare no competing interests.

Methods

STAR methods table

Cell lines

Detailed methods

Constructs

Fluorescently-tagged TIS11B and SEC61B constructs. The eGFP/mCherry/BFP fusion constructs for TIS11B and SEC61B expression were described previously (Ma and Mayr, 2018). They were generated in the pcDNA3.1-puro expression vector. The TIS11B and SEC61B coding regions were PCR amplified from HeLa cDNA and inserted downstream of eGFP/mCherry/BFP using BsrGI/EcoRI or BsrGI/HindIII restriction sites, respectively.

Constructs for RNA-FISH. All coding regions were amplified from HeLa cDNA with their respective F and R primers and inserted in-frame, downstream of GFP (GFP lacking a stop codon) between BsrGI and XbaI sites into pcDNA3.1-puro-GFP vector. The corresponding 3′UTRs were amplified from HeLa genomic DNA and inserted downstream of the stop codon into the multiple cloning site using XbaI and ApaI. All primers are listed in Table S5.

Constructs to generate the mRNA localization reporter. To investigate the influence of RBPs on mRNA localization of a GFP mRNA reporter, RBPs were fused to MCP and tethered to a GFP mRNA reporter containing MS2 binding sites as 3′UTR (Bertrand et al., 1998; Berkovits and Mayr, 2015). To investigate mRNA localization-dependent protein expression of the GFP mRNA reporter, subcellular localization signals were fused to MCP or to MCP-RBP fusions.

GFP mRNA reporter. To generate the GFP mRNA reporter, the GFP-BIRC3-MS2-SU (Lee and Mayr, 2019) vector was used the BIRC3 coding region was replaced with the THAP1 coding region. It was PCR amplified from the GFP-THAP1 vector using THAP1-MS2 F and THAP1-MS2 R primers and inserted between the BsrGI and AgeI sites. The SU fragment was removed with HindIII and XhoI and blunt end ligated, resulting in GFP-THAP1-MS2.

MCP-mCherry RBP fusion constructs. To generate MCP-mCherry, the MCP coding sequence was PCR amplified from UBC NLS-HA-2XMCP-tagRFPt vector (Addgene 64541) using MCP F and MCP R primers and inserted in-frame, upstream of mCherry (mCherry lacking a start codon) between BmtI and BamHI sites in pcDNA3.1-puro-mCherry vector (Ma and Mayr, 2018). To generate MCP-mCherry-TIS11B and MCP-mCherry-TIAL1, their coding sequences were inserted in-frame, downstream of mCherry between the BsrGI and XbaI sites. The TIS11B coding sequence was amplified from pcDNA3.1-puro-GFP-TIS11B using TIS11B MCP F and TIS11B MCP R primers and the TIAL1 coding sequence was PCR amplified from pFRT_TO_FlagHA_TIAL1 (Addgene 106090) using TIAL1 MCP F and TIAL1 MCP R primers.

MCP-mCherry fusion constructs with subcellular localization signals. To generate pcDNA3.1-puro-MCP-mCherry-SEC61B, the MCP-mCherry coding sequence was cut from MCP-mCherry vector using BmtI and BsrGI and pasted in-frame, upstream of SEC61B in pcDNA3.1-mCherry-SEC61B (replacing mCherry). To generate the TIS11B-MCP-mCherry-SEC61B vector, TIS11B coding sequence was PCR amplified from pcDNA3.1-puro-GFP-TIS11B using TIS-SEC F and TIS-SEC R primers and pasted in-frame, upstream of MCP into the BmtI site in the MCP-mCherry-SEC61B vector. To generate TRAPα-MCP-mCherry, the TRAPα coding sequence (encoded by the *SSR1* gene) was PCR amplified from HeLa cDNA using TRAPα MCP F and TRAPa MCP R and inserted in-frame, upstream of MCP in the pcDNA3.1-puro-MCP-mCherry vector.

For plasma membrane localization, the CAAX prenylation signal was added to the C-terminus of MCP-mCherry or MCP-mCherry-TIAL1. The CAAX coding sequence was purchased as a gene fragment from Azenta as described (Yan et al., 2016) and PCR amplified using TIAL1 CAAX F and CAAX R primers. It was inserted in-frame using the BsrGI and ApaI sites, located downstream of mCherry to generate pcDNA3.1-puro-MCP-mCherry-CAAX. It was inserted in-frame using EcoNI and ApaI sites to generate MCP-mCherry-TIAL1-CAAX.

SunTag constructs. To generate the SunTag-FOS vector, the FOS coding region was PCR amplified from HeLa cDNA using FOS 2F and FOS 2R primers and inserted between AgeI and BmtI sites in pcDNA4-TO-24xGCN4_v4-KIF18B-24xPP7 vector (Addgene 74928), replacing KIF18B. The FOS 3′UTR was PCR amplified from HeLa genomic DNA using FOS UTR 2F and FOS UTR 2R primers and inserted in EcoRI site downstream of the PP7 region in SunTag-FOS.

Isolation of subcytoplasmic compartments

Transfection. HEK293T cells were seeded in six 10 cm dishes at 80% confluency in antibiotic free media. After 24 hours, cells were transfected by calcium phosphate with either 3 µg mCherry-TIS11B or 3 µg GFP-SEC61B per dish.

Particle purification. 20 hours after transfection, cells were rinsed once with ice-cold PBS, scraped in 10 ml ice-cold PBS, and pelleted at 300 x g. Pellets from two plates were resuspended in 1 ml ice-cold hypotonic isolation buffer (225 mM mannitol, 75 mM sucrose, 20 mM Tris-HCl pH 7.4, 0.1 mM EDTA). Cells were lysed with 50 strokes in a 1 ml dounce-homogenizer with pestle on ice in order to shear the nuclei from the ER. Nuclei were pelleted with a two-minute spin at 600 x g. The supernatant contains the cytoplasmic membrane fraction, which was pelleted with a 15-minute spin at 7000 x g and resuspended in ice-cold PBS for fluorescent particle sorting.

Fluorescent particle sorting. Particles were sorted on a BD FACSAria III cell sorter equipped with a 70 µm nozzle. The forward-scatter threshold was decreased from 5,000 to 800 in order to visualize subcellular particles. Particles were first detected by fluorescence using the 594 nm and 488 nm excitation lasers, for mCherry-TIS11B and GFP-SEC61B respectively, and 405 nm excitation laser for DAPI. A sorting gate was drawn on particles that were either mCherry-positive or GFP-positive, but DAPI-negative, to exclude any remaining nuclei. Sorting was performed in purity mode with an average speed of 150 particles/second. Particles were sorted directly into 1 ml of TRIzol solution in Eppendorf tubes, holding 180,000 particles per tube. RNA extraction was performed for each tube separately and total RNA for each sample was combined for library preparation. Two biological replicates for each particle prep were sequenced. For each replicate, about 1.5 million TIS11B granule particles and 2.0 million ER particles were collected.

Cytosol extraction. The cytosol was extracted as previously described (Liu and Fagotto, 2011). HEK293T cells were plated in a six-well plate at 80% confluency. After 24 hours, cells were rinsed once in the dish with ice-cold PBS. After aspirating PBS, 300 µl ice-cold digitonin solution (40 µg/ml digitonin, 150 mM NaCl, 20 mM HEPES pH 7.4, 0.2 mM EDTA, 2 mM DTT, 2 mM MgCl2) was added and incubated on a shaker at 4°C for ten minutes. After incubation, the digitonin-derived cytosolic extract was pipetted from the plate and spun at 20,000 x g for one minute to pellet any floating cells. 200 µl of cytosolic extract was added to 1 ml TRIzol solution for RNA extraction.

RNA-seq library preparation

RiboGreen RNA Reagent (ThermoFisher) was used for RNA quantification and quality control was performed by Agilent BioAnalyzer. 50-500 ng of total RNA underwent polyA selection and TruSeq library preparation according to instructions provided by Illumina (TruSeq Stranded

mRNA LT Kit, catalog # RS-122-2102), with eight cycles of PCR. Samples were barcoded and run on a HiSeq 4000 in a PE50 run, using the HiSeq 3000/4000 SBS Kit (Illumina). An average of 27 million paired reads was generated per sample.

Western Blotting

For whole cell lysate preparation, cells were trypsinized and washed twice with PBS and lysed in 2x Laemmli Sample buffer (Alfa Aesar, J61337). For cytosolic lysate, cytosol was extracted with digitonin as described above and one volume of 2x Laemmli Sample buffer was added. Laemmli lysates were boiled for 10 min at 95°C. Samples were subjected to SDS-PAGE on NuPAGE 4%–12% Bis-Tris gradient protein gel (Invitrogen). Imaging was captured on the Odyssey DLx imaging system (Li-Cor). The antibodies used are listed in the Key Resources Table.

TIS11B iCLIP

Transfection. HEK293T cells were seeded in 10 cm dishes at 80% confluency in antibiotic free media. After 24 hours, cells were transfected by calcium phosphate with either 3 µg GFP-TIS11B or 1.5 µg GFP-only per dish.

Sample preparation. 20 hours after transfection, cells were rinsed once with ice-cold PBS and 6 ml of fresh PBS was added to each plate before crosslinking. Cells were irradiated once with 150 mJ/cm^2 in a Spectroline UV Crosslinker at 254 nm. Irradiated cells were scraped into Eppendorf tubes, spun at 500 x g for one minute, and snap-frozen. Crosslinked cell pellets were lysed in iCLIP lysis buffer (50 mM Tris-HCl pH 7.4, 100 mM NaCl, 1% Igepal CA-630 (Sigma I8896), 0.1% SDS, 0.5% sodium deoxycholate), sonicated with the Bioruptor Pico for 10 cycles 30 seconds ON/30 seconds OFF, and supplemented with 0.5 U of RNase I per 1 mg/ml lysate for RNA fragmentation. Lysates were pre-cleared by centrifugation at 20,000 x g at 4°C. A mix of Protein A/G Dynabeads (50 µl of each per sample, Life Technologies) were coupled to 10 µg of rabbit anti-GFP antibody (Abcam ab290). TIS11B protein-RNA complexes were immunoprecipitated from 1 ml of crosslinked lysate and washed with high salt and PNK buffer (NEB). RNA was repaired by 3′ dephosphorylation and ligated to L3-IR adaptor on beads (Zarnegar et al., 2016). Excess adaptor was removed by incubation with 5′ deadenylase and the exonuclease RecJf (NEB). TIS11B protein-RNA complexes were eluted from the beads by heating at 70°C for one minute. The complexes were then visualized via the infrared-labeled adaptor, purified with SDS-PAGE, and transferred to nitrocellulose membrane. cDNA was synthesized with Superscript IV Reverse Transcriptase (Life Technologies) and circularized by CircLigase II. Circularized cDNA was purified with AmPURE bead-based purification (A63880, Beckman Coulter), amplified by PCR and sequenced by Novaseq.

RNA-FISH

Single molecule RNA-FISH for endogenous mRNAs. Probe design. Primary probes were designed using the ProbeDealer package in MATLAB (Hu et al., 2020). Each primary probe contains 30 transcript-targeting nucleotides preceded by 20 common nucleotides that are complementary to the secondary probe. At least 30 probes were designed for each transcript, purchased in a pool from IDT. The secondary probes are 5′ conjugated to AlexaFluor 633 and were purchased from IDT.

Transfection. Prior to cell seeding, 35 mm glass cover slips were sterilized with ethanol then incubated in 1 µg/ml fibronectin in PBS at room temperature for one hour. Cover slips were rinsed in PBS and HeLa cells were seeded at 100,000 per coverslip. 24 hours after seeding, cells were transfected with 500 ng GFP-TIS11B using Lipofectamine 3000 (Invitrogen).

Sample preparation. 20 hours after transfection, cells were rinsed once with PBS then fixed in 4% paraformaldehyde for 10 minutes at room temperature. All steps were performed at room temperature if not otherwise noted. Cells were rinsed twice with PBS and permeabilized with 0.5% Triton-X solution for 10 minutes. Cells were rinsed twice with PBS and incubated for five minutes in pre-hybridization buffer (2xSSC, 50% formamide). Cells were incubated in primary probe hybridization solution (40 µM primary probe, 2xSSC, 50% formamide, 10% dextran sulfate (Sigma), 200 µg/ml yeast tRNA (Sigma), 1:100 Murine RNase Inhibitor (NEB)), for at least 15 hours at 37°C. To remove excess or unbound primary probes, cells were then rinsed twice in 2xSSC + 0.1% Tween for 15 minutes at 60°C then once more for 15 minutes at room temperature. Cells were incubated in secondary probe solution (4 nM secondary probe, 2xSSC, 50% ethylene carbonate, 1:100 Murine RNase Inhibitor) for 30 minutes in the dark. Secondary probes were rinsed twice in 50% ethylene carbonate, 2xSSC solution for five minutes then mounted with Prolong Diamond mounting solution (Invitrogen). For both endogenous and GFP-fusion constructs, RNA-FISH images were captured using confocal ZEISS LSM 880 with Airyscan super-resolution mode.

Cytosol extraction. To visualize and validate cytosolic versus ER-associated endogenous mRNAs, HeLa cells were seeded as described above, then incubated in 2 ml digitonin solution described above (40 µg/ml digitonin, 150 mM NaCl, 20 mM HEPES pH 7.4, 0.2 mM EDTA, 2 mM DTT, 2 mM MgCl2) for 10 min at 4°C. Digitonin solution was removed, coverslips were rinsed with 2 ml PBS, and RNA-FISH was performed as described above.

Line profile analysis. To quantify colocalization of two fluorescence signals (mRNA vs TGER or mRNA vs ER), line profiles were generated with FIJI (ImageJ). For each cell, 2-4 straight lines were drawn to cross TGER (or the ER) in different directions, indicated by the white arrows shown in the figures. Fluorescence signal along the straight line of TGER (or ER) and the examined mRNA was calculated for each channel using the plot profile tool in FIJI. The values of the Pearson's correlation coefficient r were calculated using Excel. Perfect correlation of protein-mRNA is indicated by r = 1, perfect exclusion is indicated by r = -1, and random distribution is indicated by r = 0.

Enrichment analysis of endogenous mRNAs. Enrichment of endogenous mRNAs in TGER was determined using FIJI. The total area of the cell and the total area occupied by TIS granules was calculated for each cell. A mask was created from the GFP-TIS11B signal and the mask area was divided by the total cell area to generate the granule area fraction. The total number of transcripts per cell (number of foci) was quantified. This value was multiplied by the granule area fraction to yield the number of transcripts expected to be present in TIS granules by chance. The observed number of transcripts in the TIS granule area was then divided by the expected value to obtain the enrichment fold-change. The fold-change values were log2-transformed. An enrichment score of 0 indicates 'no enrichment' and is observed when the observed and expected numbers of transcripts in TIS granules are the same. A positive enrichment score indicates that there are more transcripts localized to TIS granules than one would expect by chance and a negative enrichment score indicates fewer transcripts in TIS granules than one would expect by chance.

RNA-FISH after transfection of constructs. RNA-FISH experiments probing for GFP-fusion constructs were performed as described previously (Ma and Mayr, 2018). Stellaris FISH probes for eGFP with Quasar 670 Dye were used.

Confocal microscopy

Confocal imaging was performed using ZEISS LSM 880 with Airyscan super-resolution mode. A Plan-Apochromat 63x/1.4 Oil objective (Zeiss) was used. For live cell imaging, cells were incubated with a LiveCell imaging chamber (Zeiss) at 37°C and 5% CO2 and imaged in cell

culture media. Excitations were performed sequentially using 405, 488, 594 or 633 nm laser wavelength and imaging conditions were experimentally optimized to minimize bleed-through. Images were prepared with FIJI (ImageJ) software.

TMT mass spectrometry

To obtain protein expression levels, TMT mass spectrometry analysis was performed on HEK293T cells cultivated in steady-state conditions. Cells were trypsinized and washed three times with ice-cold PBS. Pelleted cells were snap-frozen in liquid nitrogen. Cell pellets were lysed with 200 µl buffer containing 8 M urea and 200 mM EPPS (pH at 8.5) with protease inhibitor (Roche) and phosphatase inhibitor cocktails 2 and 3 (Sigma). Benzonase (Millipore) was added to a concentration of 50 µg/ml and incubated at room temperature for 15 min followed by water bath sonication. Samples were centrifuged at 14,000 g at 4°C for 10 min, and supernatant extracted. The Pierce bicinchoninic acid (BCA) protein concentration assay was used to determine protein concentration. Protein disulfide bonds were reduced with 5 mM tris (2-carboxyethyl) phosphine at room temperature for 15 min, and alkylated with 10 mM iodoacetamide at room temperature for 30 min in the dark. The reaction was quenched with 10 mM dithiothreitol at room temperature for 15 min. Aliquots of 100 µg were taken for each sample and diluted to 100 µl with lysis buffer. Samples were subject to chloroform/methanol precipitation as previously described (Navarrete-Perea et al., 2018). Pellets were reconstituted in 200 mM EPPS buffer and digested with Lys-C (1:50 enzyme-to-protein ratio) and trypsin (1:50 enzyme-to-protein ratio), and digested at 37°C overnight.

Peptides were TMT-labeled as described (Navarrete-Perea et al., 2018). Briefly, peptides were TMT-tagged by the addition of anhydrous ACN and TMTPro reagents (16plex) for each respective sample and incubated for 1 hour at room temperature. A ratio check was performed by taking a 1 µl aliquot from each sample and desalted by StageTip method (Rappsilber et al., 2007). TMT tags were then quenched with hydroxylamine to a final concentration of 0.3% for 15 min at room temperature. Samples were pooled 1:1 based on the ratio check and vacuum-centrifuged to dryness. Dried peptides were reconstituted in 1 ml of 3% ACN/1% TFA, desalted using a 100 mg tC18 SepPak (Waters), and vacuum-centrifuged overnight.

Peptides were centrifuged to dryness and reconstituted in 1 ml of 1% ACN/25mM ABC. Peptides were fractionated into 48 fractions. Briefly, an Ultimate 3000 HPLC (Dionex) coupled to an Ultimate 3000 Fraction Collector using a Waters XBridge BEH130 C18 column (3.5 um 4.6 x 250 mm) was operated at 1 ml/min. Buffer A, B, and C consisted of 100% water, 100% ACN, and 25mM ABC, respectively. The fractionation gradient operated as follows: 1% B to 5% B in 1 min, 5% B to 35% B in 61 min, 35% B to 60% B in 5 min, 60% B to 70% B in 3 min, 70% B to 1% B in 10 min, with 10% C the entire gradient to maintain pH. The 48 fractions were then concatenated to 12 fractions, (i.e. fractions 1, 13, 25, 37 were pooled, followed by fractions 2, 14, 26, 38, etc.) so that every 12th fraction was used to pool. Pooled fractions were vacuum-centrifuged and then reconstituted in 1% ACN/0.1% FA for LC-MS/MS.

Fractions were analyzed by LC-MS/MS using a NanoAcquity (Waters) with a 50 cm (inner diameter 75 µm) EASY-Spray Column (PepMap RSLC, C18, 2 µm, 100 Å) heated to 60°C coupled to an Orbitrap Eclipse Tribrid Mass Spectrometer (Thermo Fisher Scientific). Peptides were separated by direct injection at a flow rate of 300 nl/min using a gradient of 5 to 30% acetonitrile (0.1% FA) in water (0.1% FA) over 3 hours and then to 50% ACN in 30 min and analyzed by SPS-MS3. MS1 scans were acquired over a range of m/z 375-1500, 120K resolution, AGC target (standard), and maximum IT of 50 ms. MS2 scans were acquired on MS1 scans of charge 2-7 using isolation of 0.5 m/z, collision-induced dissociation with activation of 32%, turbo scan, and max IT of 120 ms. MS3 scans were acquired using specific precursor

selection (SPS) of 10 isolation notches, m/z range 110-1000, 50K resolution, AGC target (custom, 200%), HCD activation of 65%, max IT of 150 ms, and dynamic exclusion of 60 s.

Visualization of translation in TGER

The SunTag system was used to visualize mRNA translation in the cytosol and the TGER domain. Stable expression of td-PP7-3xmCherry (Addgene 74926) and scFv-GCN4-sfGFP (Addgene 60907) was achieved by generating virus in HEK293T cells and transducing HeLa cells. Cells were seeded on 3.5 cm glass bottom dishes (Cellvis, D35-20-1-N). 20 hours later, cells were transfected with either the SunTag vector expressing KIF18B (Addgene 74928) or SunTag-FOS-UTR. At 15 hours post transfection, cells were treated with 100 ng/ml doxycycline for one hour to induce SunTag expression. Confocal imaging was performed as described above. Colocalization of puncta was quantified using FIJI.

mRNA localization-dependent GFP protein expression

Transfection. HeLa cells were seeded in 12-well plates at 80% confluency and transfected with 250 ng GFP-THAP1-MS2 and 250 ng of the MCP-mCherry fusion constructs indicated in the figure (Lipofectamine 3000, Invitrogen). When indicated, GFP-THAP1 or GFP-BIRC3-MS2-SU was used instead of GFP-THAP1-MS2. At 13-15 hours post transfection, cells were analyzed by FACS. For RNA-FISH experiments, cells were seeded at 80% confluency in 4-well slide chambers (Millipore Sigma) and cotransfected with 75 ng GFP-THAP1-MS2, 100 ng BFP-SEC61B, and 75 ng of the indicated MCP-mCherry fusion constructs.

FACS analysis to measure GFP protein expression. Cells were trypsinized, washed once in complete media, then resuspended in FACS buffer (PBS plus 1% FCS). At least 5,000 cells were measured on a BD LSR-Fortessa Cell Analyzer and FACS data were analyzed using FlowJo software. GFP protein expression corresponds to GFP mean fluorescence intensity (MFI). To determine the effect of MCP-tethered RBPs on protein output of the GFP reporter mRNA, only cells that were successfully cotransfected with both the MCP-mCherry fusion and the GFP reporter constructs were analyzed. To do so, the double-positive cells (mCherry+/GFP+) were gated, and all single positive and unstained cells were excluded from the analysis. The reported GFP MFI was calculated from the double-positive cells. Untransfected cells were used to draw the gates for mCherry+ or GFP+ cells.

Data analysis

RNA-seq of subcytoplasmic fractions

RNA-seq. Raw reads were processed by trimmomatic (version: 0.39) to trim low-quality ends (average quality per base < 15, 4 bp window) and adapters (Bolger et al., 2014). Trimmed reads were mapped to the human genome (hg19) using hisat2 (version: 2.1.0) (Kim et al., 2019). Reads mapped to each gene were counted using featureCounts (version: 1.6.4) (Liao et al., 2014). RPKM values for each gene were calculated using a custom Perl script. The mean RPKM values of all biological replicates were calculated and used for downstream analyses. Only protein-coding genes were analyzed. A gene is considered expressed if the RPKM value is 3 or greater. The RPKM values of the biological replicates correlated strongly (Fig. S1E).

Classification of membrane/secretory proteins versus non-membrane proteins. Information on the presence of transmembrane domains or a signal sequence was obtained from uniprot. All expressed genes were separated into mRNAs that encode membrane/secretory proteins or non-membrane proteins. If a protein contains a signal sequence but not a transmembrane domain, it is considered as secretory protein. All proteins with transmembrane domains are considered membrane proteins and all remaining proteins are classified as non-membrane

proteins. Among the 9155 mRNAs expressed in HEK293T cells, 2140 were classified as membrane/secretory proteins, whereas 7015 were classified as non-membrane proteins (Table S1).

Compartment-specific partition coefficients. The sum of RPKM values obtained from TGER particles, CRER particles, and the cytosol was considered as total cytoplasmic mRNA expression. For each gene, the fraction of transcripts that localize to each of the three compartments was calculated by dividing its compartment-specific RPKM value by the total cytoplasmic mRNA expression (Fig. S1F). The compartment-specific partition coefficient of a gene is the fraction of mRNA transcripts that localize to the compartment.

Compartment-specific enrichment of mRNAs that encode membrane/secretory proteins. We considered an mRNA to be CRER-enriched if the ratio of partition coefficients (CRER/TGER) was greater than 1.25 and classified it as TGER-enriched if it was smaller than 0.8. The median partition coefficient of membrane/secretory mRNAs in the cytosol was 0.09. If the cytosolic partition coefficient of an mRNA was greater than 0.36, it was considered enriched in the cytosol. If the CRER and TGER-specific partition coefficients were similar and the cytosolic partition coefficient was smaller than 0.18, the mRNA was assigned to the CRER, whereas it was considered not localized if the cytosolic partition coefficient was smaller than 0.18 (Fig. S1G).

Compartment-specific enrichment of mRNAs that encode non-membrane proteins. For all mRNAs that encode non-membrane proteins, the medians of the partition coefficients for each compartment were calculated. For TGER particles the median was 0.32, for CRER particles, it was 0.30 and for the cytosol, the median was 0.34. An mRNA was considered to have a biased localization to a specific compartment if its compartment-specific partition coefficient exceeded 1.25-fold of the median partition coefficient of the compartment. For example, the minimum partition coefficient for TGER-enriched mRNAs was 0.42, it was 0.38 for CRER-enriched mRNAs, and 0.43 for CY-biased mRNAs. If the enrichment was observed in two compartments, the mRNA was assigned to the compartment with the higher value. This strategy resulted in 1246 mRNAs considered to be TGER-enriched, 919 mRNAs to be ER-enriched, and 1481 mRNAs to be enriched in the cytosol. The remaining 3369 mRNAs (48%) do not have a compartment-biased mRNA localization pattern and were called (unbiased, UB).

mRNA and protein features of the localized mRNAs

RPKM values of mRNAs were obtained from RNA-seq data of unfractionated HEK293T cells and were determined for the compartment-biased mRNAs. Pro-seq and RNA-seq from HEK293 cells were obtained from GEO (GSE140365: PRO-seq; GSE142895: RNA-seq) (Patel et al., 2020). Raw reads were processed by trimmomatic (version: 0.39) to trim low-quality ends (average quality per base < 15, 4 bp window) and adapters (Bolger et al., 2014). Trimmed reads were mapped to the human genome (hg19) using hisat2 (version: 2.1.0) (Kim et al., 2019). Reads mapped to each gene were counted by featureCounts (version: 1.6.4) (Liao et al., 2014). To estimate mRNA stability rates, log2-normalized counts of Pro-seq data were divided by the log2-normalized RNA-seq data, as described previously (Blumberg et al., 2021). 3′UTR length of each mRNA was obtained from Ref-seq. The longest 3′UTR isoform of each gene is reported. AU-content in 3′UTRs is the sum of all adenosines and uridines in annotated 3′UTRs divided by the total number of nucleotides in 3′UTRs. The number of AUUUAs (AU-rich elements) in 3′UTRs were counted. Protein length was obtained from uniprot.

Protein expression

Protein expression was obtained from TMT-based quantitative mass spectrometry analysis of unfractionated HEK293T cells. Precursor protein abundance was calculated for each protein

and scaled to the TMT abundance for each channel. Relative abundance was then calculated by averaging biological replicates.

CLIP data analysis

iCLIP analysis of TIS11B in HEK293T cells. Raw fastq files were demultiplexed using the iCount python package (https://icount.readthedocs.io). 5′ and 3′ adapters were trimmed by Cutadapt (Martin, 2011). Trimmed reads were mapped to human genome using STAR and reads mapping to tRNA/rRNA were discarded (Dobin et al., 2013). Crosslink sites were called from bam files using the "xlsites" function of iCount. CLIP-seq analysis was carried out on the iMaps platform (https://imaps.genialis.com/iclip), where peak calling was performed by analysing cDNA counts at crosslink sites using Paraclu (Frith et al., 2008). Motif analysis was carried out using HOMER software. Enrichment was calculated within the genomic coordinates of a total of 57,714 TIS11B CLIP peaks found in 3′UTRs. Total peaks: 190,920; peaks in 3′UTRs: 57,714.

POSTAR3 CLIP data. CLIP data on 168 RBPs were downloaded from Postar3 (Zhao et al., 2021) and peak counts that overlapped with annotated 3′UTRs from Ref-seq in all mRNAs that encode non-membrane proteins were recorded. For each RBP, the median number of 3′UTRs CLIP peaks was calculated and all 3′UTRs with peaks counts greater than the median were considered as targets. Based on the fraction of mRNAs that are considered compartment-specific (TG: 17.8%; ER 13.1%; CY: 21.1%; unbiased: 48.0%), we determined the expected number of target genes for each compartment. If the observed number of targets divided by the expected number of targets in a compartment was greater than 1.5, the RBP was added to our short-list (Table S4). As TIS11B and TIA1/L1 are known to bind to AU-rich sequences, we added the processed PAR-CLIP data of the LARP4B RBP as it was reported to bind to AU-rich elements (Küspert et al., 2015).

Logistic regression. The R package `nnet` (v7.3-17) was used to fit a logistic regression model using the CLIP peak counts from the RBPs on the short list (N = 25) to predict the subcytoplasmic mRNA localization of non-membrane proteins. Covariates with missing values were imputed as zeros. All covariates were first `sqrt` transformed and then standardized. The 'not localized' category was used as the base level. The R package `broom` (v0.8.0) was used to compute t-test statistics for the model coefficients. The code is available on github (github.com/Mayrlab/tiger-seq).

Confirmation of the logistic regression. To validate the contribution of each individual RBP, we used more stringent criteria to determine their targets. Among all mRNAs that encode non-membrane proteins with at least one CLIP peak in the 3′UTR, we considered the top third of mRNAs as targets of each RBP (TIS11B: 1781 targets; TIA1/L1: 1313 targets; LARP4B: 1621 targets; METAP2: 256 targets; HuR: 1124 targets; PUM2: 427 targets; HNRNPC: 232 targets).

Intersection of membrane/secretory mRNAs with previous datasets. The mRNAs that are coexpressed in our RNA-seq dataset (N = 9155 mRNAs) and the ER membrane-localized mRNAs from the APEX-seq dataset (N = 1045) were determined (Fazal et al., 2019). The overlapping 845 mRNAs were intersected with the mRNAs that encode membrane/secretory proteins found to be enriched on the ER in our analysis (N = 1476). We detected 673 mRNAs which correspond to 80% of all APEX-seq mRNAs that are considered to be ER membrane-enriched. The universe used to test for enrichment were all mRNAs that encode non-membrane proteins (N = 2140). A similar analysis was performed for the fractionation dataset from Reid (2012) (Reid and Nicchitta, 2012). Among the 385 coexpressed mRNAs that are enriched on the ER according to Reid, we detected 308 in our ER-enriched fraction when focusing on membrane/secretory protein encoding mRNAs. This group represents 80% of all ER-enriched mRNAs detected by Reid.

Gene ontology analysis

Gene ontology (GO) analysis was performed using DAVID (Huang da et al., 2009).

Further statistical analysis

Statistical parameters are reported in the figures and figure legends, including the definitions and exact values of *N* and experimental measures (mean ± std or boxplots depicting median, 25th and 75th percentile (boxes) and 5% and 95% confidence intervals (error bars). Pair-wise transcriptomic feature comparisons were performed using a two-sided Mann-Whitney test. For transcriptomic analyses, statistical significance is indicated by asterisks *, $1 \times 10^{-3} > P > 1 \times 10^{-9}$; **, $1 \times 10^{-10} > P > 1 \times 10^{-20}$; ***, $1 \times 10^{-21} > P > 1 \times 10^{-80}$; ****, $1 \times 10^{-81} > P > 0$. Enrichment was determined using a X^2 test. The *P* value was calculated using a two-sided Fisher's exact test. When indicated, a two-sided t-test with assumption of equal variance was applied. Statistical significance for experimental data is indicated by asterisks *, $P < 0.05$, **, $P < 0.01$, ***, $P < 0.001$, ****, $P < 0.0001$.

Data and code availability

The mass spectrometry data are reported in Table S1. The RNA-seq samples obtained from the subcytoplasmic fractionation and the TIS11B iCLIP data obtained from HEK293T cells are available at GEO (Accession number: GSE215770). The code for logistic regression is available on github.

Figure Legends

Figure 1. Strategy to determine subcytoplasmic mRNA localization.

1A. Confocal live cell imaging of HeLa cells after transfection of mCherry (mC)-TIS11B (magenta) to visualize TIS granules and of GFP-SEC61B to visualize the rough ER (teal). Scale bar, 5 µm.

1B. Schematic showing purification strategy to identify mRNAs within three cytoplasmic compartments, including TGER (beige), CRER (blue), and the cytosol (grey).

1C. As in (A), but after sorting of fluorescent particles. Shown is a TGER particle (left) and a CRER particle (right). Scale bar, 5 µm.

1D. Stacked bar plot showing fraction of transcripts that localize to each of the three cytoplasmic compartments for TGER-enriched (TGER+, *N* = 1246), CRER-enriched (CRER+, *N* = 919), cytosol-enriched (CY+, *N* = 1481) mRNAs or for mRNAs without enrichment in a single compartment (unbiased, *N* = 3369). Shown is the mean ± standard deviation for each compartment.

1E. As in (D), but shown is the fraction of transcripts that localize to each of the three subcytoplasmic compartments for representative examples (partition coefficient). Shown are examples from the top 10%, the bottom 10%, and the median of TGER-enriched, CRER-enriched, and cytosol-enriched mRNAs.

1F. The number of compartment-enriched mRNAs is shown separately for mRNAs that encode membrane or secretory proteins versus non-membrane proteins.

1G. Single-molecule (sm) RNA-FISH of the indicated endogenous mRNAs (teal) in HeLa cells. TIS granules were visualized by using GFP-TIS11B (magenta). Cell and nuclear boundaries are indicated by the dotted lines. Representative images are shown. Scale bar, 5 µm.

1H. Quantification of (G). Colocalization of smRNA-FISH foci and TIS granules was determined. Shown is the log2 fold-change (FC) of the observed over expected TGER localization based on the relative area of TIS granules and the cytosol in each cell. Each cell is represented by one dot and the summarized data from three independent experiments is shown. Number of cells analyzed, *DUSP1*, $N = 21$; *BAG3*, $N = 25$; *DNAJB1*, $N = 32$; *MAP2K2*, $N = 45$; *MLST8*, $N = 38$; *SF3A2*, $N = 37$. Representative images are shown in Fig. S1J and S1K. Differential localization between TGER+ and CY+ mRNAs: Mann-Whitney test, ****, $P = 3 \times 10^{-20}$. *SF3A2* mRNA is significantly depleted from TIS granules, Mann-Whitney test, $P = 0.004$.

1I. Shown are smRNA-FISH foci of endogenous mRNAs in HeLa cells before (-) and after (+) digitonin treatment. Cell and nuclear boundaries are indicated by the dotted lines. Representative images are shown. Scale bar, 5 µm.

1J. Quantification of (I). Shown is the fraction of digitonin-resistant smRNA-FISH foci of endogenous mRNAs as mean ± std of three independent experiments. Number of cells analyzed, *MLST8*, $N = 70$; *SF3A2*, $N = 67$; *MAP2K2*, $N = 48$; *ALDH18A1*, $N = 63$; *TES,* $N = 81$; *IQGAP3*, $N = 50$. Representative images are shown in Fig. S1L and S1M. T-test for independent samples, **, $P = 0.008$.

Figure 2. Characteristics of compartment-enriched mRNAs.

2A. Steady-state mRNA abundance levels obtained from whole cell lysates. TGER+, $N = 1246$; CRER+, $N = 919$, CY+, $N = 1481$; unbiased, $N = 3369$. Mann Whitney test: *, $1 \times 10^{-3} > P > 1 \times 10^{-9}$; **, $1 \times 10^{-10} > P > 1 \times 10^{-20}$; ***, $1 \times 10^{-21} > P > 1 \times 10^{-80}$; ****, $1 \times 10^{-81} > P > 0$. RPKM, reads per kilobase of transcript per million reads mapped.

2B. As in (A), but steady-state protein levels obtained from whole cell lysates. TGER+, $N = 469$; CRER+, $N = 638$; CY+, $N = 833$; unbiased, $N = 2001$. *P* value categories as in (A), exact *P* values are listed in Table S3.

2C. As in (A), but Pro-seq levels are shown, which indicate transcription rates. TGER+, $N = 1222$; CRER+, $N = 896$; CY+, $N = 1425$; unbiased, $N = 3268$. *P* value categories as in (A), exact *P* values are listed in Table S3.

2D. As in (C), but estimated mRNA half-lives are shown. *P* value categories as in (A), exact *P* values are listed in Table S3.

2E. Gene ontology analysis for TGER-enriched mRNAs. Shown are the top six functional gene classes and their Benjamini-Hochberg adjusted *P* values for categories that are significantly and uniquely enriched in TGER+ mRNAs. The Benjamini-Hochberg adjusted *P* values for the same categories for CRER+ and CY+ mRNAs are shown for comparison reasons.

2F. As in (E), but for CRER-enriched mRNAs.

2G. As in (E), but for mRNAs enriched in the cytosol.

Figure 3. Presence of AU-RBPs promotes mRNA localization to TGER or CRER.

3A. 3′UTR-bound RBPs that are positively or negatively associated with mRNAs enriched in the three subcytoplasmic compartments. Shown are the -log10 transformed *P* values obtained from logistic regression (see Table S4).

3B. Predicted and observed subcytoplasmic mRNA localization for experimentally validated candidates. Shown are the number of RBP CLIP peaks used for localization prediction for each candidate.

3C. RNA-FISH of GFP mRNA after transfection of a GFP-fused LHPP coding region together with the LHPP 3′UTR (LHPP-UTR) or without the LHPP 3′UTR (LHPP-NU, no UTR) in HeLa cells (teal). Cotransfection of GFP-TIS11B to visualize TIS granules (magenta). Scale bar, 5 μm.

3D. Line diagrams showing the fluorescence intensities obtained at the position of the arrows from (C). The Pearson's correlation coefficients of the fluorescence intensities are shown.

3E. The number of 3′UTR CLIP peaks is shown for the following mRNA groups: mRNAs not bound by any of the seven RBPs (N = 2154), bound by AU-RBPs (N = 1695), bound by L/M-RBP (sum of LARP4B and METAP2 CLIP peaks), N = 825.

3F. Shown is the fraction of mRNA transcripts that localize to TGER for the groups from (E). Mann Whitney tests were performed. P value categories as in Fig. 2A, exact P values are listed in Table S3.

3G. As in (F), but shown is the fraction of mRNA transcripts that localize to CRER for the groups from (E).

3H. As in (F), but shown is the fraction of mRNA transcripts that localize to the cytosol for the groups from (E).

3I. RNA-FISH of GFP mRNA after transfection of a GFP-fused FOS coding region together with the FOS 3′UTR (FOS-UTR) or without the FOS 3′UTR (FOS-NU, no UTR) in HeLa cells (teal). Cotransfection of GFP-TIS11B to visualize TIS granules (magenta). Scale bar, 5 μm.

3J. Line diagrams showing the fluorescence intensities obtained at the position of the arrows from (I). The Pearson's correlation coefficients of the fluorescence intensities are shown.

3K. As in (J) but shown are the Pearson's correlation coefficients of additional mRNAs expressed from cDNAs either containing or lacking their corresponding 3′UTRs. Corresponding RNA-FISH images are shown in Fig. 3C and S4. Two line profiles were generated for each cell. Number of cells analyzed, *FOS-UTR* N = 14, *FOS-NU* N = 18, *THAP1-UTR* N = 15, *THAP1-NU* N = 18, *HSPA1B-UTR* N = 18, *HSPA1B-NU* N = 15, *DNAJB1-UTR* N = 13, *DNAJB1-NU* N = 18, *FBXL3-UTR* N = 12, *FBXL3-NU* N = 16, *LHPP-UTR* N = 16, *LHPP-NU* N = 12, *PTP4A3-UTR* N = 14, *PTP4A3-NU* N = 11. Mann-Whitney test, ****, $P < 0.0001$, NS, not significant; LHPP: UTR vs NU; P = 0.1447; PTP4A3 UTR vs NU; P = 0.1126.

3L. As in (F), but shown is the AU content in 3′UTRs. Mann Whitney test, P value categories as in Fig. 2A, exact P values are listed in Table S3.

3M. As in (L), but the number of AU-rich elements in 3′UTRs is shown.

3N. As in (M), but estimated mRNA half-lives are shown.

Figure 4. The ratio of 3′UTR-bound TIS11B over TIA1/L1 differentiates between TGER and CRER.

4A. The number of CLIP peaks for subgroups of AU-RBPs is shown. (-/-), no RBP, N = 2154; TIS11B only (+/-), N = 441; TIA1/L1 only (-/++), N = 230; TIS11B > TIA1/L1 (+++/+), N = 431; TIS11B < TIA1/L1 (++/+++), N = 431.

4B. Shown is the fraction of mRNA transcripts that localize to TGER for the groups from (A). P value categories as in Fig. 2A, exact P values are listed in Table S3.

4C. Shown is the fraction of mRNA transcripts that localize to CRER for the groups from (A). *P* value categories as in Fig. 2A, exact *P* values are listed in Table S3.

4D. Number of AU-rich elements in 3′UTRs is shown for the groups from (A). *P* value categories as in Fig. 3C, exact *P* values are listed in Table S3.

4E. As in (D), but shown are Pro-seq levels.

4F. As in (D), but shown are estimated mRNA half-lives.

4G. As in (D), but shown are steady-state mRNA abundance levels obtained from whole cell lysates.

4H. As in (D), but shown are steady-state protein levels obtained from whole cell lysates.

Figure 5. TIAL1-dependent mRNA localization to the rough ER increases protein expression.

5A. Schematic of the mRNA reporter used to validate the effect of a single 3′UTR-bound RBP on mRNA localization and to investigate the resulting protein expression. The GFP-tagged reporter mRNA contains the THAP1 coding region and MS2 hairpins as a 3′UTR, which allow binding of the cotransfected MS2 coat protein (mCherry-tagged MCP). Fusion of TIAL1 to MCP tethers it to the 3′UTR of the reporter mRNA. mC, mCherry.

5B. Confocal live cell imaging of HeLa cells expressing mC-tagged MCP (top) or mC-tagged MCP-TIAL1 (bottom). Scale bar, 5 μm.

5C. RNA-FISH of the GFP reporter mRNA (teal) from (A) in HeLa cells coexpressing the indicated MCP-fusion construct together with BFP-SEC61B to visualize the rough ER (magenta). Representative confocal images are shown. Scale bar, 5 μm.

5D. Line profiles of the fluorescence intensities obtained from the arrows shown in (C) together with the obtained Pearson's correlation coefficients.

5E. Quantification of the Pearson's correlation coefficients between the GFP reporter mRNA and the rough ER in the experiment shown in (C). Two line profiles were generated for each cell. For MCP, $N = 26$ cells were analyzed and for MCP-TIAL1 $N = 21$ were analyzed. The horizontal line denotes the median and the error bars denote the 25th and 75th percentiles. Mann-Whitney test, ****, $P < 0.0001$.

5F. GFP protein expression of the reporter mRNA in HeLa cells measured by FACS for the samples from (A). Representative histograms are shown. The histograms on the left indicate GFP-negative cell populations.

5G. Quantification of the experiment shown in (F). Shown is the mean ± std of five independent experiments. T-test for independent samples, ****, $P = 0.0003$.

Figure 6. 3′UTR-bound TIAL1 cooperates with the rough ER membrane environment to increase protein expression.

6A. Schematic of a GFP-tagged mRNA reporter that investigates the influence of subcellular mRNA localization on protein expression. Fusion of MCP to SEC61B localizes the GFP reporter mRNA (shown as in Fig. 5A) to the rough ER membrane, whereas MCP alone localizes it to the cytosol.

6B. Confocal live cell imaging of HeLa cells expressing mC-tagged MCP (left) or mC-tagged MCP-SEC61B (right). Scale bar, 5 µm.

6C. GFP protein expression of the mRNA reporter measured by FACS in HeLa cells coexpressing the mRNA reporter together with the indicated MCP-fusion constructs. Representative histograms are shown. GFP-negative populations are plotted on the left side.

6D. Quantification of the experiment from (C). Shown is the mean ± std of four independent experiments. T-test for independent samples, **, P =0.0026.

6E. As in Fig. 4D, but addition of a prenylation signal (CAAX) localizes the TIAL1-bound GFP reporter mRNA to the plasma membrane. In the absence of CAAX, the TIAL1-bound reporter mRNA localizes to the rough ER.

6F. Confocal live cell imaging of HeLa cells expressing the indicated constructs. Scale bar, 5 µm.

6G. GFP protein expression of the mRNA reporter measured by FACS in HeLa cells coexpressing the mRNA reporter together with the indicated MCP-fusion constructs. Representative histograms are shown. GFP-negative populations are plotted on the left side.

6H. Quantification of the experiment from (G). Shown is the mean ± std of four independent experiments. T-test for independent samples, ****, $P < 0.0006$, **, $P = 0.002$.

Figure 7. Relocalization of cytosolic mRNAs to the rough ER membrane increases their protein expression.

7A. Schematic of a GFP-tagged reporter mRNA bound by TIS11B that allows investigation of localization-dependent GFP protein expression. Fusion of MCP and TIS11B localizes the mRNA reporter to the cytosol, whereas the TIS11B-MCP-SEC61B fusion localizes the mRNA to the rough ER membrane.

7B. Confocal live cell imaging of HeLa cells expressing the indicated constructs (described in A). Scale bar, 5 µm.

7C. GFP protein expression of the mRNA reporter measured by FACS in HeLa cells coexpressing the mRNA reporter together with the indicated MCP-fusion constructs. Representative histograms are shown. GFP-negative populations are plotted on the left side.

7D. Quantification of the experiment from (C). Shown is the mean ± std of four independent experiments. T-test for independent samples, ****, $P < 0.0001$, **, $P = 0.03$, NS, not significant.

7E. Model. Characteristics of subcytoplasmic compartments. Shown are mRNA features of compartment-enriched mRNAs. mRNA relocalization from the cytosol to the ER increased protein expression by two-fold independently of the bound RBPs. nt, nucleotide.

Supplementary Figures

Figure S1. Strategy to determine subcytoplasmic mRNA localization.

S1A. Cell fractionation strategy to obtain the cytoplasmic membrane fraction. Transfected HEK293T cells were lysed in hypotonic buffer, followed by douncing and differential centrifugation at 600 g to pellet nuclei and the supernatant was subsequently spun at 7000 g.

The pellet contains the cytoplasmic membrane fraction that was used for subsequent fluorescent particle sorting.

S1B. FACS plot showing mCherry-TIS11B-positive TGER particles costained with DAPI to segregate TGER particles from nuclear contamination. Gate (1) contains TGER particles, whereas gate (2) contains TGER particles bound to nuclei, indicated by DAPI stain and larger size.

S1C. As in (B) but shown are GFP-SEC61B-positive CRER particles costained with DAPI. Gate (1) contains CRER particles, whereas gate (2) contains CRER particles bound to nuclei, indicated by DAPI stain and larger size.

S1D. Immunoblot showing markers used to evaluate the quality of the digitonin-based cytosol extraction. H2A antibody was used as marker for nuclear components, Calnexin was used as ER marker and GAPDH was used as cytosolic protein. Unassembled TIS11B was observed in the cytosol after transfection with mCherry-tagged TIS11B. Marker expression in whole cell lysates serves as control. mC, mCherry.

S1E. Pearson correlation coefficients for mRNA expression levels for biological replicates on subcytoplasmic compartments.

S1F. Baseline distribution of partition coefficients across the three investigated cytoplasmic compartments is shown separately for mRNAs that encode membrane/secretory proteins and mRNAs that encode non-membrane proteins.

S1G. Distribution of partition coefficients in each fractionation sample for compartment-enriched mRNAs that encode membrane/secretory proteins.

S1H. Overlap of CRER-enriched mRNAs that encode membrane/secretory proteins (N = 1476) with previous datasets that used alternative isolation methods. APEX-seq, X^2 =127, $P < 0.0001$ Fractionation dataset, X^2 = 803, $P < 0.0001$.

S1I. Distribution of partition coefficients in each fractionation sample for compartment-enriched mRNAs that encode non-membrane proteins.

S1J. smRNA-FISH of endogenous mRNAs (teal), predicted to localize to the TGER in HeLa cells. The TGER domain is visualized by GFP-TIS11B (magenta). Cell and nuclear boundaries are indicated by the dotted lines. Representative images are shown. Scale bar, 5 µm. Shown are representative images for *DUSP1* and *DNAJB1.*

S1K. As in (J), but for endogenous mRNAs predicted to localize to the cytosol in HeLa cells. Shown are representative images for *MAP2K2 and SF3A2.*

S1L. smRNA-FISH of endogenous mRNAs predicted to localize to the CRER. Shown are HeLa cells before (-) and after (+) digitonin treatment. Cell and nuclear boundaries are indicated by the dotted lines, number of foci counted in each image indicated in white. Representative images for *TES* and *IQGAP3* are shown. Scale bar, 5 µm.

S1M. As in (L), but for endogenous mRNAs predicted to localize to the cytosol in HeLa cells. Shown are representative images for *SF3A2 and MAP2K2.*

Figure S2. The TGER domain is an active translation compartment.

S2A. As in Fig. 2C, but steady-state mRNA abundance levels of compartment-enriched mRNAs obtained by RNA-seq from whole cell lysates of HEK293 cells. This sample was used together with the Pro-seq sample to estimate mRNA half-lives. Mann Whitney test: *, $1 \times 10^{-3} > P > 1 \times 10^{-}$

^{9}; **, 1 x 10^{-10} >*P*> 1 x 10^{-20}; ***, 1 x 10^{-21} >*P*> 1 x 10^{-80}; ****, 1 x 10^{-81} >*P*> 0. RPKM, reads per kilobase of transcript per million reads mapped.

S2B. As in Fig. 2A, but 3′UTR length of mRNAs enriched in the indicated compartments is shown. *P* value categories as in (A), exact *P* values are listed in Table S3.

S2C. As in (B), but the fraction of adenosines or uridines in 3′UTRs of mRNAs enriched in the indicated compartments is shown. *P* value categories as in (A), exact *P* values are listed in Table S3.

S2D. As in (B), but the number of AU-rich elements (AUUUA) in 3′UTRs of mRNAs enriched in the indicated compartments is shown. *P* value categories as in (A), exact *P* values are listed in Table S3.

S2E. As in (B), but size of mRNA-encoded proteins enriched in the indicated compartments is shown. *P* value categories as in (A), exact *P* values are listed in Table S3.

S2F. Schematic of the reporter mRNA used with the SunTag system to measure nascent protein synthesis. CDS, coding sequence. The KIF18B construct was used previously (Yan et al., 2016).

S2G. Confocal imaging of HeLa cells stably expressing SunTag reporter proteins svFc-GFP and mCherry-tagged PP7 protein (mC-PP7) co-transfected with two constructs (i) BFP-TIS11B to visualize the TGER domain and (ii) SunTag-labeled mRNA encoding KIF18B and PP7-binding sites. The *KIF18B* mRNA is visualized by mC-PP7 binding (teal) whereas the KIF18B protein is visualized by svFc-GFP binding (magenta). Foci with co-localization of mRNA and protein represent nascent protein synthesis and are indicative of active translation. A representative example is shown. White box indicates area depicted at 6X magnification in the lower panel. Scale bar, 5 μm (top panel), 1 μm (bottom panel).

S2H. Quantification of the experiment from (G). Shown are the number of mRNA foci in TGER or the cytosol (CY) using the Suntag reporter from (F). *N* = 24 cells were analyzed.

S2I. As in (H), but shown are the mRNAs that are actively translated in each compartment, which were identified by counting the teal and magenta-double positive foci.

Figure S3. CLIP analysis of RBPs.

S3A. Gel showing samples used for iCLIP of GFP-tagged TIS11B. The region outlined in red was used for iCLIP sample preparation.

S3B. TIS11B iCLIP tag distribution obtained from HEK293T cells.

S3C. The top five motifs that were enriched within TIS11B peaks in 3′UTRs compared to all nucleotides in 3′UTRs. Shown are *P* values obtained by HOMER.

S3D. Fraction of mRNA transcripts that localize to TGER, CRER, or the cytosol for the indicated groups of mRNAs. mRNAs that are not bound by any of the seven RBPs (no RBP, *N* = 2154) are compared to mRNAs that are targets for at least one of the seven RBPs (RBP, *N* = 4861). Mann Whitney test was performed. *P* value categories as in (A), exact *P* values are listed in Table S3.

S3E. The number of 3′UTR CLIP peaks is shown for the mRNA groups from (D).

S3F. Fraction of mRNA transcripts that localize to TGER, CRER, or the cytosol for the indicated groups of mRNAs. mRNAs that are not bound by any of the seven RBPs (*N* = 2154) are compared to mRNAs that are only bound by LARP4B (*N* = 740), or METAP2 (*N* = 90), or both

(*N* = 85). Mann Whitney test was performed. *P* value categories as in (A), exact *P* values are listed in Table S3.

S3G. The number of CLIP peaks is shown for the mRNA groups from (F).

S3H. As in Fig. 3L, but 3′UTR length is shown. Mann Whitney test, *P* value categories as in Fig. 2A, exact *P* values are listed in Table S3.

S3I. As in (H), but Pro-seq values are shown.

Figure S4. mRNA localization to TGER is controlled by 3′UTRs.

S4. RNA-FISH of mRNAs after transfection of cDNA GFP-fusion constructs containing the indicated coding regions, either including (UTR) or excluding the respective 3'UTRs (NU, no UTR) in HeLa cells (teal). BFP-TIS11B was cotransfected to visualize the TGER domain (magenta). Scale bar, 5 µm. Line diagrams depicting the fluorescence intensities obtained at the position of the arrows are shown with the Pearson's correlation coefficients of the fluorescence intensities. Shown are representative images for cytosol- or TGER-enriched mRNAs.

S4A. *PTP4A* does not contain 3'UTR peaks for any of the seven RBPs and is predicted to localize to the cytosol.

S4B. *THAP1, FBXL3, DNAJB1,* and *HSPA1B* are predicted to localize to TGER in the presence of their 3'UTRs.

Figure S5. CLIP peaks that differentiate between TGER and CRER.

S5A. Fraction of mRNA transcripts that localize to TGER for different groups of mRNAs: no RBP, *N* = 2154; TIS11B only, *N* = 441; HuR only, *N* = 124; PUM2 only, *N* = 38; HNRNPC only, *N* = 2 (not shown); any combination of the four RBPs, *N* = 372. Mann Whitney test, *P* value categories as in Fig. 2A, exact *P* values are listed in Table S3.

S5B. The number of CLIP peaks for the groups from (A) are shown.

S5C. As in Fig. 4D, but 3′UTR length is shown. Mann Whitney test, *P* value categories as in Fig. 2A, exact *P* values are listed in Table S3.

S5D. As in (C), but AU content in the 3′UTR is shown.

Figure S6. mRNA localization-dependent protein expression of the GFP reporter.

S6A. Gating strategy to assess GFP protein expression of the reporter mRNA by FACS. Left panel shows the ungated population of HeLa cells coexpressing MCP-mCherry and the GFP-THAP1-MS2 reporter, separated by size (forward scatter) and granularity (side scatter). The black circle indicates the live cells that were used for subsequent analysis. Middle panel, the GFP- and mCherry-double positive population was gated to obtain the GFP mean fluorescence values (MFI, right panel) which corresponds to the reported GFP protein expression values.

S6B. As in (A), but HeLa cells coexpressing MCP-mCherry-TIAL1 and the GFP-THAP1-MS2 reporter.

S6C. As in Fig. 5A and 5G, but the MS2 sites in the GFP reporter were omitted. Coexpression of MCP-mCherry-TIAL1 does not result in the binding of MCP to the reporter mRNA without MS2 sites. This experiment serves as control for the effect of TIA1L1 overexpression on reporter mRNA expression.

S6D. Schematic of a second mRNA reporter used to validate the effect of a single 3′UTR-bound RBP on protein expression. The GFP-tagged reporter mRNA contains the BIRC3 coding region and MS2 hairpins as 3′UTR, which allow binding of the co-transfected MS2 coat protein (mCherry-tagged MCP). Fusion of TIAL1 to MCP tethers TIAL1 to the 3′UTR of the reporter mRNA. mC, mCherry.

S6E. GFP protein expression of the reporter mRNA from (D) in HeLa cells, coexpressing the indicated MCP-fusion constructs, measured by FACS. Representative histograms are shown. The histograms on the left indicate GFP-negative cell populations.

S6F. Quantification of the experiment shown in (E). Shown is the mean ± std of five independent experiments. T-test for independent samples, **, $P = 0.005$.

S6G. RNA-FISH of the GFP reporter mRNA (teal) from Fig. 6A in HeLa cells coexpressing MCP-mCherry-SEC61B (magenta) to visualize colocalization between the mRNA and the rough ER membrane. Representative confocal images are shown. Scale bar, 5 µm.

S6H. Line profiles of the fluorescence intensities of the arrows from (G).

S6I. Quantification of the experiment from (G). Two line profiles were generated for each cell. The Pearson's correlation coefficients between the reporter mRNA and the ER were determined. For MCP, $N = 26$ cells were analyzed, for MCP-SEC61B, $N = 26$ cells were analyzed. The horizontal line denotes the median and the error bars denote the 25th and 75th percentiles. Mann-Whitney test, ****, $P < 0.0001$.

S6J. Schematic of a second GFP-tagged mRNA reporter that investigates the influence of subcellular mRNA localization on protein expression. Fusion of MCP to TRAPα localizes the GFP reporter mRNA to the ER membrane, whereas MCP alone localizes it to the cytosol.

S6K. Confocal live cell imaging of HeLa cells expressing mC-tagged TRAPα-MCP. Scale bar, 5 µm.

S6L. GFP protein expression of the reporter mRNAs from (J) coexpressing the indicated MCP-fusion constructs in HeLa cells measured by FACS. Representative histograms are shown. The histograms on the left indicate GFP-negative cell populations.

S6M. Quantification of the experiment from (L). Shown is the mean ± std of four independent experiments. T-test for independent samples, ****, $P < 0.0001$.

Figure S7. Redirecting mRNA localization from the cytosol to the rough ER overcomes the repressive effect of a bound RBP.

S7A. Confocal live cell imaging of HeLa cells expressing the indicated constructs. Shown are representative images with TIS granules or unassembled TIS11B. mC, mCherry. Scale bar, 5 µm.

S7B. Quantification from (A). The fraction of HeLa cells with TIS granules is shown after transfection of the indicated TIS11B fusion constructs. $N = 165$ cells were analyzed for mCherry-TIS11B and $N = 198$ cells were analyzed for MCP-mCherry-TIS11B. MCP-mCherry-TIS11B largely prevents TIS granule formation.

S7C. Schematic of a second TIS11B-bound mRNA reporter that allows investigation of mRNA localization-dependent GFP expression. The coding region of the reporter is provided by BIRC3, followed by MS2 binding sites. Tethering of MCP or TIS11B localizes the mRNA reporter to the cytosol, whereas the MCP-TIS11B-SEC61B fusion localizes the mRNA reporter to the rough ER.

S7D. GFP protein expression of the reporter mRNA from (C) in HeLa cells, coexpressing the indicated MCP-fusion constructs, measured by FACS. Representative histograms are shown. The histograms on the left indicate GFP-negative cell populations.

S7E. Quantification of the experiment from (D). Shown is the mean ± std of four independent experiments. T-test for independent samples, ****, $P < 0.0001$, MCP vs TIS11B-SEC61B: $P = 0.058$; NS).

References

Banani, S.F., Lee, H.O., Hyman, A.A., and Rosen, M.K. (2017). Biomolecular condensates: organizers of cellular biochemistry. Nature reviews Molecular cell biology *18*, 285-298.

Berkovits, B.D., and Mayr, C. (2015). Alternative 3' UTRs act as scaffolds to regulate membrane protein localization. Nature *522*, 363-367.

Bertolotti, A. (2018). The split protein phosphatase system. The Biochemical journal *475*, 3707-3723.

Bertrand, E., Chartrand, P., Schaefer, M., Shenoy, S.M., Singer, R.H., and Long, R.M. (1998). Localization of ASH1 mRNA particles in living yeast. Mol Cell *2*, 437-445.

Biever, A., Donlin-Asp, P.G., and Schuman, E.M. (2019). Local translation in neuronal processes. Current opinion in neurobiology *57*, 141-148.

Blumberg, A., Zhao, Y., Huang, Y.-F., Dukler, N., Rice, E.J., Chivu, A.G., Krumholz, K., Danko, C.G., and Siepel, A. (2021). Characterizing RNA stability genome-wide through combined analysis of PRO-seq and RNA-seq data. BMC biology *19*, 30.

Bolger, A.M., Lohse, M., and Usadel, B. (2014). Trimmomatic: a flexible trimmer for Illumina sequence data. Bioinformatics *30*, 2114-2120.

Boraas, L., Hu, M., Thornton, L., Vejnar, C.E., Zhen, G., Giraldez, A.J., Mayr, C., Wang, S., and Nicoli, S. (2021). Non-coding function for mRNAs in Focal Adhesion Architecture and Mechanotransduction. bioRxiv, 2021.2010.2004.463097.

Buxbaum, A.R., Haimovich, G., and Singer, R.H. (2015). In the right place at the right time: visualizing and understanding mRNA localization. Nature reviews Molecular cell biology *16*, 95-109.

Chao, J.A., Patskovsky, Y., Patel, V., Levy, M., Almo, S.C., and Singer, R.H. (2010). ZBP1 recognition of beta-actin zipcode induces RNA looping. Genes Dev *24*, 148-158.

Chen, Q., Jagannathan, S., Reid, D.W., Zheng, T., and Nicchitta, C.V. (2011). Hierarchical regulation of mRNA partitioning between the cytoplasm and the endoplasmic reticulum of mammalian cells. Molecular biology of the cell *22*, 2646-2658.

Courel, M., Clément, Y., Bossevain, C., Foretek, D., Vidal Cruchez, O., Yi, Z., Bénard, M., Benassy, M.N., Kress, M., Vindry, C*., et al.* (2019). GC content shapes mRNA storage and decay in human cells. eLife *8*.

Cui, X.A., Zhang, H., and Palazzo, A.F. (2012). p180 promotes the ribosome-independent localization of a subset of mRNA to the endoplasmic reticulum. PLoS Biol *10*, e1001336.

Diehn, M., Bhattacharya, R., Botstein, D., and Brown, P.O. (2006). Genome-scale identification of membrane-associated human mRNAs. PLoS Genet *2*, e11.

Dobin, A., Davis, C.A., Schlesinger, F., Drenkow, J., Zaleski, C., Jha, S., Batut, P., Chaisson, M., and Gingeras, T.R. (2013). STAR: ultrafast universal RNA-seq aligner. Bioinformatics *29*, 15-21.

Fazal, F.M., Han, S., Parker, K.R., Kaewsapsak, P., Xu, J., Boettiger, A.N., Chang, H.Y., and Ting, A.Y. (2019). Atlas of Subcellular RNA Localization Revealed by APEX-Seq. Cell *178*, 473-490.e426.

Frith, M.C., Valen, E., Krogh, A., Hayashizaki, Y., Carninci, P., and Sandelin, A. (2008). A code for transcription initiation in mammalian genomes. Genome Res *18*, 1-12.

Galloway, A., Saveliev, A., Lukasiak, S., Hodson, D.J., Bolland, D., Balmanno, K., Ahlfors, H., Monzon-Casanova, E., Mannurita, S.C., Bell, L.S.*, et al.* (2016). RNA-binding proteins ZFP36L1 and ZFP36L2 promote cell quiescence. Science *352*, 453-459.

Gebauer, F., Schwarzl, T., Valcárcel, J., and Hentze, M.W. (2021). RNA-binding proteins in human genetic disease. Nature reviews Genetics *22*, 185-198.

Gilks, N., Kedersha, N., Ayodele, M., Shen, L., Stoecklin, G., Dember, L.M., and Anderson, P. (2004). Stress granule assembly is mediated by prion-like aggregation of TIA-1. Molecular biology of the cell *15*, 5383-5398.

Glock, C., Biever, A., Tushev, G., Nassim-Assir, B., Kao, A., Bartnik, I., Tom Dieck, S., and Schuman, E.M. (2021). The translatome of neuronal cell bodies, dendrites, and axons. Proc Natl Acad Sci U S A *118*.

Hafner, M., Landthaler, M., Burger, L., Khorshid, M., Hausser, J., Berninger, P., Rothballer, A., Ascano, M., Jungkamp, A.C., Munschauer, M.*, et al.* (2010). PAR-CliP--a method to identify transcriptome-wide the binding sites of RNA binding proteins. Journal of visualized experiments : JoVE.

Han, X., Zhou, Z., Fei, L., Sun, H., Wang, R., Chen, Y., Chen, H., Wang, J., Tang, H., Ge, W.*, et al.* (2020). Construction of a human cell landscape at single-cell level. Nature *581*, 303-309.

Hu, M., Yang, B., Cheng, Y., Radda, J.S.D., Chen, Y., Liu, M., and Wang, S. (2020). ProbeDealer is a convenient tool for designing probes for highly multiplexed fluorescence in situ hybridization. Sci Rep *10*, 22031.

Huang da, W., Sherman, B.T., and Lempicki, R.A. (2009). Systematic and integrative analysis of large gene lists using DAVID bioinformatics resources. Nature protocols *4*, 44-57.

Hubstenberger, A., Courel, M., Benard, M., Souquere, S., Ernoult-Lange, M., Chouaib, R., Yi, Z., Morlot, J.B., Munier, A., Fradet, M.*, et al.* (2017). P-Body Purification Reveals the Condensation of Repressed mRNA Regulons. Mol Cell *68*, 144-157 e145.

Huttelmaier, S., Zenklusen, D., Lederer, M., Dictenberg, J., Lorenz, M., Meng, X., Bassell, G.J., Condeelis, J., and Singer, R.H. (2005). Spatial regulation of beta-actin translation by Src-dependent phosphorylation of ZBP1. Nature *438*, 512-515.

Jan, C.H., Williams, C.C., and Weissman, J.S. (2014). Principles of ER cotranslational translocation revealed by proximity-specific ribosome profiling. Science *346*, 1257521.

Kedersha, N.L., Gupta, M., Li, W., Miller, I., and Anderson, P. (1999). RNA-binding proteins TIA-1 and TIAR link the phosphorylation of eIF-2 alpha to the assembly of mammalian stress granules. The Journal of cell biology *147*, 1431-1442.

Keene, J.D. (2007). RNA regulons: coordination of post-transcriptional events. Nature reviews Genetics *8*, 533-543.

Khong, A., Matheny, T., Jain, S., Mitchell, S.F., Wheeler, J.R., and Parker, R. (2017). The Stress Granule Transcriptome Reveals Principles of mRNA Accumulation in Stress Granules. Mol Cell *68*, 808-820 e805.

Kim, D., Paggi, J.M., Park, C., Bennett, C., and Salzberg, S.L. (2019). Graph-based genome alignment and genotyping with HISAT2 and HISAT-genotype. Nat Biotechnol *37*, 907-915.

Küspert, M., Murakawa, Y., Schäffler, K., Vanselow, J.T., Wolf, E., Juranek, S., Schlosser, A., Landthaler, M., and Fischer, U. (2015). LARP4B is an AU-rich sequence associated factor that promotes mRNA accumulation and translation. Rna *21*, 1294-1305.

Lawrence, J.B., and Singer, R.H. (1986). Intracellular localization of messenger RNAs for cytoskeletal proteins. Cell *45*, 407-415.

Lebedeva, S., Jens, M., Theil, K., Schwanhausser, B., Selbach, M., Landthaler, M., and Rajewsky, N. (2011). Transcriptome-wide analysis of regulatory interactions of the RNA-binding protein HuR. Mol Cell *43*, 340-352.

Lecuyer, E., Yoshida, H., Parthasarathy, N., Alm, C., Babak, T., Cerovina, T., Hughes, T.R., Tomancak, P., and Krause, H.M. (2007). Global analysis of mRNA localization reveals a prominent role in organizing cellular architecture and function. Cell *131*, 174-187.

Lee, S.H., and Mayr, C. (2019). Gain of Additional BIRC3 Protein Functions through 3'-UTR-Mediated Protein Complex Formation. Mol Cell *74*, 701-712 e709.

Lerner, R.S., Seiser, R.M., Zheng, T., Lager, P.J., Reedy, M.C., Keene, J.D., and Nicchitta, C.V. (2003). Partitioning and translation of mRNAs encoding soluble proteins on membrane-bound ribosomes. Rna *9*, 1123-1137.

Liao, Y., Smyth, G.K., and Shi, W. (2014). featureCounts: an efficient general purpose program for assigning sequence reads to genomic features. Bioinformatics *30*, 923-930.

Litterman, A.J., Kageyama, R., Le Tonqueze, O., Zhao, W., Gagnon, J.D., Goodarzi, H., Erle, D.J., and Ansel, K.M. (2019). A massively parallel 3' UTR reporter assay reveals relationships between nucleotide content, sequence conservation, and mRNA destabilization. Genome Res *29*, 896-906.

Liu, X., and Fagotto, F. (2011). A method to separate nuclear, cytosolic, and membrane-associated signaling molecules in cultured cells. Science signaling *4*, pl2.

Lykke-Andersen, J., and Wagner, E. (2005). Recruitment and activation of mRNA decay enzymes by two ARE-mediated decay activation domains in the proteins TTP and BRF-1. Genes Dev *19*, 351-361.

Ma, W., and Mayr, C. (2018). A Membraneless Organelle Associated with the Endoplasmic Reticulum Enables 3'UTR-Mediated Protein-Protein Interactions. Cell *175*, 1492-1506 e1419.

Ma, W., Zheng, G., Xie, W., and Mayr, C. (2021). In vivo reconstitution finds multivalent RNA-RNA interactions as drivers of mesh-like condensates. eLife *10*.

Martin, M. (2011). Cutadapt removes adapter sequences from high-throughput sequencing reads. 2011 *17*, 3.

Mazan-Mamczarz, K., Lal, A., Martindale, J.L., Kawai, T., and Gorospe, M. (2006). Translational repression by RNA-binding protein TIAR. Mol Cell Biol *26*, 2716-2727.

Meyer, C., Garzia, A., Mazzola, M., Gerstberger, S., Molina, H., and Tuschl, T. (2018). The TIA1 RNA-Binding Protein Family Regulates EIF2AK2-Mediated Stress Response and Cell Cycle Progression. Mol Cell *69*, 622-635 e626.

Mili, S., Moissoglu, K., and Macara, I.G. (2008). Genome-wide screen reveals APC-associated RNAs enriched in cell protrusions. Nature *453*, 115-119.

Miller, S., Yasuda, M., Coats, J.K., Jones, Y., Martone, M.E., and Mayford, M. (2002). Disruption of dendritic translation of CaMKIIalpha impairs stabilization of synaptic plasticity and memory consolidation. Neuron *36*, 507-519.

Moor, A.E., Golan, M., Massasa, E.E., Lemze, D., Weizman, T., Shenhav, R., Baydatch, S., Mizrahi, O., Winkler, R., Golani, O.*, et al.* (2017). Global mRNA polarization regulates translation efficiency in the intestinal epithelium. Science *357*, 1299-1303.

Moretti, F., Rolando, C., Winker, M., Ivanek, R., Rodriguez, J., Von Kriegsheim, A., Taylor, V., Bustin, M., and Pertz, O. (2015). Growth Cone Localization of the mRNA Encoding the Chromatin Regulator HMGN5 Modulates Neurite Outgrowth. Mol Cell Biol *35*, 2035-2050.

Mukherjee, N., Corcoran, D.L., Nusbaum, J.D., Reid, D.W., Georgiev, S., Hafner, M., Ascano, M., Jr., Tuschl, T., Ohler, U., and Keene, J.D. (2011). Integrative regulatory mapping

indicates that the RNA-binding protein HuR couples pre-mRNA processing and mRNA stability. Mol Cell *43*, 327-339.

Navarrete-Perea, J., Yu, Q., Gygi, S.P., and Paulo, J.A. (2018). Streamlined Tandem Mass Tag (SL-TMT) Protocol: An Efficient Strategy for Quantitative (Phospho)proteome Profiling Using Tandem Mass Tag-Synchronous Precursor Selection-MS3. Journal of proteome research *17*, 2226-2236.

Patel, R.K., West, J.D., Jiang, Y., Fogarty, E.A., and Grimson, A. (2020). Robust partitioning of microRNA targets from downstream regulatory changes. Nucleic Acids Res *48*, 9724-9746.

Peeples, W., and Rosen, M.K. (2021). Mechanistic dissection of increased enzymatic rate in a phase-separated compartment. Nature chemical biology *17*, 693-702.

Qin, W., Myers, S.A., Carey, D.K., Carr, S.A., and Ting, A.Y. (2021). Spatiotemporally-resolved mapping of RNA binding proteins via functional proximity labeling reveals a mitochondrial mRNA anchor promoting stress recovery. Nature communications *12*, 4980.

Rappsilber, J., Mann, M., and Ishihama, Y. (2007). Protocol for micro-purification, enrichment, pre-fractionation and storage of peptides for proteomics using StageTips. Nature protocols *2*, 1896-1906.

Reid, D.W., and Nicchitta, C.V. (2012). Primary role for endoplasmic reticulum-bound ribosomes in cellular translation identified by ribosome profiling. J Biol Chem *287*, 5518-5527.

Shin, Y., and Brangwynne, C.P. (2017). Liquid phase condensation in cell physiology and disease. Science *357*.

Smalec, B.M., Ietswaart, R., Choquet, K., McShane, E., West, E.R., and Churchman, L.S. (2022). Genome-wide quantification of RNA flow across subcellular compartments reveals determinants of the mammalian transcript life cycle. bioRxiv, 2022.2008.2021.504696.

Staudacher, J.J., Naarmann-de Vries, I.S., Ujvari, S.J., Klinger, B., Kasim, M., Benko, E., Ostareck-Lederer, A., Ostareck, D.H., Bondke Persson, A., Lorenzen, S.*, et al.* (2015). Hypoxia-induced gene expression results from selective mRNA partitioning to the endoplasmic reticulum. Nucleic Acids Res *43*, 3219-3236.

Stoecklin, G., Colombi, M., Raineri, I., Leuenberger, S., Mallaun, M., Schmidlin, M., Gross, B., Lu, M., Kitamura, T., and Moroni, C. (2002). Functional cloning of BRF1, a regulator of ARE-dependent mRNA turnover. EMBO J *21*, 4709-4718.

Tushev, G., Glock, C., Heumuller, M., Biever, A., Jovanovic, M., and Schuman, E.M. (2018). Alternative 3' UTRs Modify the Localization, Regulatory Potential, Stability, and Plasticity of mRNAs in Neuronal Compartments. Neuron *98*, 495-511 e496.

Vaquerizas, J.M., Kummerfeld, S.K., Teichmann, S.A., and Luscombe, N.M. (2009). A census of human transcription factors: function, expression and evolution. Nature reviews Genetics *10*, 252-263.

Voigt, F., Zhang, H., Cui, X.A., Triebold, D., Liu, A.X., Eglinger, J., Lee, E.S., Chao, J.A., and Palazzo, A.F. (2017). Single-Molecule Quantification of Translation-Dependent Association of mRNAs with the Endoplasmic Reticulum. Cell reports *21*, 3740-3753.

Wang, Z., Kayikci, M., Briese, M., Zarnack, K., Luscombe, N.M., Rot, G., Zupan, B., Curk, T., and Ule, J. (2010). iCLIP predicts the dual splicing effects of TIA-RNA interactions. PLoS Biol *8*, e1000530.

Xia, C., Fan, J., Emanuel, G., Hao, J., and Zhuang, X. (2019). Spatial transcriptome profiling by MERFISH reveals subcellular RNA compartmentalization and cell cycle-dependent gene expression. Proc Natl Acad Sci U S A *116*, 19490-19499.

Yan, X., Hoek, T.A., Vale, R.D., and Tanenbaum, M.E. (2016). Dynamics of Translation of Single mRNA Molecules In Vivo. Cell *165*, 976-989.

Yugami, M., Okano, H., Nakanishi, A., and Yano, M. (2020). Analysis of the nucleocytoplasmic shuttling RNA-binding protein HNRNPU using optimized HITS-CLIP method. PLoS One *15*, e0231450.

Zarnegar, B.J., Flynn, R.A., Shen, Y., Do, B.T., Chang, H.Y., and Khavari, P.A. (2016). irCLIP platform for efficient characterization of protein-RNA interactions. Nat Methods *13*, 489-492.

Zhao, W., Zhang, S., Zhu, Y., Xi, X., Bao, P., Ma, Z., Kapral, Thomas H., Chen, S., Zagrovic, B., Yang, Yucheng T.*, et al.* (2021). POSTAR3: an updated platform for exploring post-transcriptional regulation coordinated by RNA-binding proteins. Nucleic Acids Research *50*, D287-D294.

Horste et al., Figure 1

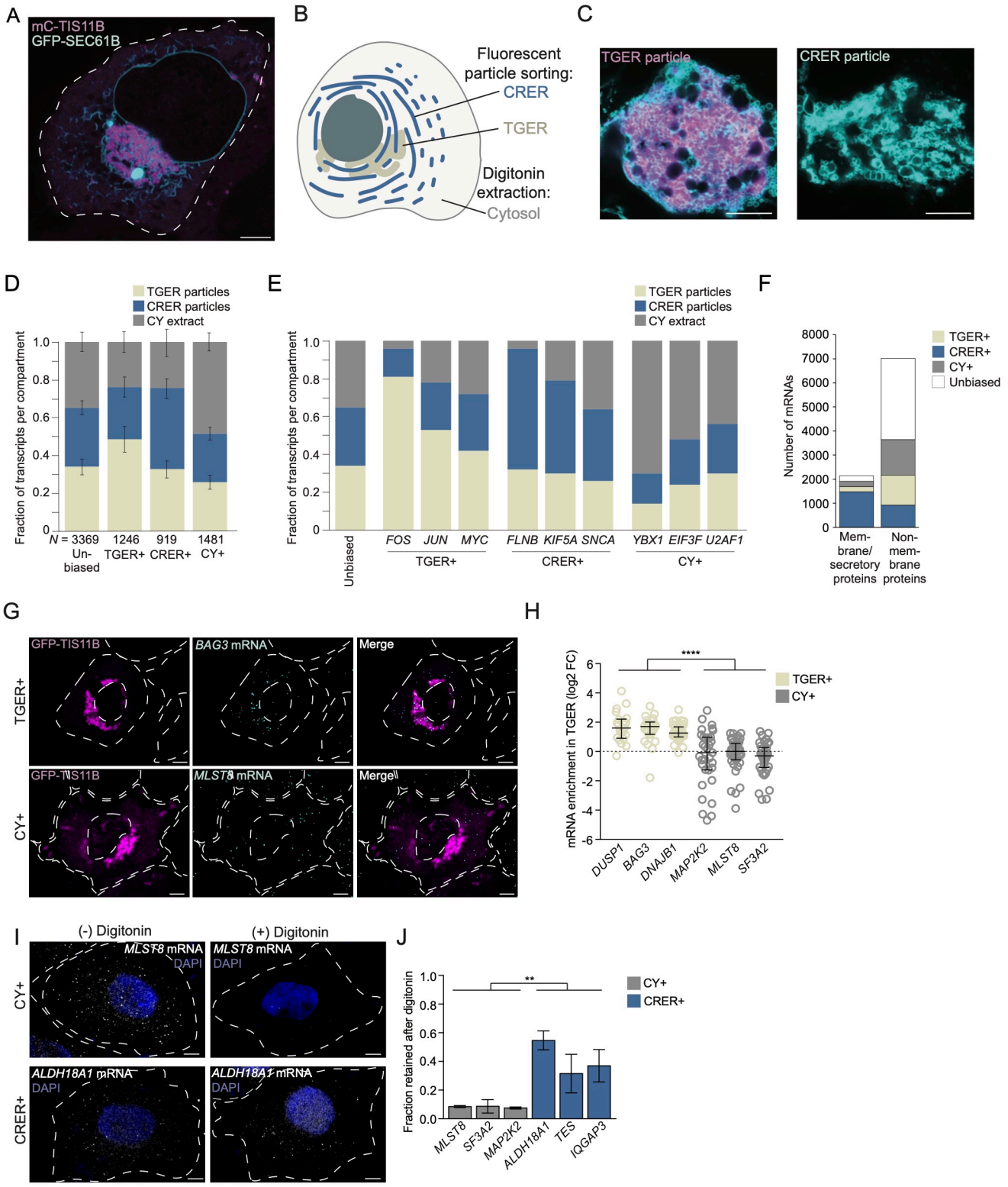

Figure 1. Strategy to determine subcytoplasmic mRNA localization.
(A) Confocal live cell imaging of HeLa cells after transfection of mCherry (mC)-TIS11B (magenta) to visualize TIS granules and of GFP-SEC61B to visualize the rough ER (teal). Scale bar, 5 µm.
(B) Schematic showing purification strategy to identify mRNAs within three cytoplasmic compartments, including TGER (beige), CRER (blue), and the cytosol (grey).
(C) As in (A), but after sorting of fluorescent particles. Shown is a TGER particle (left) and a CRER particle (right). Scale bar, 5 µm.
(D) Stacked bar plot showing fraction of transcripts that localize to each of the three cytoplasmic compartments for TGER-enriched (TGER+, *N* = 1246), CRER-enriched (CRER+, *N* = 919), cytosol-enriched (CY+, *N* = 1481) mRNAs or for mRNAs without enrichment in a single compartment (unbiased, *N* = 3369). Shown is the mean ± standard deviation for each compartment.
(E) As in (D), but shown is the fraction of transcripts that localize to each of the three subcytoplasmic compartments for representative examples (partition coefficient). Shown are examples from the top 10%, the bottom 10%, and the median of TGER-enriched, CRER-enriched, and cytosol-enriched mRNAs.
(F) The number of compartment-enriched mRNAs is shown separately for mRNAs that encode membrane or secretory proteins versus non-membrane proteins.
(G) Single-molecule (sm) RNA-FISH of the indicated endogenous mRNAs (teal) in HeLa cells. TIS granules were visualized by using GFP-TIS11B (magenta). Cell and nuclear boundaries are indicated by the dotted lines. Representative images are shown. Scale bar, 5 µm.
(H) Quantification of (G). Colocalization of smRNA-FISH foci and TIS granules was determined. Shown is the log2 fold-change (FC) of the observed over expected TGER localization based on the relative area of TIS granules and the cytosol in each cell. Each cell is represented by one dot and the summarized data from three independent experiments is shown. Number of cells analyzed, *DUSP1, N* = 21; *BAG3, N* = 25; *DNAJB1, N* = 32; *MAP2K2, N* = 45; *MLST8, N* = 38; *SF3A2, N* = 37. Representative images are shown in Fig. S1J and S1K. Differential localization between TGER+ and CY+ mRNAs: Mann-Whitney test, ****, *P* = 3 x 10-20. SF3A2 mRNA is significantly depleted from TIS granules, Mann-Whitney test, *P* = 0.004.
(I) Shown are smRNA-FISH foci of endogenous mRNAs in HeLa cells before (-) and after (+) digitonin treatment. Cell and nuclear boundaries are indicated by the dotted lines. Representative images are shown. Scale bar, 5 µm.
(J) Quantification of (I). Shown is the fraction of digitonin-resistant smRNA-FISH foci of endogenous mRNAs as mean ± std of three independent experiments. Number of cells analyzed, *MLST8, N* = 70; *SF3A2, N* = 67; *MAP2K2, N* = 48; *ALDH18A1, N* = 63; *TES, N* = 81; *IQGAP3, N* = 50. Representative images are shown in Fig. S1L and S1M. T-test for independent samples, **, P = 0.008.

Horste et al., Figure 2

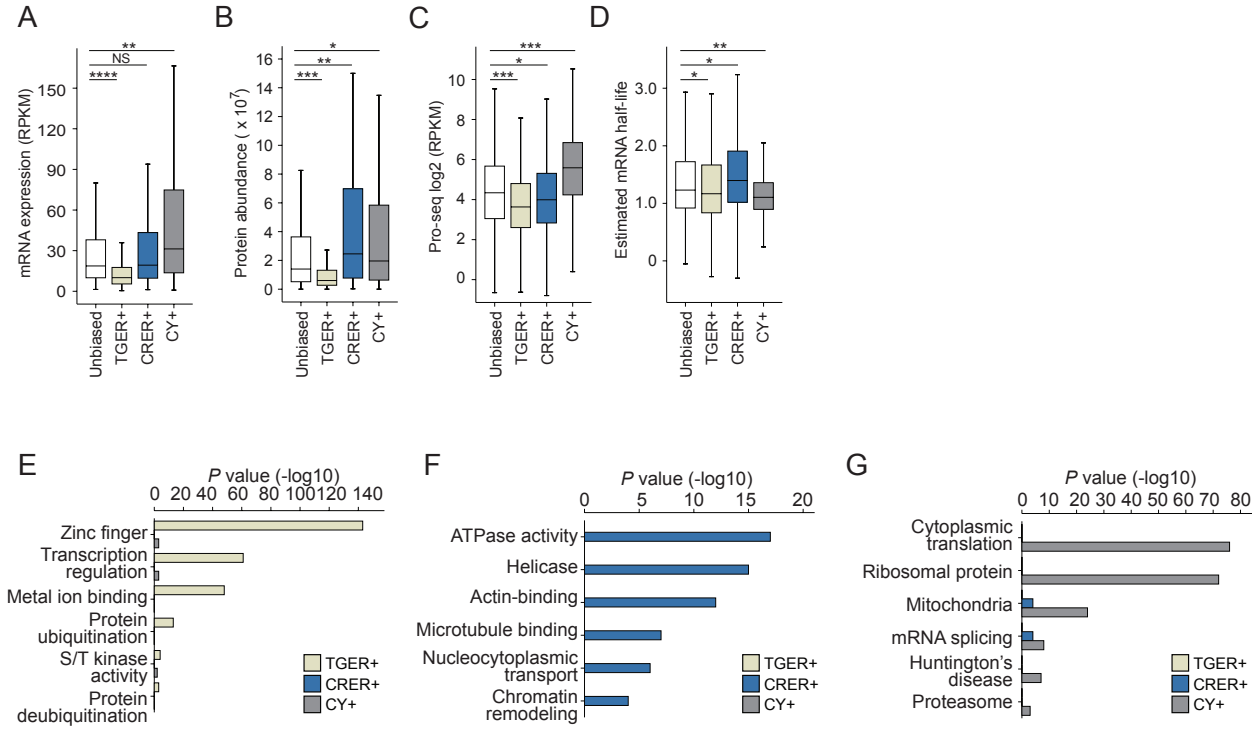

Figure 2. Characteristics of compartment-enriched mRNAs.
(A) Steady-state mRNA abundance levels obtained from whole cell lysates. TGER+, *N* = 1246; CRER+, *N* = 919, CY+, *N* = 1481; unbiased, *N* = 3369. Mann Whitney test: *, 1 x 10-3 >*P*> 1 x 10-9; **, 1 x 10-10 >*P*> 1 x 10-20; ***, 1 x 10-21 >*P*> 1 x 10-80; ****, 1 x 10-81 >*P*> 0. RPKM, reads per kilobase of transcript per million reads mapped.
(B) As in (A), but steady-state protein levels obtained from whole cell lysates. TGER+, *N* = 469; CRER+, *N* = 638; CY+, *N* = 833; unbiased, *N* = 2001. *P* value categories as in (A), exact *P* values are listed in Table S3.
(C) As in (A), but Pro-seq levels are shown, which indicate transcription rates. TGER+, *N* = 1222; CRER+, *N* = 896; CY+, *N* = 1425; unbiased, *N* = 3268. *P* value categories as in (A), exact *P* values are listed in Table S3.
(D) As in (C), but estimated mRNA half-lives are shown. *P* value categories as in (A), exact *P* values are listed in Table S3.
(E) Gene ontology analysis for TGER-enriched mRNAs. Shown are the top six functional gene classes and their Benjamini-Hochberg adjusted *P* values for categories that are significantly and uniquely enriched in TGER+ mRNAs. The Benjamini-Hochberg adjusted *P* values for the same categories for CRER+ and CY+ mRNAs are shown for comparison reasons.
(F) As in (E), but for CRER-enriched mRNAs.
(G) As in (E), but for mRNAs enriched in the cytosol.

Horste et al., Figure 3

A

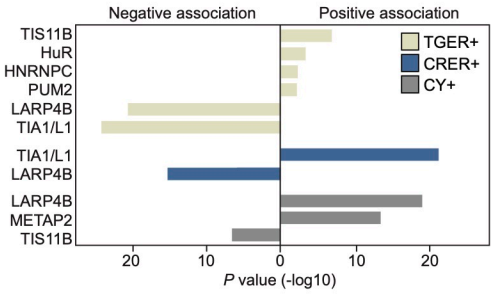

B

	Number of RBP peaks in 3'UTR							Predicted by CLIP	Observed experimentally
Gene name	TIS11B	HuR	PUM2	HNRNPC	TIA1/L1	LARP4B	METAP2		
LHPP	0	0	0	0	0	0	0	CY	CY
PTP4A3	0	0	0	0	0	0	0	CY	CY
MAP2K2	0	0	0	0	0	0	5	CY	CY
MLST8	0	0	0	0	0	6	4	CY	CY
SF3A2	0	0	0	0	0	5	0	CY	CY
FOS	3	0	0	0	0	0	0	TGER	TGER
THAP1	15	2	4	0	0	0	0	TGER	TGER
FBXL3	45	2	4	0	8	0	0	TGER	TGER
HSPA1B	10	0	0	0	49	0	0	CRER	TGER
DNAJB1	21	0	0	0	3	7	0	TGER	TGER
BAG3	11	0	4	0	0	0	0	TGER	TGER
DUSP1	7	0	2	4	32	8	0	CRER	TGER
ALDH18A1	10	0	0	0	16	5	0	CRER	CRER
TES	11	2	5	3	58	7	0	CRER	CRER
IQGAP3	0	0	0	0	4	0	0	CRER	CRER

C

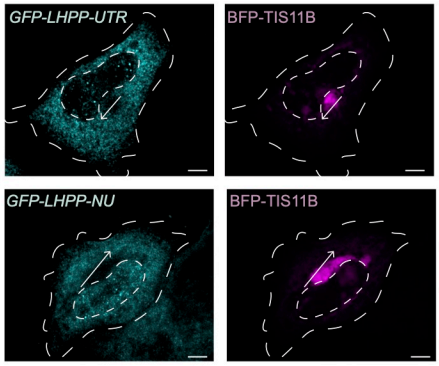

D

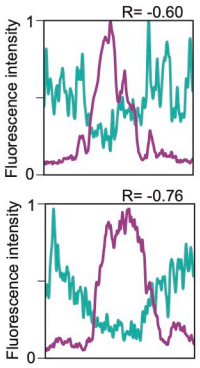

E

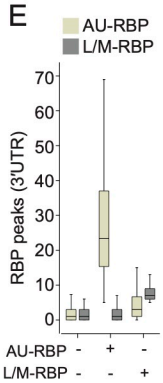

F

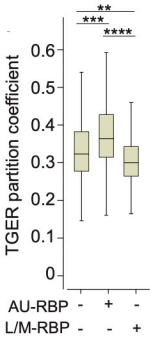

G

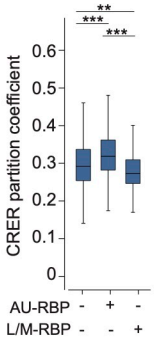

H

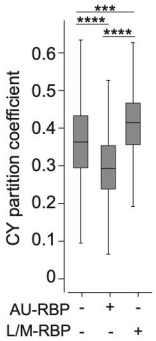

I

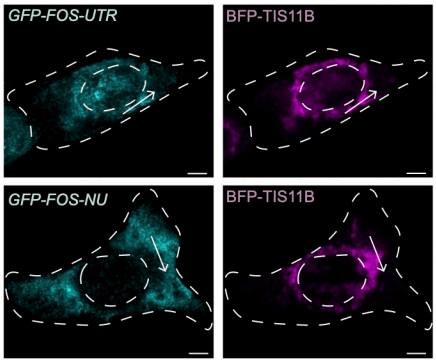

J

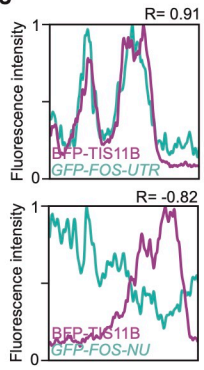

K

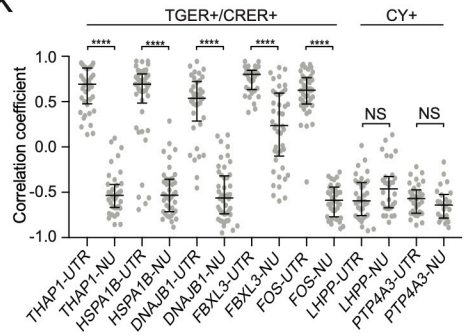

L

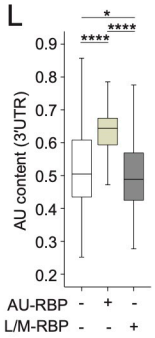

M

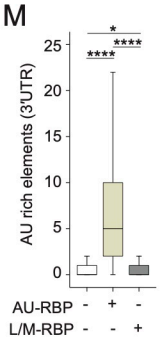

N

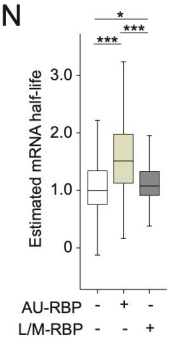

Figure 3. Presence of AU-RBPs promotes mRNA localization to TGER or CRER.
(A) 3′UTR-bound RBPs that are positively or negatively associated with mRNAs enriched in the three subcytoplasmic compartments. Shown are the -log10 transformed *P* values obtained from logistic regression (see Table S4).
(B) Predicted and observed subcytoplasmic mRNA localization for experimentally validated candidates. Shown are the number of RBP CLIP peaks used for localization prediction for each candidate.
(C) RNA-FISH of GFP mRNA after transfection of a GFP-fused LHPP coding region together with the *LHPP 3'UTR* (*LHPP-UTR*) or without the *LHPP 3'UTR* (*LHPP-NU*, no UTR) in HeLa cells (teal). Cotransfection of GFP-TIS11B to visualize TIS granules (magenta). Scale bar, 5 µm.
(D) Line diagrams showing the fluorescence intensities obtained at the position of the arrows from (C). The Pearson's correlation coefficients of the fluorescence intensities are shown.
(E) The number of 3′UTR CLIP peaks is shown for the following mRNA groups: mRNAs not bound by any of the seven RBPs (*N* = 2154), bound by AU-RBPs (*N* = 1695), bound by L/M-RBP (sum of LARP4B and METAP2 CLIP peaks), *N* = 825.
(F) Shown is the fraction of mRNA transcripts that localize to TGER for the groups from (E). Mann Whitney tests were performed. *P* value categories as in Fig. 2A, exact *P* values are listed in Table S3.
(G) As in (F), but shown is the fraction of mRNA transcripts that localize to CRER for the groups from (E).
(H) As in (F), but shown is the fraction of mRNA transcripts that localize to the cytosol for the groups from (E).
(I) RNA-FISH of GFP mRNA after transfection of a GFP-fused *FOS* coding region together with the *FOS 3'UTR* (*FOS-UTR*) or without the *FOS 3'UTR* (*FOS-NU*, no UTR) in HeLa cells (teal). Cotransfection of GFP-TIS11B to visualize TIS granules (magenta). Scale bar, 5 µm.
(J) Line diagrams showing the fluorescence intensities obtained at the position of the arrows from (I). The Pearson's correlation coefficients of the fluorescence intensities are shown.
(K) As in (J) but shown are the Pearson's correlation coefficients of additional mRNAs expressed from cDNAs either containing or lacking their corresponding 3′UTRs. Corresponding RNA-FISH images are shown in Fig. C and S4. Two line profiles were generated for each cell. Number of cells analyzed, *FOS-UTR N* = 14, *FOS-NU N* = 18, *THAP1-UTR N* = 15, *THAP1-NU N* = 18, *HSPA1B-UTR N* = 18, *HSPA1B-NU N* = 15, *DNAJB1-UTR N* = 13, DNAJB1-NU *N* = 18, FBXL3-UTR *N* = 12, FBXL3-NU *N* = 16, LHPP-UTR *N* = 16, LHPP-NU *N* = 12, *PTP4A3-UTR N* = 14, *PTP4A3-NU N* = 11. Mann-Whitney test, ****, *P* < 0.0001, NS, not significant; *LHPP: UTR* vs *NU*; *P* = 0.1447; *PTP4A3 UTR* vs *NU*; *P* = 0.1126.
(L) As in (F), but shown is the AU content in 3′UTRs. Mann Whitney test, *P* value categories as in Fig. 2A, exact *P* values are listed in Table S3.
(M) As in (L), but the number of AU-rich elements in 3′UTRs is shown.
(N) As in (M), but estimated mRNA half-lives are shown.

Horste, et al, Figure 4

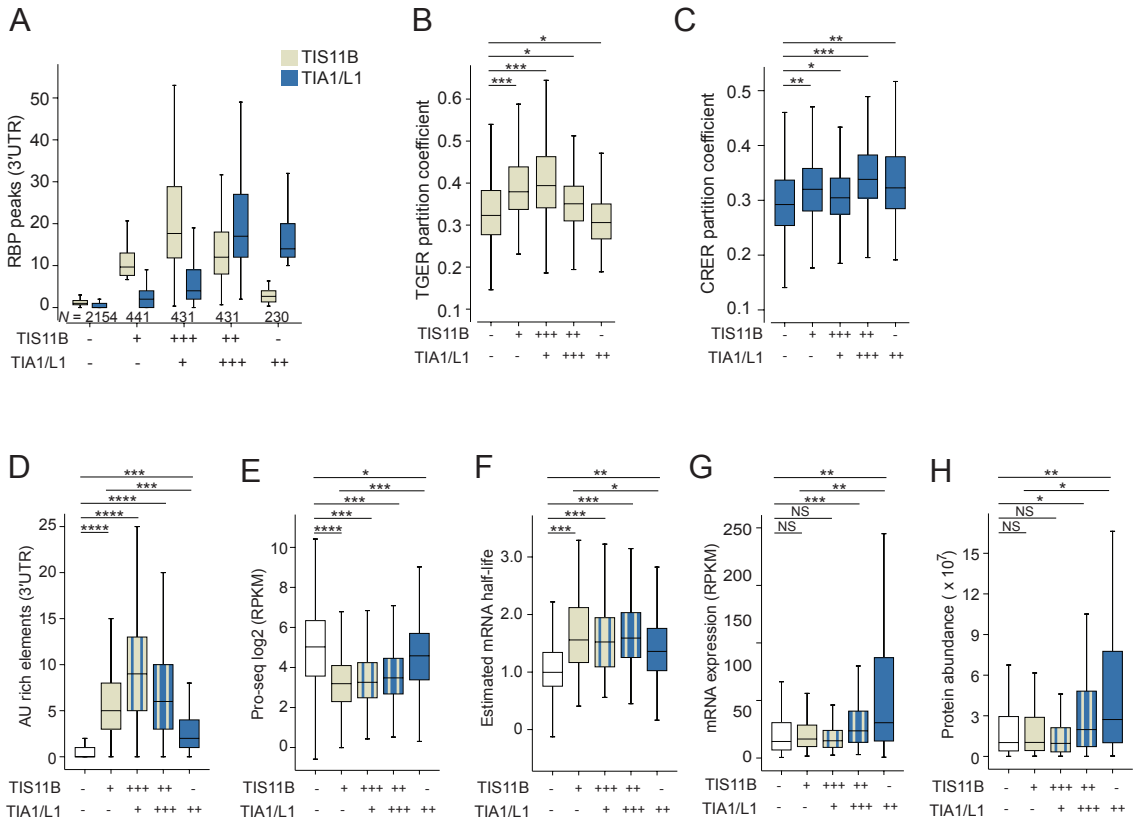

Figure 4. The ratio of 3′UTR-bound TIS11B over TIA1/L1 differentiates between TGER and CRER.
(A) The number of CLIP peaks for subgroups of AU-RBPs is shown. (-/-), no RBP, *N* = 2154; TIS11B only (+/-), N = 441; TIA1/L1 only (-/++), *N* = 230; TIS11B > TIA1/L1 (+++/+), *N* = 431; TIS11B < TIA1/L1 (++/+++), *N* = 431.
(B) Shown is the fraction of mRNA transcripts that localize to TGER for the groups from (A). *P* value categories as in Fig. 2A, exact *P* values are listed in Table S3.
(C) Shown is the fraction of mRNA transcripts that localize to CRER for the groups from (A). *P* value categories as in Fig. A, exact *P* values are listed in Table S3.
(D) Number of AU-rich elements in 3′UTRs is shown for the groups from (A). *P* value categories as in Fig. 3C, exact *P* values are listed in Table S3.
(E) As in (D), but shown are Pro-seq levels.
(F) As in (D), but shown are estimated mRNA half-lives.
(G) As in (D), but shown are steady-state mRNA abundance levels obtained from whole cell lysates.
(H) As in (D), but shown are steady-state protein levels obtained from whole cell lysates.

Horste et al., Figure 5

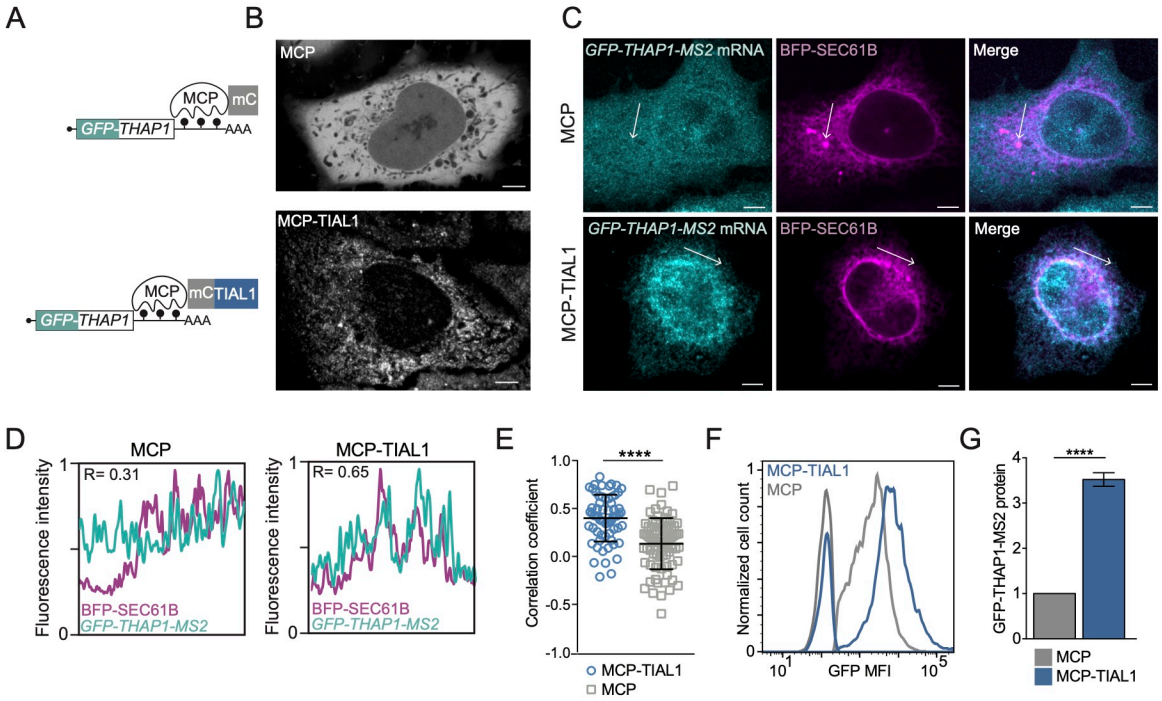

Figure 5. TIAL1-dependent mRNA localization to the rough ER increases protein expression.
(A) Schematic of the mRNA reporter used to validate the effect of a single 3′UTR-bound RBP on mRNA localization and to investigate the resulting protein expression. The GFP-tagged reporter mRNA contains the THAP1 coding region and MS2 hairpins as a 3′UTR, which allow binding of the cotransfected MS2 coat protein (mCherry-tagged MCP). Fusion of TIAL1 to MCP tethers it to the 3′UTR of the reporter mRNA. mC, mCherry.
(B) Confocal live cell imaging of HeLa cells expressing mC-tagged MCP (top) or mC-tagged MCP-TIAL1 (bottom). Scale bar, 5 µm.
(C) RNA-FISH of the GFP reporter mRNA (teal) from (A) in HeLa cells coexpressing the indicated MCP-fusion construct together with BFP-SEC61B to visualize the rough ER (magenta). Representative confocal images are shown.
Scale bar, 5 µm.
(D) Line profiles of the fluorescence intensities obtained from the arrows shown in (C) together with the obtained Pearson's correlation coefficients.
(E) Quantification of the Pearson's correlation coefficients between the GFP reporter mRNA and the rough ER in the experiment shown in (C). Two line profiles were generated for each cell. For MCP, $N = 26$ cells were analyzed and for MCP-TIAL1 $N = 21$ were analyzed. The horizontal line denotes the median and the error bars denote the 25th and 75th percentiles. Mann-Whitney test, ****, $P < 0.0001$.
(F) GFP protein expression of the reporter mRNA in HeLa cells measured by FACS for the samples from (A). Representative histograms are shown. The histograms on the left indicate GFP-negative cell populations.
(G) Quantification of the experiment shown in (F). Shown is the mean ± std of five independent experiments. T-test for independent samples, ****, $P = 0.0003$.

Horste et al., Figure 6

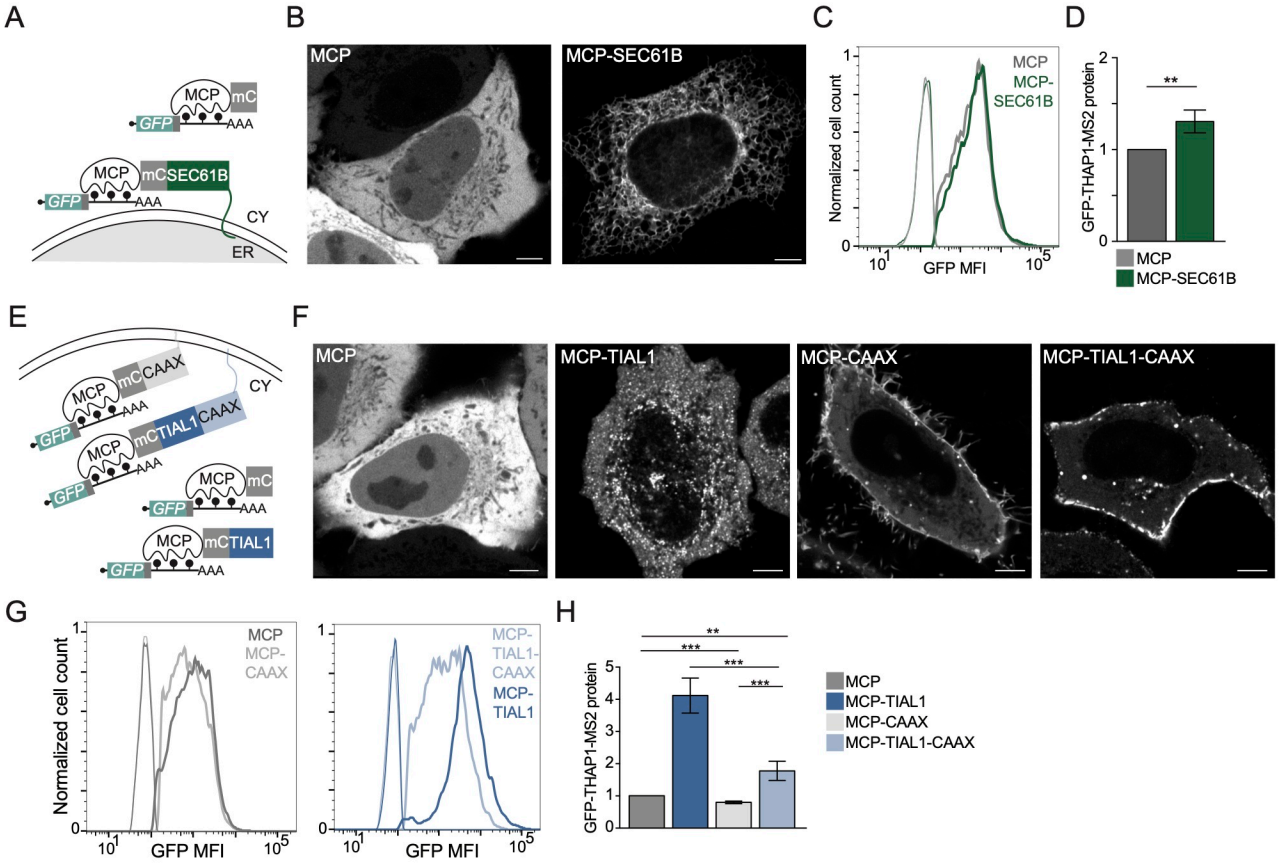

Figure 6. 3′UTR-bound TIAL1 cooperates with the rough ER membrane environment to increase protein expression.

(A) Schematic of a GFP-tagged mRNA reporter that investigates the influence of subcellular mRNA localization on protein expression. Fusion of MCP to SEC61B localizes the GFP reporter mRNA (shown as in Fig. 5A) to the rough ER membrane, whereas MCP alone localizes it to the cytosol.

(B) Confocal live cell imaging of HeLa cells expressing mC-tagged MCP (left) or mC-tagged MCP-SEC61B (right). Scale bar, 5 µm.

(C) GFP protein expression of the mRNA reporter measured by FACS in HeLa cells coexpressing the mRNA reporter together with the indicated MCP-fusion constructs. Representative histograms are shown. GFP-negative populations are plotted on the left side.

(D) Quantification of the experiment from (C). Shown is the mean ± std of four independent experiments. T-test for independent samples, **, P =0.0026.

(E) As in Fig. 4D, but addition of a prenylation signal (CAAX) localizes the TIAL1-bound GFP reporter mRNA to the plasma membrane. In the absence of CAAX, the TIAL1-bound reporter mRNA localizes to the rough ER.

(F) Confocal live cell imaging of HeLa cells expressing the indicated constructs. Scale bar, 5 µm.

(G) GFP protein expression of the mRNA reporter measured by FACS in HeLa cells coexpressing the mRNA reporter together with the indicated MCP-fusion constructs. Representative histograms are shown. GFP-negative populations are plotted on the left side.

(H) Quantification of the experiment from (G). Shown is the mean ± std of four independent experiments. T-test for independent samples, ****, $P < 0.0006$, **, P = 0.002.

Horste et al., Figure 7

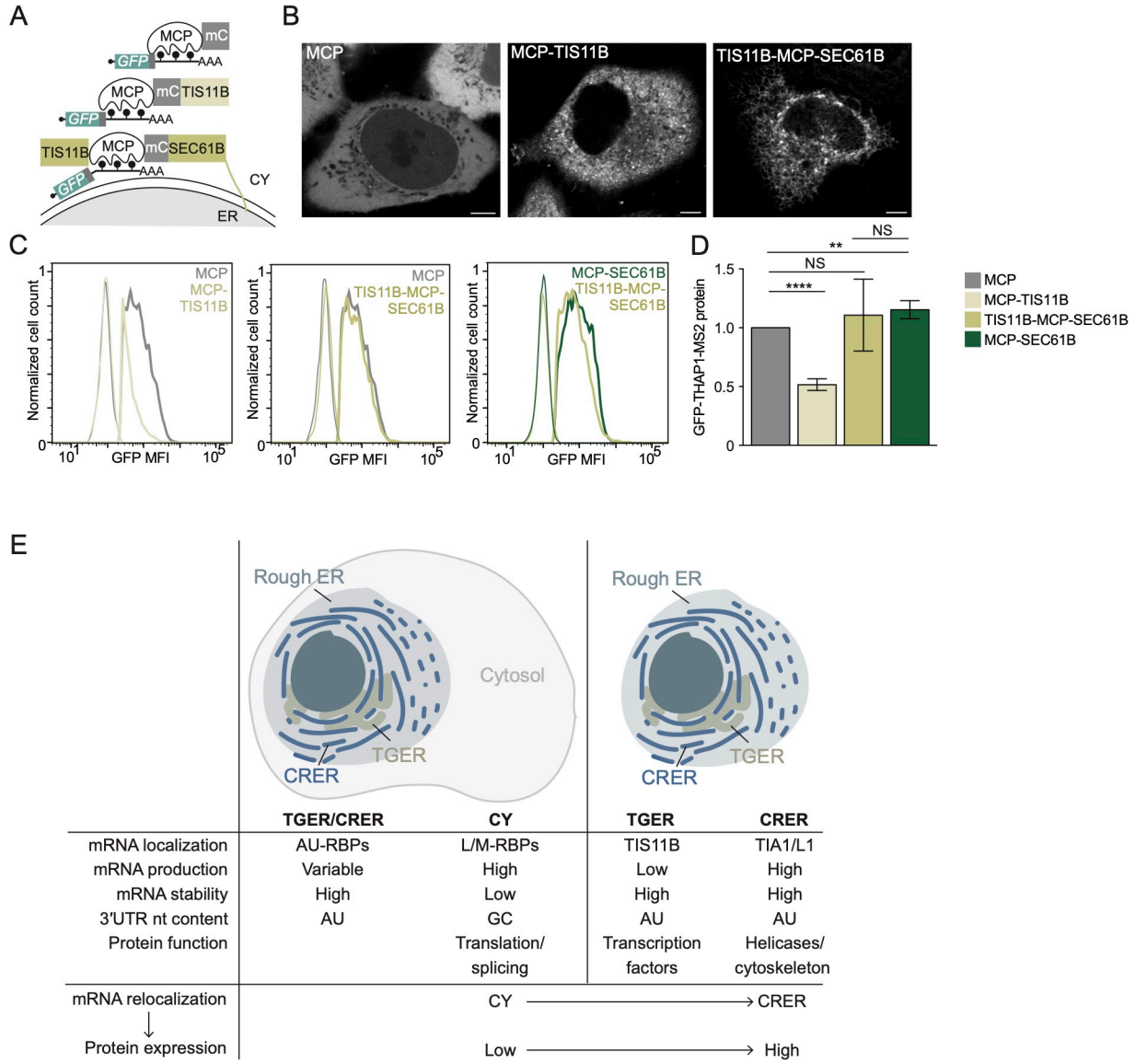

Figure 7. Relocalization of cytosolic mRNAs to the rough ER membrane increases their protein expression.
(A) Schematic of a GFP-tagged reporter mRNA bound by TIS11B that allows investigation of localization-dependent GFP protein expression. Fusion of MCP and TIS11B localizes the mRNA reporter to the cytosol, whereas the TIS11B-MCP-SEC61B fusion localizes the mRNA to the rough ER membrane.
(B) Confocal live cell imaging of HeLa cells expressing the indicated constructs (described in A). Scale bar, 5 µm.
(C) GFP protein expression of the mRNA reporter measured by FACS in HeLa cells coexpressing the mRNA reporter together with the indicated MCP-fusion constructs. Representative histograms are shown. GFP-negative populations are plotted on the left side.
(D) Quantification of the experiment from (C). Shown is the mean ± std of four independent experiments. T-test for independent samples, ****, $P < 0.0001$, **, $P = 0.03$, NS, not significant.
(E) Model. Characteristics of subcytoplasmic compartments. Shown are mRNA features of compartment-enriched mRNAs. mRNA relocalization from the cytosol to the ER increased protein expression by two-fold independently of the bound RBPs. nt, nucleotide.

KEY RESOURCES TABLE

REAGENT or RESOURCE	SOURCE	IDENTIFIER
Antibodies		
Rabbit anti-GFP	Abcam	Cat# ab290, RRID:AB_303395
Mouse anti-mCherry	Abcam	Cat# ab125096, RRID:AB_11133266
Mouse anti-GAPDH	Sigma-Aldrich	Cat# G8795, RRID:AB_1078991
Rabbit anti-Calnexin	Abcam	Cat# ab22595, RRID:AB_2069006
Rabbit anti-H2A	Millipore	Cat# 07-146, RRID:AB_11212920
Donkey anti-mouse IRDye 700	Rockland	Cat# 610-730-002, RRID:AB_1660934
Donkey anti-rabbit IRDye 800	LI-COR Biosciences	Cat# 926-32213, RRID:AB_621848
Donkey anti-mouse IRDye 800	LI-COR Biosciences	Cat# 926-32212, RRID:AB_621847
Chemicals, Peptides, and Recombinant Proteins		
Stellaris® FISH Probes, eGFP with Quasar® 670 Dye	Biosearchtech	Cat# VSMF-1015-5
Lipofectamine 3000	ThermoFisher	Cat# L3000001
Chloroquine diphosphate salt	Millipore-Sigma	Cat# 6628
Fibronectin	Millipore-Sigma	Cat# F0635
Odyssey blocking buffer (PBS)	LI-COR Biosciences	Cat# 927-40000
SeeBlue Plus2 Pre-Stained Standard	Thermo Fisher Scientific	Cat# LC5925
NuPAGE MES SDS running buffer 20x	Invitrogen	Cat# NP0002
NuPAGE Novex 4-12% Bis-Tris Protein Gels, 1.0 mm, 10 well	Invitrogen	Cat# NP0321
NuPAGE Transfer Buffer	Invitrogen	Cat# NP00061
Sample Buffer, Laemmli 2× Concentrate	Sigma-Aldrich	Cat# S3401
Tween-20	Fisher Scientific	Cat# BP337-500
Triton X-100	Fisher Scientific	Cat# BP151-100
Nonidet P-40	Sigma-Aldrich	Cat# 74385
IGEPAL CA-630	Millipore-Sigma	Cat# I8896
Doxycycline Hydrochloride	Millipore-Sigma	Cat# D3447
Ampicillin Sodium Salt	Fisher Scientific	Cat# BP176025
Puromycin Dihydrochloride	Fisher Scientific	Cat# A1113803
Bovine Serum Albumin (BSA)	Fisher Scientific	Cat# BP1605100
Tris Base	Fisher Scientific	Cat# BP152-1
Sodium Chloride	Fisher Scientific	Cat# S271-3
Dextran Sulfate Sodium Salt	Spectrum Chemical	Cat# DE131
Dextran Sulfate 50% solution	Millipore-Sigma	Cat# S4030
Ethylene Carbonate, 98%	Millipore-Sigma	Cat# E26258-500G
Ribonucleoside Vanadyl Complex	NEB	Cat# S1402
Salmon testes single stranded DNA	Sigma-Aldrich	Cat# D7656
Yeast tRNA	Life Technologies	Cat# 15401029
Formamide	Sigma-Aldrich	Cat# F7503
Murine RNase Inhibitor	NEB	Cat# M0314S

AMPure XP	Fisher Scientific	Cat# NC9959336
Protein A/G Magnetic Beads	ThermoFisher	Cat# 88802
Superscript IV Reverse Transcriptase	ThermoFisher	Cat# 18090010
DAPI (4',6-Diamidino-2-Phenylindole, Dihydrochloride)	Life Technologies	Cat# D1306
Quant-it Ribogreen RNA Reagent	ThermoFisher	Cat# R11491
TRI Reagent™ Solution	Invitrogen	Cat# AM9738
Q5 High-Fidelity DNA Polymerase	NEB	Cat# M0491L
T4 DNA Ligase	NEB	Cat# M0202L
DNA Polymerase I, Large (Klenow) Fragment	NEB	Cat# M0210L
UltraPure agarose	Invitrogen	Cat# 16500500
Ethidium Bromide	Fisher Scientific	Cat# PI17898
16% Paraformaldehde Aqueous Solution	Fisher Scientific	Cat# 50-980-487
ProLong Gold Antifade Mountant	ThermoFisher	Cat# P36934
ProLong Diamond Antifade Mountant	ThermoFisher	Cat# P36961
Methanol	Fisher Scientific	Cat# A412-4
Ethanol	Fisher Scientific	Cat# BP28184
Isopropanol	Fisher Scientific	Cat# BP26184
Chloroform	Fisher Scientific	Cat# C607-4
Critical Commercial Assays		
QIAGEN Plasmid Plus Midi Kit	Qiagen	Cat# 12945
Experimental Models: Cell Lines		
HeLa	Jonathan S. Weissman	N/A
HEK293T	ATCC	ATCC Cat# CRL-3216, RRID:CVCL_0063
Oligonucleotides	This paper	Table S4
Recombinant DNA		
pcDNA-GFP-TIS11B	Ma and Mayr, 2018	N/A
pcDNA-BFP-TIS11B	Ma and Mayr, 2018	N/A
pcDNA-mCherry-TIS11B	Ma and Mayr, 2018	N/A
pcDNA-GFP-SEC61B	Ma and Mayr, 2018	N/A
pcDNA-BFP-SEC61B	Ma and Mayr, 2018	N/A
pcDNA-mCherry-SEC61B	Ma and Mayr, 2018	N/A
pcDNA-GFP	Ma and Mayr, 2018	N/A
pcDNA-mCherry	Ma and Mayr, 2018	N/A
pcDNA-BIRC3-MS2-SU	Lee, et al., 2019	N/A
pFRT_TO_FlagHA_TIAL1	Meyer, et al., 2018	Addgene 106090
UBC NLS-HA-2XMCP-tagRFPt	Halstead, et al., 2015	Addgene 64541
pHR-tdPP7-3xmCherry	Yan, et al., 2016	Addgene 74926
pHR-scFv-GCN4-sfGFP-GB1-dWPRE	Yan, et al., 2016	Addgene 60907
pcDNA4TO-24xGCN4_v4-kif18b-24xPP7	Yan, et al., 2016	Addgene 74928
pcDNA-GFP-FOS	This paper	N/A

pcDNA-GFP-FOS-UTR	This paper	N/A
pcDNA-GFP-THAP1	This paper	N/A
pcDNA-GFP-THAP1-UTR	This paper	N/A
pcDNA-GFP-FBXL3	This paper	N/A
pcDNA-GFP-FBXL3-UTR	This paper	N/A
pcDNA-GFP-DNAJB1	This paper	N/A
pcDNA-GFP-DNAJB1-UTR	This paper	N/A
pcDNA-GFP-HSPA1B	This paper	N/A
pcDNA-GFP-HSPA1B-UTR	This paper	N/A
pcDNA-GFP-LHPP	This paper	N/A
pcDNA-GFP-LHPP-UTR	This paper	N/A
pcDNA-GFP-PTP4A3	This paper	N/A
pcDNA-GFP-PTP4A3-UTR	This paper	N/A
pcDNA-GFP-THAP1-MS2	This paper	N/A
pcDNA-MCP-mCherry	This paper	N/A
pcDNA-MCP-mCherry-TIS11B	This paper	N/A
pcDNA-MCP-mCherry-HuR	Lee, et al., 2019	N/A
pcDNA-MCP-mCherry-TIAL1	This paper	N/A
pcDNA-MCP-mCherry-TIA1	This paper	N/A
pcDNA-MCP-mCherry-SEC61B	This paper	N/A
pcDNA-TRAPa-MCP-mCherry	This paper	N/A
pcDNA-MCP-mCherry-CAAX	This paper	N/A
pcDNA-MCP-mCherry-TIAL1-CAAX	This paper	N/A
pcDNA-TIS11B-MCP-mCherry-SEC61B	This paper	N/A
SunTag-FOS-UTR	This paper	N/A
Software and Algorithms		
FIJI	NIH	https://fiji.sc/
Imaris	BitPlane	http://www.bitplane.com/imaris
MATLAB	MATLAB	https://www.mathworks.com/products/matlab.html
HOMER	UCSD	http://homer.ucsd.edu/homer/
GraphPad Prism 8	GraphPad Software	https://www.graphpad.com/scientific-software/prism
FlowJo_V10	FlowJo	https://www.flowjo.com
SPSS Software Version 14	IBM SPSS Statistics	https://www.ibm.com/products/spss-statistics
R Studio	R Project	https://www.r-project.org/
Odyssey	LI-COR Biosciences	https://www.licor.com/bio/products/imaging_systems/odyssey/

CONTACT FOR REAGENT AND RESOURCE SHARING

Further information and requests for resources and reagents may be directed to and will be fulfilled by the Lead Contact, Christine Mayr (mayrc@mskcc.org).

Experimental Model and Subject Details

Cell lines

HEK293T (human immortalized embryonic kidney cells, female origin) was purchased from ATCC. HeLa, a human cervical cancer cell line (female origin), was a gift from the lab of Jonathan S. Weissman (UCSF), provided by Calvin H. Jan. All cells were maintained at 37°C with 5% CO2 injection in Dulbecco's Modified Eagle Medium (DMEM) containing 4,500 mg/L glucose, 10% heat inactivated fetal bovine serum, 100 U/ml penicillin and 100 µg/ml streptomycin.

Horste et al., Figure S1

A

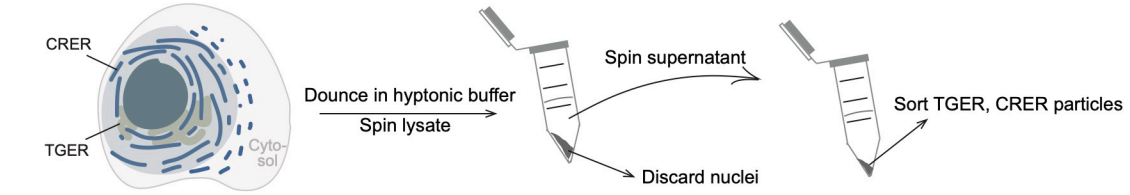

B

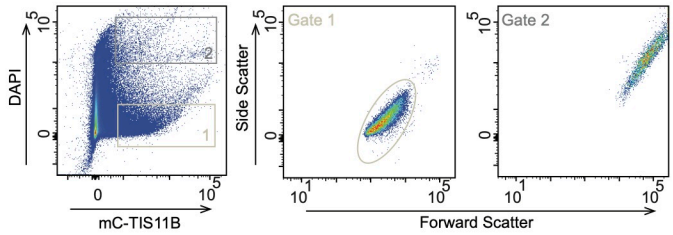

C

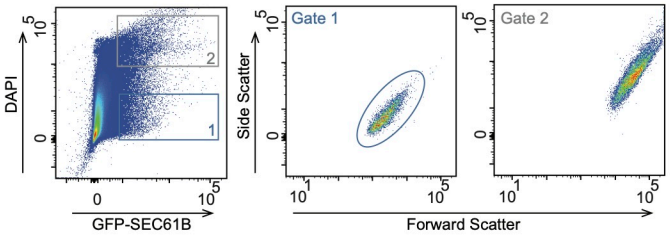

D

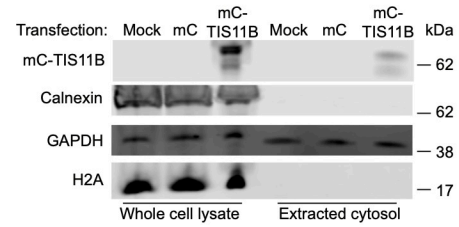

E

Pair-wise replicate comparison	Pearson correlation coefficient
TGER1 vs TGER2	0.961
TGER1 vs TGER3	0.911
TGER2 vs TGER3	0.970
CRER1 vs CRER2	0.959
CRER1 vs CRER3	0.947
CRER2 vs CRER3	0.992
CY1 vs CY2	0.938
CY1 vs CY3	0.893
CY2 vs CY3	0.954

F

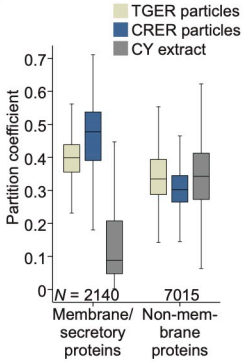

G

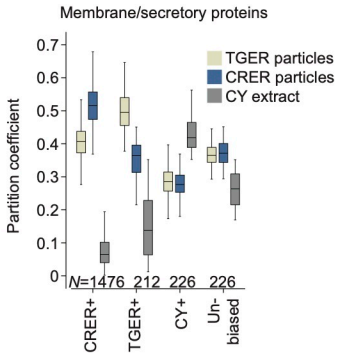

H

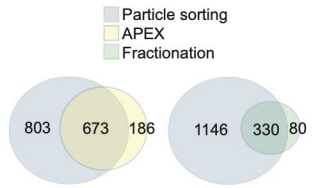

I

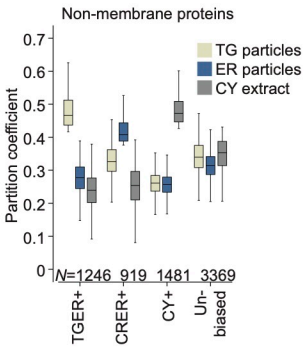

J

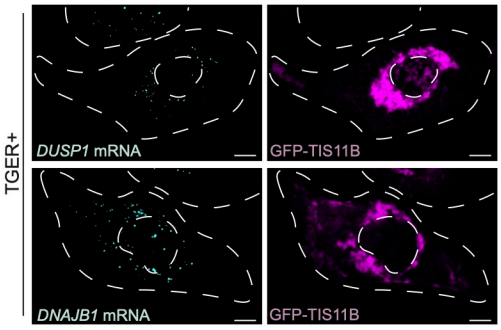

L

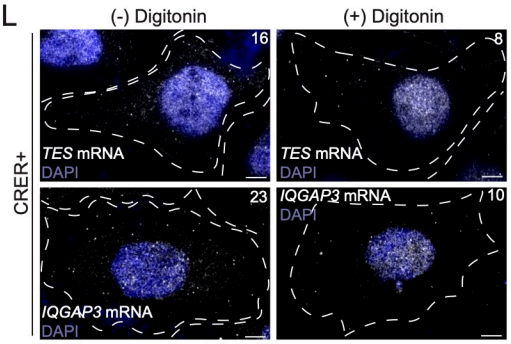

K

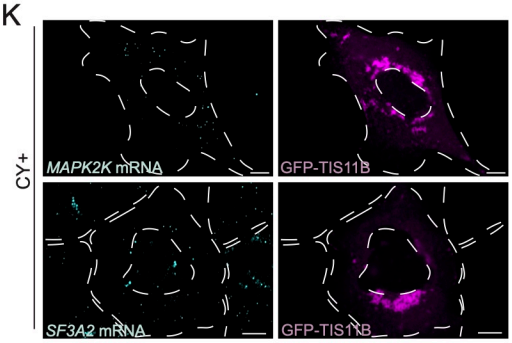

M

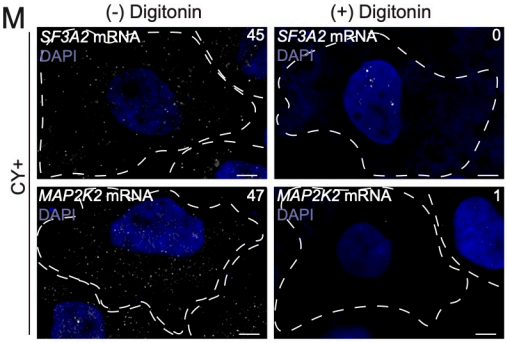

Figure S1. Strategy to determine subcytoplasmic mRNA localization.

(A) Cell fractionation strategy to obtain the cytoplasmic membrane fraction. Transfected HEK293T cells were lysed in hypotonic buffer, followed by douncing and differential centrifugation at 600 g to pellet nuclei and the supernatant was subsequently spun at 7000 g. The pellet contains the cytoplasmic membrane fraction that was used for subsequent fluorescent particle sorting.

(B) FACS plot showing mCherry-TIS11B-positive TGER particles costained with DAPI to segregate TGER particles from nuclear contamination. Gate (1) contains TGER particles, whereas gate (2) contains TGER particles bound to nuclei, indicated by DAPI stain and larger size.

(C) As in (B) but shown are GFP-SEC61B-positive CRER particles costained with DAPI. Gate (1) contains CRER particles, whereas gate (2) contains CRER particles bound to nuclei, indicated by DAPI stain and larger size.

(D) Immunoblot showing markers used to evaluate the quality of the digitonin-based cytosol extraction. H2A antibody was used as marker for nuclear components, Calnexin was used as ER marker and GAPDH was used as cytosolic protein. Unassembled TIS11B was observed in the cytosol after transfection with mCherry-tagged TIS11B. Marker expression in whole cell lysates serves as control. mC, mCherry.

(E) Pearson correlation coefficients for mRNA expression levels for biological replicates on subcytoplasmic compartments.

(F) Baseline distribution of partition coefficients across the three investigated cytoplasmic compartments is shown separately for mRNAs that encode membrane/secretory proteins and mRNAs that encode non-membrane proteins.

(G) Distribution of partition coefficients in each fractionation sample for compartment-enriched mRNAs that encode membrane/secretory proteins.

(H) Overlap of CRER-enriched mRNAs that encode membrane/secretory proteins (N = 1476) with previous datasets that used alternative isolation methods. APEX-seq, $X2$ =127, P < 0.0001 Fractionation dataset, $X2$ = 803, P < 0.0001.

(I) Distribution of partition coefficients in each fractionation sample for compartment-enriched mRNAs that encode non-membrane proteins.

(J) smRNA-FISH of endogenous mRNAs (teal), predicted to localize to the TGER in HeLa cells. The TGER domain is visualized by GFP-TIS11B (magenta). Cell and nuclear boundaries are indicated by the dotted lines. Representative images are shown. Scale bar, 5 µm. Shown are representative images for *DUSP1* and *DNAJB1.*

(K) As in (J), but for endogenous mRNAs predicted to localize to the cytosol in HeLa cells. Shown are representative images for *MAP2K2* and *SF3A2*.

(L) smRNA-FISH of endogenous mRNAs predicted to localize to the CRER. Shown are HeLa cells before (-) and after (+) digitonin treatment. Cell and nuclear boundaries are indicated by the dotted lines, number of foci counted in each image indicated in white. Representative images for *TES* and *IQGAP3* are shown. Scale bar, 5 µm.

(M) As in (L), but for endogenous mRNAs predicted to localize to the cytosol in HeLa cells. Shown are representative images for *SF3A2* and *MAP2K2.*

Horste et al., Figure S2

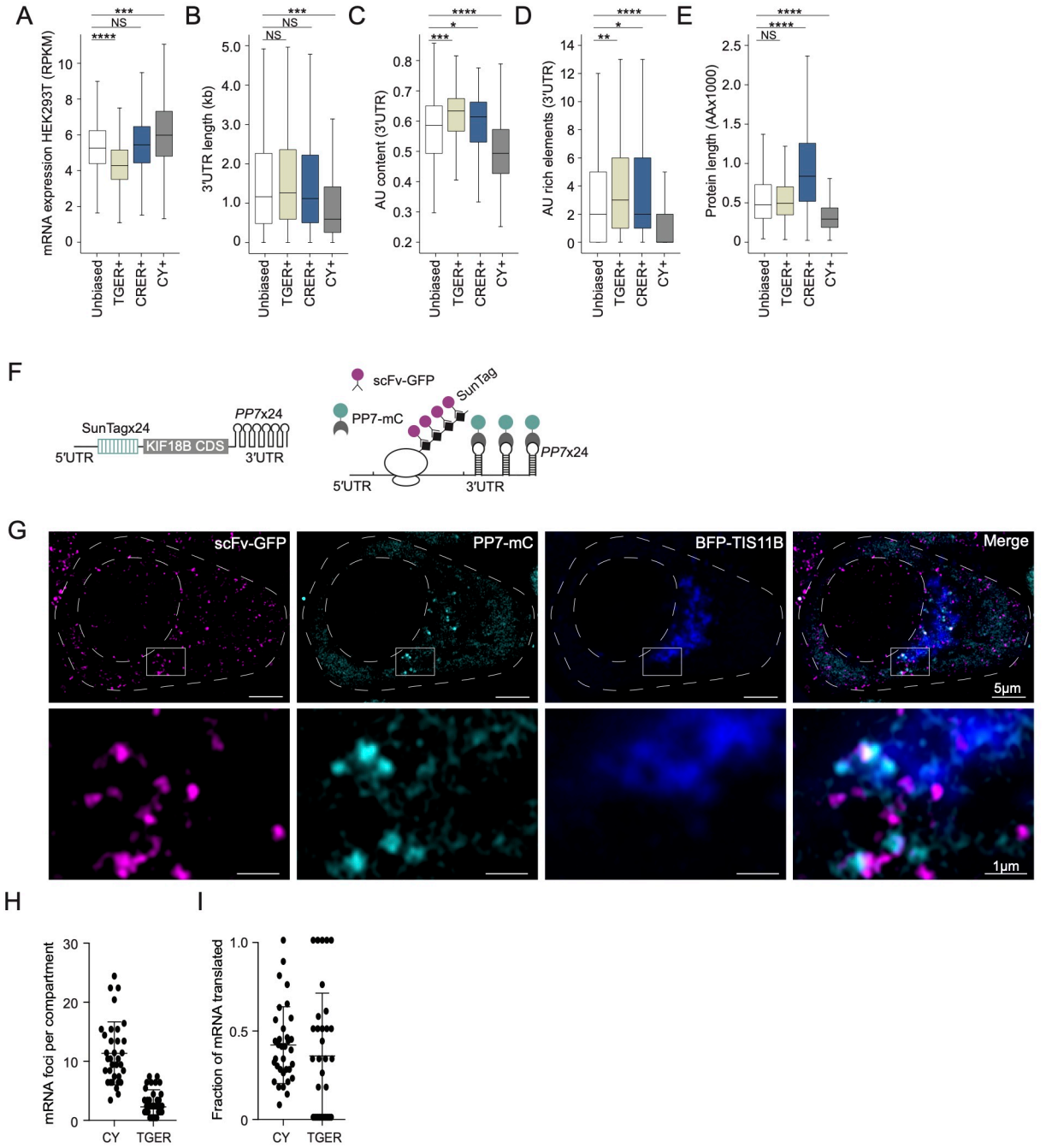

Figure S2. The TGER domain is an active translation compartment.

(A) As in Fig. 2C, but steady-state mRNA abundance levels of compartment-enriched mRNAs obtained by RNA-seq from whole cell lysates of HEK293 cells. This sample was used together with the Pro-seq sample to estimate mRNA half-lives. Mann Whitney test: *, 1 x 10-3 >*P*> 1 x 10-9; **, 1 x 10-10 >*P*> 1 x 10-20; ***, 1 x 10-21 >*P*> 1 x 10-80; ****, 1 x 10-81 >*P*> 0. RPKM, reads per kilobase of transcript per million reads mapped.

(B) As in Fig. 2A, but 3′UTR length of mRNAs enriched in the indicated compartments is shown. *P* value categories as in (A), exact *P* values are listed in Table S3.

(C) As in (B), but the fraction of adenosines or uridines in 3′UTRs of mRNAs enriched in the indicated compartments is shown. *P* value categories as in (A), exact *P* values are listed in Table S3.

(D) As in (B), but the number of AU-rich elements (AUUUA) in 3′UTRs of mRNAs enriched in the indicated compartments is shown. *P* value categories as in (A), exact *P* values are listed in Table S3.

(E) As in (B), but size of mRNA-encoded proteins enriched in the indicated compartments is shown. *P* value categories as in (A), exact *P* values are listed in Table S3.

(F) Schematic of the reporter mRNA used with the SunTag system to measure nascent protein synthesis. CDS, coding sequence. The KIF18B construct was used previously (Yan et al., 2016).

(G) Confocal imaging of HeLa cells stably expressing SunTag reporter proteins svFc-GFP and mCherry-tagged PP7 protein (mC-PP7) co-transfected with two constructs (i) BFP-TIS11B to visualize the TGER domain and (ii) SunTag-labeled mRNA encoding KIF18B and PP7-binding sites. The *KIF18B* mRNA is visualized by mC-PP7 binding (teal) whereas the KIF18B protein is visualized by svFc-GFP binding (magenta). Foci with co-localization of mRNA and protein represent nascent protein synthesis and are indicative of active translation. A representative example is shown. White box indicates area depicted at 6X magnification in the lower panel. Scale bar, 5 μm (top panel), 1 μm (bottom panel).

(H) Quantification of the experiment from (G). Shown are the number of mRNA foci in TGER or the cytosol (CY) using the Suntag reporter from (F). *N* = 24 cells were analyzed.

(I) As in (H), but shown are the mRNAs that are actively translated in each compartment, which were identified by counting the teal and magenta-double positive foci.

Horste et al., Figure S3

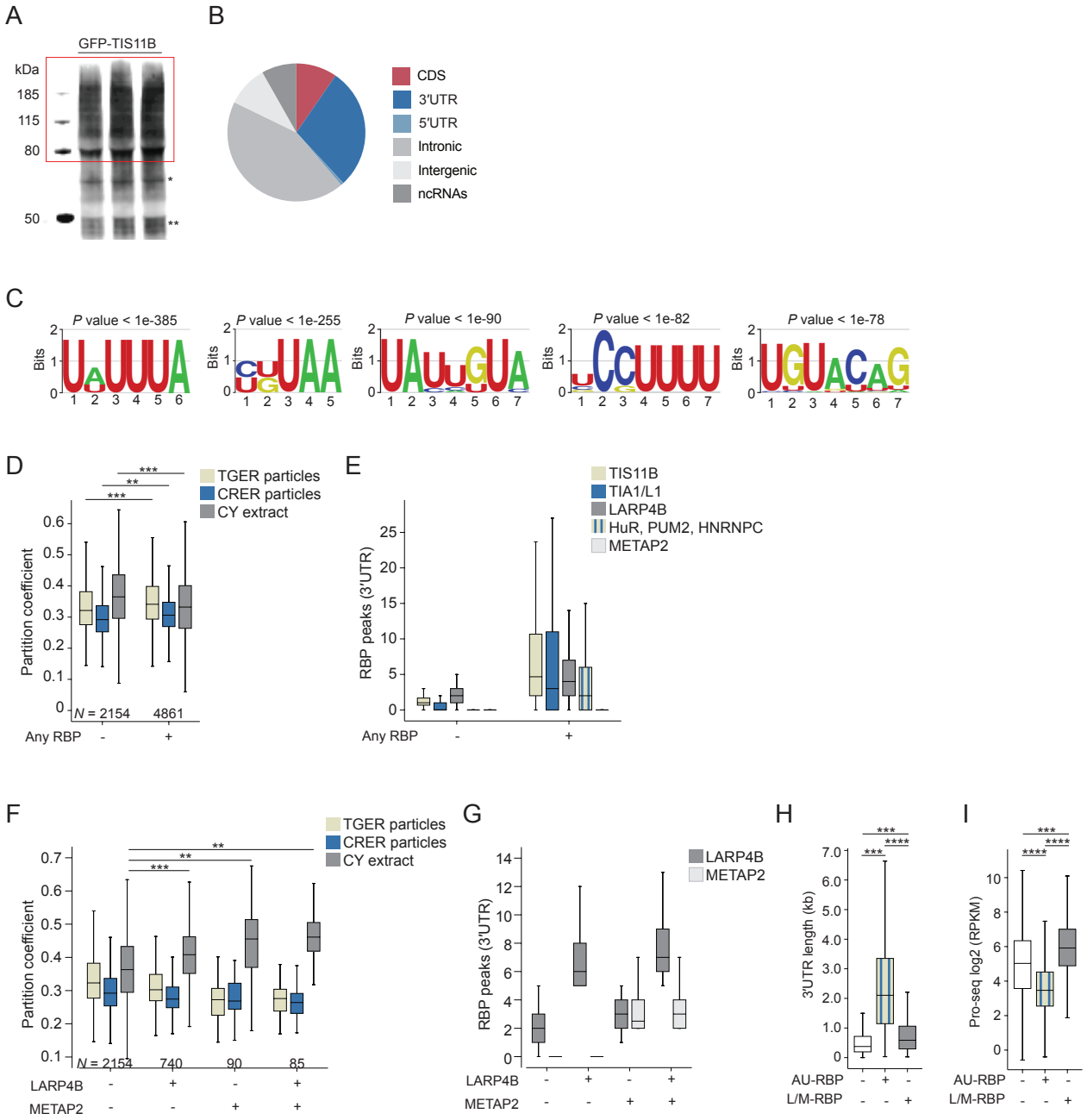

Figure S3. CLIP analysis of RBPs.
(A) Gel showing samples used for iCLIP of GFP-tagged TIS11B. The region outlined in red was used for iCLIP sample preparation.
(B) TIS11B iCLIP tag distribution obtained from HEK293T cells.
(C) The top five motifs that were enriched within TIS11B peaks in 3′UTRs compared to all nucleotides in 3′UTRs. Shown are *P* values obtained by HOMER.
(D) Fraction of mRNA transcripts that localize to TGER, CRER, or the cytosol for the indicated groups of mRNAs. mRNAs that are not bound by any of the seven RBPs (no RBP, $N = 2154$) are compared to mRNAs that are targets for at least one of the seven RBPs (RBP, $N = 4861$). Mann Whitney test was performed. *P* value categories as in (A), exact *P* values are listed in Table S3.
(E) The number of 3′UTR CLIP peaks is shown for the mRNA groups from (D).
(F) Fraction of mRNA transcripts that localize to TGER, CRER, or the cytosol for the indicated groups of mRNAs. mRNAs that are not bound by any of the seven RBPs ($N = 2154$) are compared to mRNAs that are only bound by LARP4B ($N = 740$), or METAP2 ($N = 90$), or both ($N = 85$). Mann Whitney test was performed. *P* value categories as in (A), exact *P* values are listed in Table S3.
(G) The number of CLIP peaks is shown for the mRNA groups from (F).
(H) As in Fig. 3L, but 3′UTR length is shown. Mann Whitney test, *P* value categories as in Fig. 2A, exact *P* values are listed in Table S3.
(I) As in (H), but Pro-seq values are shown.

Horste, et al., Figure S4

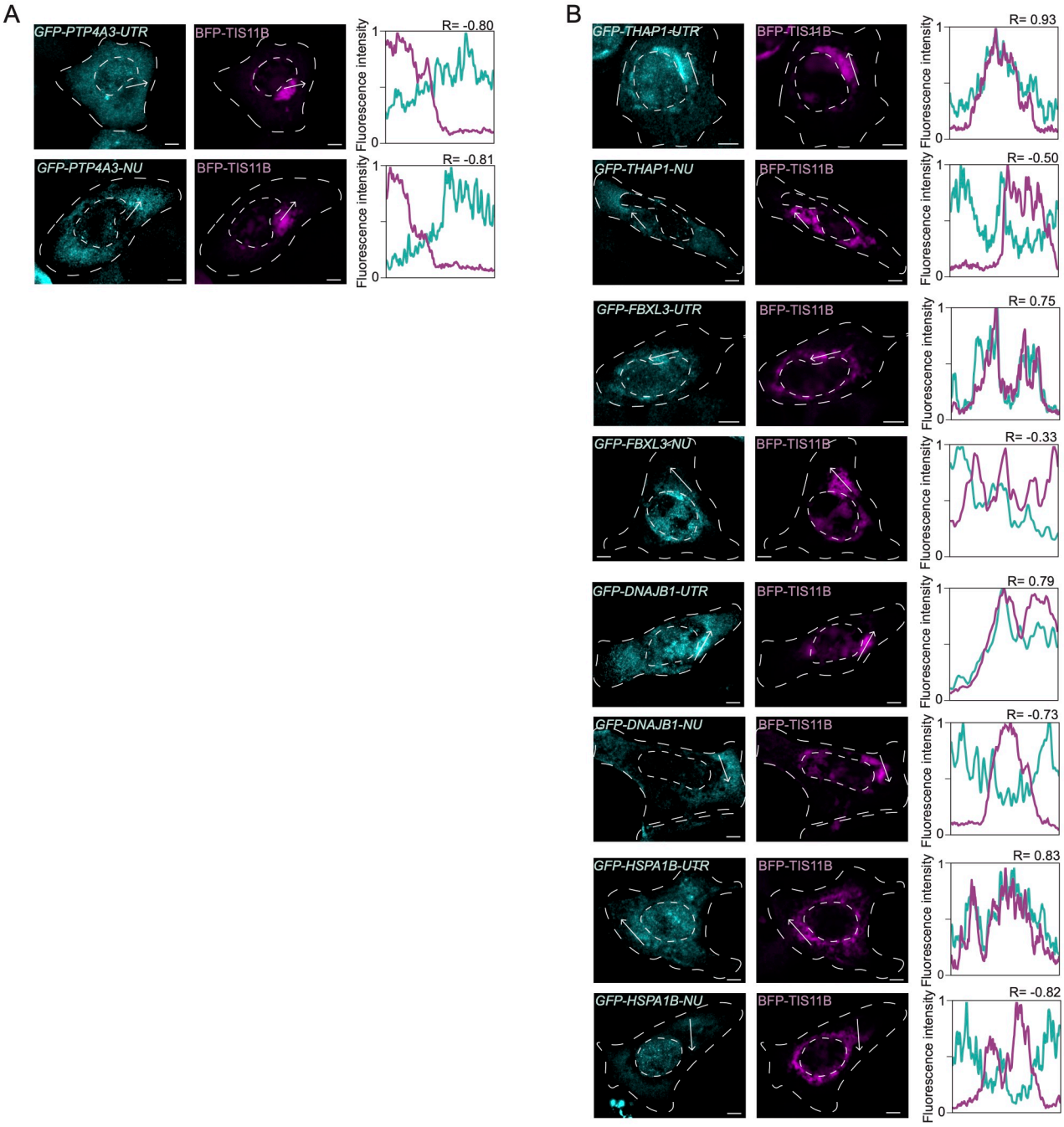

Figure S4. mRNA localization to TGER is controlled by 3′UTRs.
RNA-FISH of mRNAs after transfection of cDNA GFP-fusion constructs containing the indicated coding regions, either including (UTR) or excluding the respective 3'UTRs (NU, no UTR) in HeLa cells (teal). BFP-TIS11B was cotransfected to visualize the TGER domain (magenta). Scale bar, 5 µm. Line diagrams depicting the fluorescence intensities obtained at the position of the arrows are shown with the Pearson's correlation coefficients of the fluorescence intensities. Shown are representative images for cytosol- or TGER-enriched mRNAs.
(A) *PTP4A* does not contain 3'UTR peaks for any of the seven RBPs and is predicted to localize to the cytosol.
(B) *THAP1, FBXL3, DNAJB1,* and *HSPA1B* are predicted to localize to TGER in the presence of their 3'UTRs.

Horste, et al, Figure S5

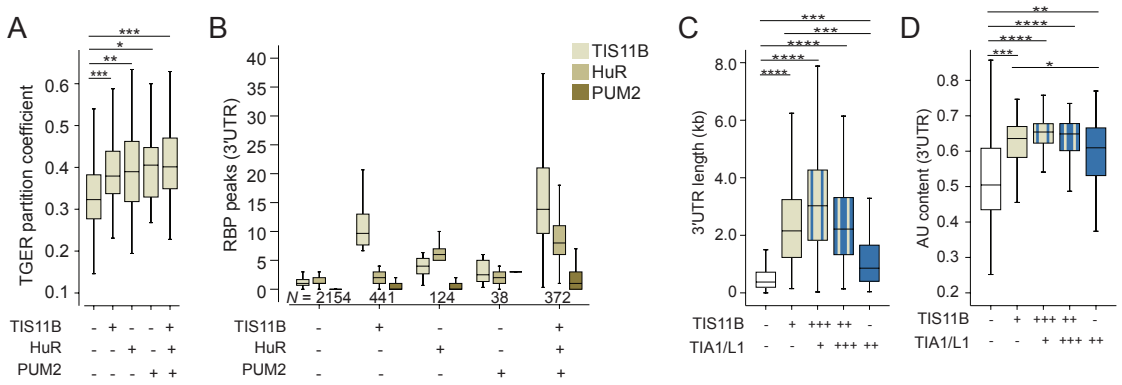

Figure S5. CLIP peaks that differentiate between TGER and CRER.
(A) Fraction of mRNA transcripts that localize to TGER for different groups of mRNAs: no RBP, *N* = 2154; TIS11B only, *N* = 441; HuR only, *N* = 124; PUM2 only, *N* = 38; HNRNPC only, *N* = 2 (not shown); any combination of the four RBPs, *N* = 372. Mann Whitney test, *P* value categories as in Fig. 2A, exact *P* values are listed in Table S3.
(B) The number of CLIP peaks for the groups from (A) are shown.
(C) As in Fig. 4D, but 3′UTR length is shown. Mann Whitney test, *P* value categories as in Fig. 2A, exact *P* values are listed in Table S3.
(D) As in (C), but AU content in the 3′UTR is shown.

Horste, et al., Figure S6

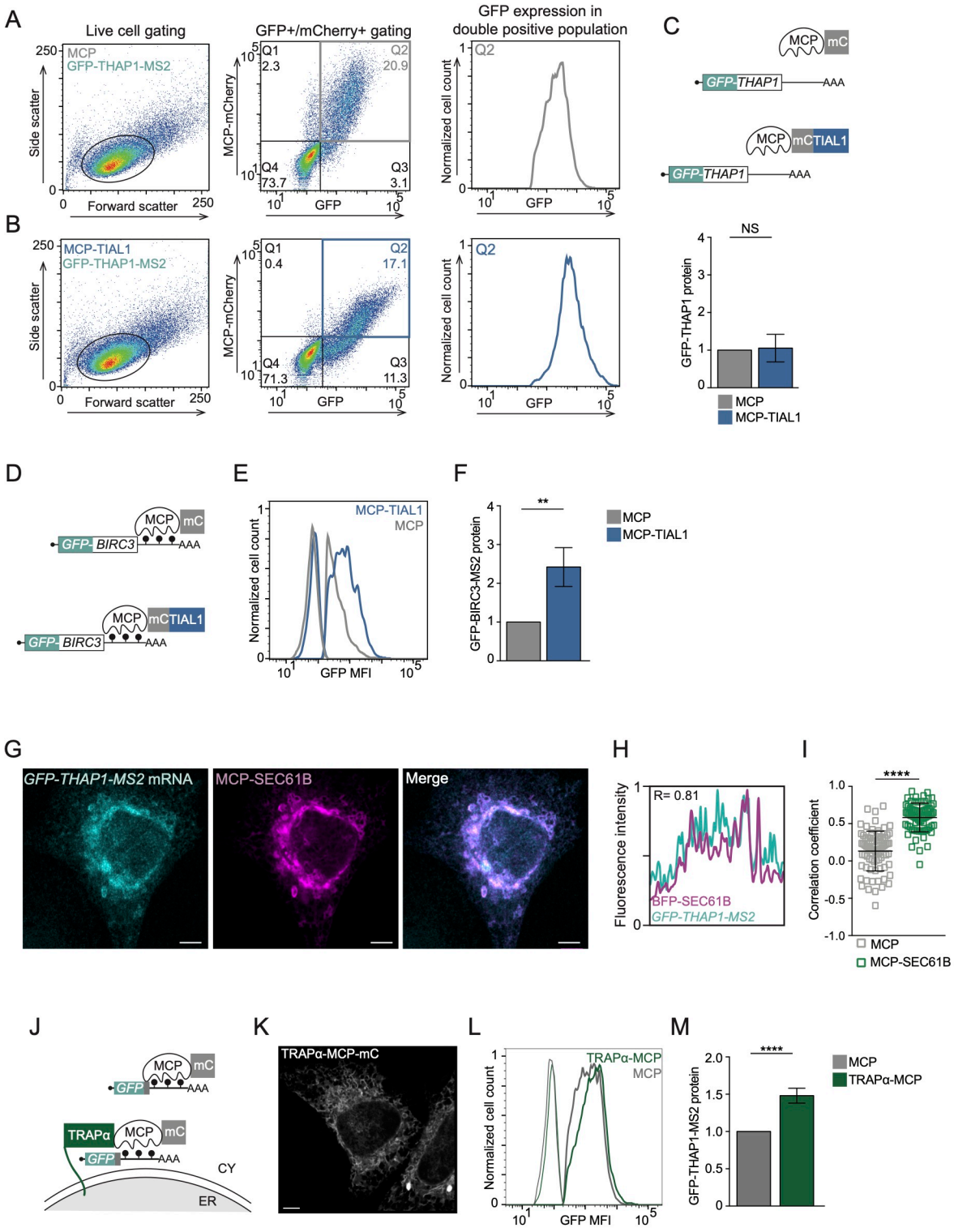

Figure S6. mRNA localization-dependent protein expression of the GFP reporter.
(A) Gating strategy to assess GFP protein expression of the reporter mRNA by FACS. Left panel shows the ungated population of HeLa cells coexpressing MCP-mCherry and the *GFP-THAP1-MS2* reporter, separated by size (forward scatter) and granularity (side scatter). The black circle indicates the live cells that were used for subsequent analysis. Middle panel, the GFP- and mCherry-double positive population was gated to obtain the GFP mean fluorescence values (MFI, right panel) which corresponds to the reported GFP protein expression values.
(B) As in (A), but HeLa cells coexpressing MCP-mCherry-TIAL1 and the *GFP-THAP1-MS2* reporter.
(C) As in Fig. 5A and 5G, but the MS2 sites in the GFP reporter were omitted. Coexpression of MCP-mCherry-TIAL1 does not result in the binding of MCP to the reporter mRNA without MS2 sites. This experiment serves as control for the effect of TIA1L1 overexpression on reporter mRNA expression.
(D) Schematic of a second mRNA reporter used to validate the effect of a single 3′UTR-bound RBP on protein expression. The GFP-tagged reporter mRNA contains the BIRC3 coding region and MS2 hairpins as 3′UTR, which allow binding of the co-transfected MS2 coat protein (mCherry-tagged MCP). Fusion of TIAL1 to MCP tethers TIAL1 to the 3′UTR of the reporter mRNA. mC, mCherry.
(E) GFP protein expression of the reporter mRNA from (D) in HeLa cells, coexpressing the indicated MCP-fusion constructs, measured by FACS. Representative histograms are shown. The histograms on the left indicate GFP-negative cell populations.
(F) Quantification of the experiment shown in (E). Shown is the mean ± std of five independent experiments. T-test for independent samples, **, $P = 0.005$.
(G) RNA-FISH of the GFP reporter mRNA (teal) from Fig. 6A in HeLa cells coexpressing MCP-mCherry-SEC61B (magenta) to visualize colocalization between the mRNA and the rough ER membrane. Representative confocal images are shown. Scale bar, 5 µm.
(H) Line profiles of the fluorescence intensities of the arrows from (G).
(I) Quantification of the experiment from (G). Two line profiles were generated for each cell. The Pearson's correlation coefficients between the reporter mRNA and the ER were determined. For MCP, $N = 26$ cells were analyzed, for MCP-SEC61B, $N = 26$ cells were analyzed. The horizontal line denotes the median and the error bars denote the 25th and 75th percentiles. Mann-Whitney test, ****, $P < 0.0001$.
(J) Schematic of a second GFP-tagged mRNA reporter that investigates the influence of subcellular mRNA localization on protein expression. Fusion of MCP to TRAPα localizes the GFP reporter mRNA to the ER membrane, whereas MCP alone localizes it to the cytosol.
(K) Confocal live cell imaging of HeLa cells expressing mC-tagged TRAPα-MCP. Scale bar, 5 µm.
(L) GFP protein expression of the reporter mRNAs from (J) coexpressing the indicated MCP-fusion constructs in HeLa cells measured by FACS. Representative histograms are shown. The histograms on the left indicate GFP-negative cell populations.
(M) Quantification of the experiment from (L). Shown is the mean ± std of four independent experiments. T-test for independent samples, ****, $P < 0.0001$.

Horste, et al., Figure S7

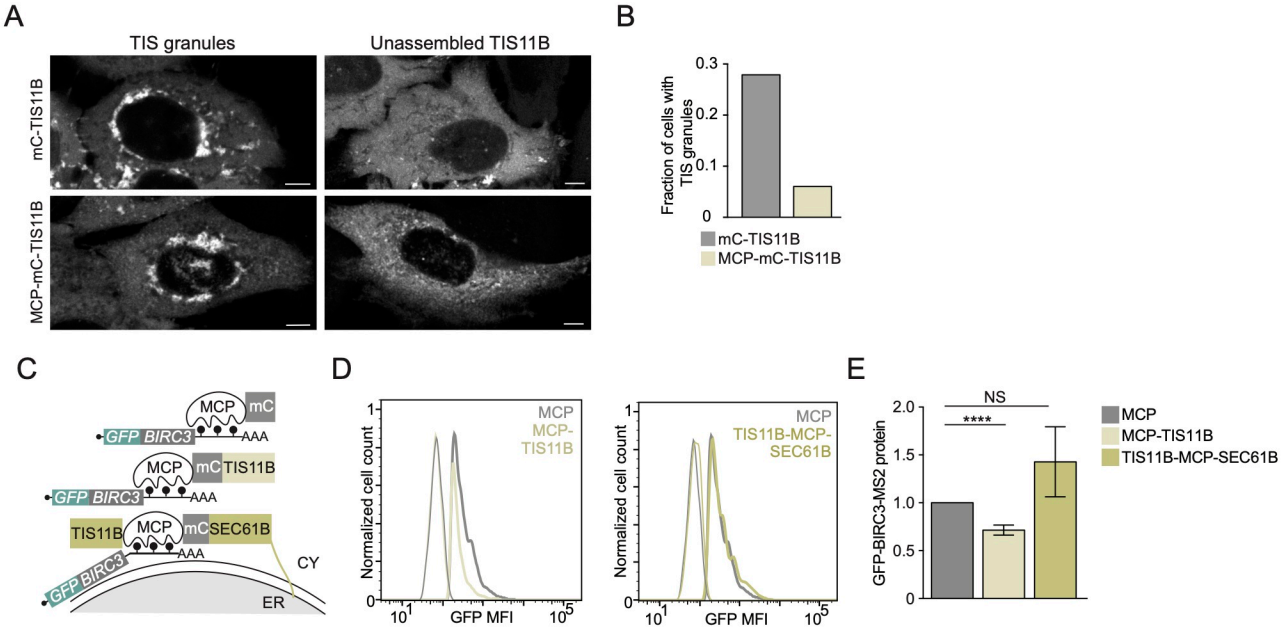

Figure S7. Redirecting mRNA localization from the cytosol to the rough ER overcomes the repressive effect of a bound RBP.

(A) Confocal live cell imaging of HeLa cells expressing the indicated constructs. Shown are representative images with TIS granules or unassembled TIS11B. mC, mCherry. Scale bar, 5 µm.

(B) Quantification from (A). The fraction of HeLa cells with TIS granules is shown after transfection of the indicated TIS11B fusion constructs. *N* = 165 cells were analyzed for mCherry-TIS11B and *N* = 198 cells were analyzed for MCP-mCherry-TIS11B. MCP-mCherry-TIS11B largely prevents TIS granule formation.

(C) Schematic of a second TIS11B-bound mRNA reporter that allows investigation of mRNA localization-dependent GFP expression. The coding region of the reporter is provided by BIRC3, followed by MS2 binding sites. Tethering of MCP or TIS11B localizes the mRNA reporter to the cytosol, whereas the MCP-TIS11B-SEC61B fusion localizes the mRNA reporter to the rough ER.

(D) GFP protein expression of the reporter mRNA from (C) in HeLa cells, coexpressing the indicated MCP-fusion constructs, measured by FACS. Representative histograms are shown. The histograms on the left indicate GFP-negative cell populations.

(E) Quantification of the experiment from (D). Shown is the mean ± std of four independent experiments. T-test for independent samples, ****, $P < 0.0001$, MCP vs TIS11B-SEC61B: $P = 0.058$; NS).

Table S2. Partition coefficients for mRNAs validated by RNA-FISH.

	Partition coefficient		
Genes	**TGER**	**CRER**	**CY**
LHPP	0.14	0.25	0.61
PTP4A3	0.24	0.23	0.53
MAP2K2	0.21	0.21	0.58
MLST8	0.21	0.17	0.62
SF3A2	0.23	0.26	0.51
FOS	0.82	0.15	0.04
THAP1	0.66	0.17	0.17
FBXL3	0.54	0.23	0.23
HSPA1B	0.75	0.19	0.06
DNAJB1	0.77	0.10	0.13
BAG3	0.62	0.22	0.16
DUSP1	0.71	0.16	0.12
ALDH18A1	0.35	0.51	0.14
TES	0.39	0.53	0.08
IQGAP3	0.34	0.54	0.12

Table S3. Mann-Whitney statistical test values.

Related to Figure	Comparison	*Z* Score	*P* Value
2A	UB vs TGER	-20.6	5.5E-94
2A	UB vs CRER	-0.87	0.39
2A	UB vs CY	-5.0	8.9E-40
2B	UB vs TGER	-11.6	3.5E-31
2B	UB vs CRER	-7.4	1.5E-13
2B	UB vs CY	-5.0	5.4E-7
2C	UB vs TGER	-10.6	2.5E-26
2C	UB vs CRER	-4.3	1.8E-5
2C	UB vs CY	-18.0	1.0E-72
2D	UB vs TGER	-3.7	2.4E-4
2D	UB vs CRER	-5.3	8.5E-8
2D	UB vs CY	-8.6	6.1E-18
3F	No RBP vs AU-RBP	-15.0	1.1E-50
3F	No RBP vs L/M-RBP	-8.7	2.5E-18
3F	AU-RBP vs L/M-RBP	-20.1	4.9E-90
3G	No RBP vs AU-RBP	-12.8	1.8E-37
3G	No RBP vs L/M-RBP	-6.8	1.1E-11
3G	AU-RBP vs L/M-RBP	-17.0	1.1E-64
3H	No RBP vs AU-RBP	-20.2	5.3E-91
3H	No RBP vs L/M-RBP	-11.9	6.7E-33
3H	AU-RBP vs L/M-RBP	-26.3	6.9E-153
3L	No RBP vs AU-RBP	-28.7	1.0E-181
3L	No RBP vs L/M-RBP	-4.3	1.5E-5
3L	AU-RBP vs L/M-RBP	-28.2	4.9E-175
3M	No RBP vs AU-RBP	-45	0
3M	No RBP vs L/M-RBP	-4.4	1.3E-5
3M	AU-RBP vs L/M-RBP	-31.2	2.2E-213
3N	No RBP vs AU-RBP	-24.6	1.0E-133
3N	No RBP vs L/M-RBP	-5.3	1.0E-7
3N	AU-RBP vs L/M-RBP	-17.9	6.0E-72
4B	No RBP vs TIS11B+	-13.3	2.0E-40
4B	No RBP vs TIS11B+++/TIA1-L1+	-15.2	3.7E-52
4B	No RBP vs TIS11B++/TIA1-L1+++	-6.2	4.7E-10
4B	No RBP vs TIA1-L1++	-3.6	3.2E-4
4C	No RBP vs TIS11B+	-7.5	5.5E-14
4C	No RBP vs TIS11B+++/TIA1-L1+	-3.8	1.5E-4
4C	No RBP vs TIS11B++/TIA1-L1+++	-13.7	1.7E-42
4C	No RBP vs TIA1-L1++	-7.8	5.5E-15
4D	No RBP vs TIS11B+	-31.1	4.6E-212
4D	No RBP vs TIS11B+++/TIA1-L1+	-32.0	5.3E-225
4D	No RBP vs TIS11B++/TIA1-L1+++	-30.7	1.3E-207
4D	No RBP vs TIA1-L1++	-14.3	1.3E-46
4D	TIS11B+/TIA1-L1++	-11.9	8.5E-33
4E	No RBP vs TIS11B+	-31.1	4.6E-212
4E	No RBP vs TIS11B+++/TIA1-L1+	-15.5	7.3E-54
4E	No RBP vs TIS11B++/TIA1-L1+++	-13.4	7.2E-41

Table S4. Sequences of oligonucleotides, related to STAR Methods

Sequences of primers for PCR	
FOS F	5´-CAGTTGTACAAGATGTTCTCGGGCTTCAAC-3´
FOS R	5´-TATATCTAGATCACAGGGCCAGCAGCGT-3´
FOS UTR F	5´-TATATCTAGAGGGCAGGGAAGGGGAGGCA-3´
FOS UTR R	5´-CGCGTCTAGATCGCATTCAACTTAAATGCT-3´
THAP1 F	5´-TAATTGTACAGTGCAGTCCTGCTCCGCC-3´
THAP1 R	5´-ACTGTCTAGATTATGCTGGTACTTCAACTA-3´
THAP1 UTR F	5´-CAGTTCTAGAAAAAATGAAATGTGTATTGA-3´
THAP1 UTR R	5´-TAATGGGCCCTGCCATTGTTTCACACCT-3´
DNAJB1 F	5´-CAGTTGTACAGGTAAAGACTACTACCAG-3´
DNAJB1 R	5´-ACTGTCTAGACTATATTGGAAGAACCTG-3´
DNAJB1 UTR F	5´-CAGTTCTAGACTATCTGAGCTCCCCAAG-3´
DNAJB1 UTR R	5´-ACTGTCTAGATGAGGTTTAGCATCAGTC-3´
HSPA1B F	5´-TAATTGTACAGCCAAAGCCGCGGCGATC-3´
HSPA1B R	5´-ACTGTCTAGACTAATCCACCTCCTCAATGG-3´
HSPA1B UTR F	5´-CATCTCTAGAGGGCCTTTGTTCTTTAGTAT-3´
HSPA1B UTR R	5´-CGTGGGGCCCAAAGTTTAACATTTTATT-3´
FBXL3 F	5´-CAGTTGTACAAAACGAGGAGGAAGAGATAG-3´
FBXL3 R	5´-TAATTCTAGATTACCAAGTGGGCATCATGT-3´
FBXL3 UTR F	5´-CAGTTCTAGAAAACTGCATGATGAATAGCA-3´
FBXL3 UTR R	5´-AATTGGGCCCAGCATTAGTAACTTTTTATT-3´
LHPP F	5´-TATATGTACAGCACCGTGGGGCAAGC-3´
LHPP R	5´-TATATCTAGATCACTTGTCGGCGTGCTG-3´
LHPP UTR F	5´-TATATCTAGATGGCCTCCTGGGAGAGCC-3´
LHPP UTR R	5´-TATGTCTAGATGCTGGTCAAGGCAGAGT-3´
PTP4A3 F	5´-TATATGTACAGCTCGGATGAACCGCCCG-3´
PTP4A3 R	5´-TATATCTAGACTACATAACGCAGCACCGGG-3´
PTP4A3 UTR F	5´-TAATTCTAGAGCTCAGGACCTTGGCTGGG-3´
PTP4A3 UTR R	5´-GACGTCTAGATTCACCCAACATGCATTGG-3´
THAP1 MS2 F	5´-ATATTGTACAAGGTGCAGTCCTGCTCCG-3´
THAP1 MS2 R	5´-CAGTACCGGTTTATGCTGGTACTTCAACTA-3´
MCP F	5´-CAGTGCTAGCATGGCTTCTAACTTTACTCA-3´
MCP R	5´-TATAGGATCCGTAGATGCCGGAGTTTGCTG-3´
TIS11B MCP F	5´-ATATGTACAAGACCACCACCCTCGTGT-3´
TIS11B MCP R	5´-CAGGTCTAGATTAGTCATCTGAGATGGAAA-3´
TIA1 MCP F	5´-TATATGTACAAGGAGGACGAGATGCCCAAG-3´
TIA1 MCP R	5´-CAGTTCTAGATCACTGGGTTTCATACCCTG-3´
TIAL1 MCP F	5´-TATATGTACAAGATGGAAGACGACGGGCAG-3´
TIAL1 MCP R	5´-GCGATCTAGATCACTGTGTTTGGTAACTTG-3´

TIS-SEC F	5´-TAATGCTAGCATGACCACCACCCTCGTGTC-3´
TIS-SEC R	5´-CAGTGCTAGCGTCATCTGAGATGGAAAGTC-3´
TRAPA MCP F	5´-TAATGCTAGCATGAGACTCCTCCCCCGCTT-3´
TRAPA MCP R	5´-CAGTGCTAGCCTCATCAGATCCCACTGATC-3´
TIAL1 CAAX F	5´-AGGTCCTCCCCAAGGACAAGCTCCTCC-3´
TIAL1 CAAX R	5´-CCTAGGGCCCTTACATGATAACACACTTGG-3´
CAAX F	5´-CAGTCTGTACAAGATGGGTGGAGGTTCTGG-3´
FOS 2F	5´-TATTACCGGTCAATGTTCTCGGGCTTCAAC-3´
FOS 2R	5´-TATAGCTAGCTCACAGGGCCAGCAGCGT-3´
FOS UTR 2F	5´-TTAAGAATTCGGGGCAGGGAAGGGGAGG-3´
FOS UTR 2R	5´-CCGCGAATTCTCGCATTCAACTTAAATGCT-3´
Sequences of RNA-FISH oligos	**5´- -3´**
2_BAG3 -_Seq_2	GGGATGTATTGAAGGAGGATGTCGCGGTCACCGTTGCCGGACGCCACCTG
4_BAG3 -_Seq_4	GGGATGTATTGAAGGAGGATTGTGGTCCACGAAGAAGGGCCAGCCGGTCT
5_BAG3 -_Seq_5	GGGATGTATTGAAGGAGGATGCGGGTCGTTCCACGTAGTGGTGCGGCTGT
7_BAG3 -_Seq_7	GGGATGTATTGAAGGAGGATCCTCCCGGGAAGGGCCATTGGCAGAGGAT
8_BAG3 -_Seq_8	GGGATGTATTGAAGGAGGATGGCCTTCCCTAGCAGGCGGCAGCCTAGAGC
10_BAG3 -_Seq_10	GGGATGTATTGAAGGAGGATCGCCTTCATGGAGCACAGGAATGGGAATGT
11_BAG3 -_Seq_11	GGGATGTATTGAAGGAGGATCATGGAAAGGGTGCACCTGCCGGTTCTCAG
13_BAG3 -_Seq_13	GGGATGTATTGAAGGAGGATTCTGAGGAGCCGCTGCTGCCGCCTCAGTTC
14_BAG3 -_Seq_14	GGGATGTATTGAAGGAGGATTCTGGCATGCCCCGCAGAGGTGACTGGGAC
16_BAG3 -_Seq_16	GGGATGTATTGAAGGAGGATGGCTGGGGGCTGGGCTGCCGCCGCCGCTGC
17_BAG3 -_Seq_17	GGGATGTATTGAAGGAGGATTGGAGACTGGGACCGCTCAGGTCCGTGGGA
19_BAG3 -_Seq_19	GGGATGTATTGAAGGAGGATGCTCCTGCCGGAGGAAGGCAGGCTGGCCGA
20_BAG3 -_Seq_20	GGGATGTATTGAAGGAGGATCCCCCGCGGGAGCTGGTGACTGCCCAGGCT
22_BAG3 -_Seq_22	GGGATGTATTGAAGGAGGATTGGTGGAAGGAGGGCTGGGCTGCTGGCCGG
23_BAG3 -_Seq_23	GGGATGTATTGAAGGAGGATTGCTGCGCTGGGTAGTGCGTCTTCTGGGCT
25_BAG3 -_Seq_25	GGGATGTATTGAAGGAGGATGGCTCCCAGTCATCCCCCTGGATCTTGTGG
26_BAG3 -_Seq_26	GGGATGTATTGAAGGAGGATGACCTGAACGGGGATGCCGCCCGCAGGGGC

28_BAG3 - _Seq_28	GGGATGTATTGAAGGAGGATTGGAGTGGCGTGCTGCTCCTGGCTGGTGAG
29_BAG3 - _Seq_29	GGGATGTATTGAAGGAGGATACGGTGTGCACACGGATGGGCGAGGGGGAG
31_BAG3 - _Seq_31	GGGATGTATTGAAGGAGGATTCAGGCTGGGAAACAGGTGCAGTTTCTCGA
32_BAG3 - _Seq_32	GGGATGTATTGAAGGAGGATACTGGGCCTGGCTTACTTTCTGGTTTGTTT
34_BAG3 - _Seq_34	GGGATGTATTGAAGGAGGATGAATCCACCTCTTTGCGGATCACTTGAATT
35_BAG3 - _Seq_35	GGGATGTATTGAAGGAGGATGGAGGTGGGGGCTTCTGGGAAACAGGTTTA
37_BAG3 - _Seq_37	GGGATGTATTGAAGGAGGATGGGCTGGGAGGAGGACAAGGAACTGGAGCA
39_BAG3 - _Seq_39	GGGATGTATTGAAGGAGGATGGGGCTGCCCTCTCTTCTGTAGCCACACTC
40_BAG3 - _Seq_40	GGGATGTATTGAAGGAGGATGGAGGTGTAGCTTCTGCAGGGGCAGTGCTG
42_BAG3 - _Seq_42	GGGATGTATTGAAGGAGGATATGGCTTCCACTTTCAGCACTCCTGGATGT
43_BAG3 - _Seq_43	GGGATGTATTGAAGGAGGATGCCTGCTCCAGCCCCTGTACCTTCTCCAGG
45_BAG3 - _Seq_45	GGGATGTATTGAAGGAGGATAAATACTCTTCGATCATCAGGTACTTTTTG
46_BAG3 - _Seq_46	GGGATGTATTGAAGGAGGATACTGAATCCAGGGCCAGCAGCTCTTTGGTC
48_BAG3 - _Seq_48	GGGATGTATTGAAGGAGGATTGAACCTTCCTGACACCGTCTCTCCTGGCC
49_BAG3 - _Seq_49	GGGATGTATTGAAGGAGGATGCTTTCTGTTCAAGTTTTTCCAAGATGGTC
51_BAG3 - _Seq_51	GGGATGTATTGAAGGAGGATTCTGCTTCAAGGTTGCTGGGCTGGAGTTCA
52_BAG3 - _Seq_52	GGGATGTATTGAAGGAGGATCCCATCTCCATGATTGCCTGCAGTGGCTGA
54_BAG3 - _Seq_54	GGGATGTATTGAAGGAGGATTCTGTGTGGGGATCTTCTGCATTTCCAGCA
55_BAG3 - _Seq_55	GGGATGTATTGAAGGAGGATGCTGCTGCTGTGGCTTCTGGCTGCTGGGTT
57_BAG3 - _Seq_57	GGGATGTATTGAAGGAGGATAGAGGCTACGGTGCTGCTGGGTTACCAGGG
58_BAG3 - _Seq_58	GGGATGTATTGAAGGAGGATCATCGGTTCCGAGTCTGATTTTTACAGGGC
60_BAG3 - _Seq_60	GGGATGTATTGAAGGAGGATTAAAAACCAACTGACTTAAAGTCTCTGAAA
61_BAG3 - _Seq_61	GGGATGTATTGAAGGAGGATCACCCAAGTTACTGCATACCAAGCAGCTAA
63_BAG3 - _Seq_63	GGGATGTATTGAAGGAGGATCAGAGTAAGAATATAGAAGAAAAGCATCAT
64_BAG3 - _Seq_64	GGGATGTATTGAAGGAGGATCTCAAACAACAAGCAACTTCTTTATTTGTA

66_BAG3 - _Seq_66	GGGATGTATTGAAGGAGGATAGGTGGTGGGGGTGCCCAAGTAGACAG GGC
67_BAG3 - _Seq_67	GGGATGTATTGAAGGAGGATTACAAAAGACAGTGCACAACCACAGCTA AC
69_BAG3 - _Seq_69	GGGATGTATTGAAGGAGGATCTGATAAATGTTTCATATTTATGTGATGG G
70_BAG3 - _Seq_70	GGGATGTATTGAAGGAGGATGAAGAAAATCATCTCATTAAAATGGCAAC A
72_BAG3 - _Seq_72	GGGATGTATTGAAGGAGGATATATTCCTATGGCTCCTGGCACATTTTAC T
73_BAG3 - _Seq_73	GGGATGTATTGAAGGAGGATAATGTAGCATTAAAGTCATCCAACATACA G
2_DUSP1 - _Seq_2	GGGATGTATTGAAGGAGGATTCGCTCCCCCAGCAGCGCCCGCAGGCC TCC
3_DUSP1 - _Seq_3	GGGATGTATTGAAGGAGGATGCGGCAGTCCAGCAGCAGGCATTGCGC CGC
4_DUSP1 - _Seq_4	GGGATGTATTGAAGGAGGATGATGTGGCCGGCGTTGAAAGCGAAGAA GGA
5_DUSP1 - _Seq_5	GGGATGTATTGAAGGAGGATGGTGCTGAAGCGCACGTTGACAGAGCC GGC
6_DUSP1 - _Seq_6	GGGATGTATTGAAGGAGGATCTCCAGGCCCATGGCGCCCTTGGCCCG GCG
7_DUSP1 - _Seq_7	GGGATGTATTGAAGGAGGATCAGCAACACCACGGCGTGGTAGGCGCC GGC
8_DUSP1 - _Seq_8	GGGATGTATTGAAGGAGGATCCAGGGTGCCGTCGCGCTTGGCGCCGT CCA
9_DUSP1 - _Seq_9	GGGATGTATTGAAGGAGGATTTGAGGAAGAAGACTTGCGCGGCGCGC GCC
10_DUSP1 - _Seq_10	GGGATGTATTGAAGGAGGATCAGGAAGCCGAAAACGCTTCGTATCCTC CT
11_DUSP1 - _Seq_11	GGGATGTATTGAAGGAGGATGGGGGTCGACTGTTTGCTGCACAGCTC CGG
12_DUSP1 - _Seq_12	GGGATGTATTGAAGGAGGATGCTAGTACTCAGGGGAAGGCTGAGCCC CAT
13_DUSP1 - _Seq_13	GGGATGTATTGAAGGAGGATACTGCACCCAGATTCCGCGCTGTCAGG GAC
15_DUSP1 - _Seq_15	GGGATGTATTGAAGGAGGATGTACAGAAAGGGCAGGATTTCCACCGG GCC
16_DUSP1 - _Seq_16	GGGATGTATTGAAGGAGGATCTTGCGGGAAGCGTGATACGCACTGCC CAG
17_DUSP1 - _Seq_17	GGGATGTATTGAAGGAGGATGGCAGTGATGCCCAAGGCATCCAGCAT GTC
18_DUSP1 - _Seq_18	GGGATGTATTGAAGGAGGATGTTGGGACAATTGGCTGAGACGTTGATC AA
19_DUSP1 - _Seq_19	GGGATGTATTGAAGGAGGATGCTCTTGTACTGGTAGTGACCCTCAAAA TG
20_DUSP1 - _Seq_20	GGGATGTATTGAAGGAGGATGTCTGCCTTGTGGTTGTCCTCCACAGGG AT
21_DUSP1 - _Seq_21	GGGATGTATTGAAGGAGGATGTCAATGGCCTCGTTGAACCAGGAGCTG AT

22_DUSP1 - _Seq_22	GGGATGTATTGAAGGAGGATTCCTCCAGCATTCTTGATGGAGTCTATGAA
23_DUSP1 - _Seq_23	GGGATGTATTGAAGGAGGATAATGCCTGCCTGGCAGTGGACAAACACCCT
24_DUSP1 - _Seq_24	GGGATGTATTGAAGGAGGATGTAAGCAAGGCAGATGGTGGCTGACCGGGA
25_DUSP1 - _Seq_25	GGGATGTATTGAAGGAGGATGTCCAGCTTGACTCGATTAGTCCTCATAAG
26_DUSP1 - _Seq_26	GGGATGTATTGAAGGAGGATTCGCCTCTGCTTCACAAACTCAAAGGCCTC
28_DUSP1 - _Seq_28	GGGATGTATTGAAGGAGGATCACCTGGGACTCAAACTGCAGCAGCTGGCC
29_DUSP1 - _Seq_29	GGGATGTATTGAAGGAGGATCCCAGCCTCTGCCGAACAGTGCGGAGCCAG
30_DUSP1 - _Seq_30	GGGATGTATTGAAGGAGGATGAGGTGCCTCGGTCGAGCACAGCCATGGCG
31_DUSP1 - _Seq_31	GGGATGTATTGAAGGAGGATGAGACGGGGAAGTTGAACACGGTGGTGGTG
32_DUSP1 - _Seq_32	GGGATGTATTGAAGGAGGATAGCGCACTGTTCGTGGAGTGGACAGGGATG
33_DUSP1 - _Seq_33	GGGATGTATTGAAGGAGGATGAGGTCGTAATGGGGCTCTGAAGGTAGCTC
34_DUSP1 - _Seq_34	GGGATGTATTGAAGGAGGATTCACCTCCCGTGGCCTTTCAGCAGCTGGGA
35_DUSP1 - _Seq_35	GGGATGTATTGAAGGAGGATGCATGGAGTCCCAATGGGATGTGAAGAGCC
36_DUSP1 - _Seq_36	GGGATGTATTGAAGGAGGATCCAGAGTTATTGCATTTCTCCTCTCAAGGA
37_DUSP1 - _Seq_37	GGGATGTATTGAAGGAGGATTAAATAAGGACCAGCCCTCTCGAGCCCCTC
38_DUSP1 - _Seq_38	GGGATGTATTGAAGGAGGATGAAACCCAGAGGAACTCGGGTGAAGTTAAA
39_DUSP1 - _Seq_39	GGGATGTATTGAAGGAGGATTTGACGCTAAGTCATCACCATAACTGCTTA
41_DUSP1 - _Seq_41	GGGATGTATTGAAGGAGGATAGATGGACTTGATGTACCCACTATATATTG
42_DUSP1 - _Seq_42	GGGATGTATTGAAGGAGGATTGAGTCCTTTCTCTTCTGCCCCATTTTGTC
43_DUSP1 - _Seq_43	GGGATGTATTGAAGGAGGATGGGCGAGCAAAAAGAAACCGGATCACACAC
44_DUSP1 - _Seq_44	GGGATGTATTGAAGGAGGATTATGTCAAGCATGAAGAGATTCTACAAAAA
45_DUSP1 - _Seq_45	GGGATGTATTGAAGGAGGATATATGTGTCGTCGGGAATAATACTGGTAGG
46_DUSP1 - _Seq_46	GGGATGTATTGAAGGAGGATCAGACACCTACACAAAAATAAATAAGGTAT
47_DUSP1 - _Seq_47	GGGATGTATTGAAGGAGGATTCTAGGAGTAGACAATGACATTTGTGAAGG
48_DUSP1 - _Seq_48	GGGATGTATTGAAGGAGGATCTCAAAAACAAAAATTGAGGTATTTGGTTC

49_DUSP1 - _Seq_49	GGGATGTATTGAAGGAGGATGCTTAAGATATATTTACAGGATAGTACAGT
50_DUSP1 - _Seq_50	GGGATGTATTGAAGGAGGATGTATTTTCCATCAGTGCTGAAAACAAACCT
51_DUSP1 - _Seq_51	GGGATGTATTGAAGGAGGATAGCAAACATACAACTGTTGGCAACTAAAAA
52_DUSP1 - _Seq_52	GGGATGTATTGAAGGAGGATCCTTATGTAACAAAATGTCTTCTTAGAAGA
1_SF3A2 - _Seq_1	GGGATGTATTGAAGGAGGATCTTGCCCCCGGGGCGATGCTGGAAGTCCAT
2_SF3A2 - _Seq_2	GGGATGTATTGAAGGAGGATGGAGGAGGAGGCCACGCCCCCGCTCCCGGT
3_SF3A2 - _Seq_3	GGGATGTATTGAAGGAGGATGAGGCGCTCCCTGCGGTCACGGTTGCTCTC
4_SF3A2 - _Seq_5	GGGATGTATTGAAGGAGGATGTGGTTCTTCATGAAGTACGGGTCCTTGTT
5_SF3A2 - _Seq_6	GGGATGTATTGAAGGAGGATCAGGCAGAGTTTGCATTCATAGGAGCCCAG
6_SF3A2 - _Seq_7	GGGATGTATTGAAGGAGGATCAGGTAGCTCCCCTCATTGTTGTGAAGTGT
7_SF3A2 - _Seq_8	GGGATGTATTGAAGGAGGATGGTCTGGTGCTTCTTCCCCTGCGTATGTGC
8_SF3A2 - _Seq_9	GGGATGTATTGAAGGAGGATGGCCTCCTTGGCTGCTCGCCGGGCCAGGTT
9_SF3A2 - _Seq_10	GGGATGTATTGAAGGAGGATTGACCTTCTCAGGCGCGGGCTGGGCAGGGG
10_SF3A2 - _Seq_11	GGGATGTATTGAAGGAGGATCGATCTTCACAAACTTCTTCACCTCCACCT
11_SF3A2 - _Seq_12	GGGATGTATTGAAGGAGGATTCTGCTTGGTCACTTTGTAGCCCGGGCGGC
12_SF3A2 - _Seq_13	GGGATGTATTGAAGGAGGATGGAGGCTCTGCTGGCCCATCTCCGAGTCTC
13_SF3A2 - _Seq_14	GGGATGTATTGAAGGAGGATCGGCGATCTCAGGGTAGTCAATCTGGAAGA
14_SF3A2 - _Seq_15	GGGATGTATTGAAGGAGGATACATGAAGCGGTGACGTGGCATGATGCCCT
15_SF3A2 - _Seq_16	GGGATGTATTGAAGGAGGATCCGGAGGCTCGATCCTCTGCTCGTACGCAG
16_SF3A2 - _Seq_17	GGGATGTATTGAAGGAGGATTCGGCGGCCATGAGCAGGTACTGCCAGCGC
17_SF3A2 - _Seq_18	GGGATGTATTGAAGGAGGATGGCACCTTGAAGGCAATGGTCTCGTAGGGC
18_SF3A2 - _Seq_19	GGGATGTATTGAAGGAGGATTTGCCCTCCGCCTTGTCGATCTCTCTGCTC
19_SF3A2 - _Seq_20	GGGATGTATTGAAGGAGGATTTGGTCTCCCGGTTCCAGTGTGTCCAGAAC
20_SF3A2 - _Seq_22	GGGATGTATTGAAGGAGGATGGGAGGCTGGGTGGAGCCGGGGGCTTCTCC
21_SF3A2 - _Seq_23	GGGATGTATTGAAGGAGGATCGGGGGTGGAGGCCGCTTCACCCCAGGGGG

22_SF3A2 - _Seq_24	GGGATGTATTGAAGGAGGATCGGTGGCCGAGGGGGCAGACCGTTCATCAG
23_SF3A2 - _Seq_25	GGGATGTATTGAAGGAGGATTGGCGGGGGCGGTGGCAAAGACTCAGGCAG
24_SF3A2 - _Seq_26	GGGATGTATTGAAGGAGGATTAGCTGGGGTGGTCCCGGGGGCCCTGAGGG
25_SF3A2 - _Seq_27	GGGATGTATTGAAGGAGGATTGCAGGGGGATGCACCACTGGGGCCGGGGG
26_SF3A2 - _Seq_28	GGGATGTATTGAAGGAGGATGACGCCAGGAGCTGGGGGATGGACCCCAGA
27_SF3A2 - _Seq_29	GGGATGTATTGAAGGAGGATGGCTGGGGGATGGACGCCAGGAGCTGGGGG
28_SF3A2 - _Seq_30	GGGATGTATTGAAGGAGGATGACCCCAGAGGTTGGTGGGTGGACCCCAGG
29_SF3A2 - _Seq_31	GGGATGTATTGAAGGAGGATGGCTGGAGGGTGGACTCCAGGAGCTGGGGG
30_SF3A2 - _Seq_32	GGGATGTATTGAAGGAGGATGACTCCGGGGGCTGGTGGGTGAACCCCGGG
31_SF3A2 - _Seq_33	GGGATGTATTGAAGGAGGATTGGTGGGTGAACCCCAGGGGCTGGTGGGTG
32_SF3A2 - _Seq_34	GGGATGTATTGAAGGAGGATCGCTGATGGGGGAGGATGGACCCCTGGGGC
33_SF3A2 - _Seq_35	GGGATGTATTGAAGGAGGATTGGGTGCACCCCCGGGGCCTGGGGGTGAAC
34_SF3A2 - _Seq_36	GGGATGTATTGAAGGAGGATTGGGGCCTGAGGGTGAACGGCGGGGGCTGC
35_SF3A2 - _Seq_37	GGGATGTATTGAAGGAGGATAGGGTGCATCCCTGGGGCTGGTGGGTGCAC
36_SF3A2 - _Seq_38	GGGATGTATTGAAGGAGGATGGGAGGTTGGGGGTGGACCCCCGGGGCCTG
37_SF3A2 - _Seq_39	GGGATGTATTGAAGGAGGATGGTGGACCCCAGGAGCCGACGGATGGACCC
38_SF3A2 - _Seq_40	GGGATGTATTGAAGGAGGATGATTTGAGGGGTGAACTCCCGGAGGCTGAG
39_SF3A2 - _Seq_41	GGGATGTATTGAAGGAGGATCCTCAGCATTGGGGGCATGGGAGTTGGGGG
40_SF3A2 - _Seq_42	GGGATGTATTGAAGGAGGATGTTCCCTGGGCCTTCGGAGGGAAGTGGGGG
41_SF3A2 - _Seq_43	GGGATGTATTGAAGGAGGATTTCTCAGTTGGTTGGGGGAGGGGGAGGTAT
42_SF3A2 - _Seq_44	GGGATGTATTGAAGGAGGATTGGCGCTGGGCTTGCTGGGGGAGGGAGCAG
43_SF3A2 - _Seq_45	GGGATGTATTGAAGGAGGATCTTCTCTCAGTGGGAAAAGGCAAGAGCACC
1_MLST8 ._Seq_1	GGGATGTATTGAAGGAGGATACTGCCCACCGTGCCTGGGGAGGTGTTCAT
2_MLST8 ._Seq_2	GGGATGTATTGAAGGAGGATGTAGCCTGCAGTGGCCAGGATGACCGGGTC
3_MLST8 ._Seq_3	GGGATGTATTGAAGGAGGATGTGGGCCTGCCAGAAGCGCACGGTGTGGTC

4_MLST8._Seq_4	GGGATGTATTGAAGGAGGATGTGCTGCACCGTCCGGGTGCAGATGCCGCT
5_MLST8._Seq_5	GGGATGTATTGAAGGAGGATGACCTCCAAGGCATTCACCTGGGAGTCCTG
6_MLST8._Seq_6	GGGATGTATTGAAGGAGGATTGCAGCAGCAATCATGCTGCGGTCCGGTGT
7_MLST8._Seq_7	GGGATGTATTGAAGGAGGATGAGATCATACATGCGGATGTGCTGGTAACC
8_MLST8._Seq_8	GGGATGTATTGAAGGAGGATGCTGATGATGGGGTTAGGGTTATTGGAGTT
9_MLST8._Seq_9	GGGATGTATTGAAGGAGGATAGACGCGATGTTCTTGTTGACGCCGTCGTA
10_MLST8._Seq_10	GGGATGTATTGAAGGAGGATCATCCAGCGGCCGTCTTCGTGGAAGCCCAC
11_MLST8._Seq_11	GGGATGTATTGAAGGAGGATCCTGGCTGTGCAGTCCTCGCCGCCCGTGTA
12_MLST8._Seq_12	GGGATGTATTGAAGGAGGATCTGCAGGTTCCGGGACCTGAGGTCCCAGAT
13_MLST8._Seq_13	GGGATGTATTGAAGGAGGATGGGTGCGTTCACCTGGAAGATCCGCTGGCA
14_MLST8._Seq_14	GGGATGTATTGAAGGAGGATCTGGTTGGGGTGCAGGCACACGCAGTTAAT
15_MLST8._Seq_15	GGGATGTATTGAAGGAGGATCCCGCTCTGGTCACCCACGATGAGCTCTGC
16_MLST8._Seq_16	GGGATGTATTGAAGGAGGATGTCTGTTTTCAAGTCCCAGATGTGGATAGC
17_MLST8._Seq_17	GGGATGTATTGAAGGAGGATCTCGGGCTCAGGGATCAGCTGCTCGTTGTG
18_MLST8._Seq_18	GGGATGTATTGAAGGAGGATGGGATCGATGTGGGCGGACGTGATGGAGAC
19_MLST8._Seq_19	GGGATGTATTGAAGGAGGATGCTATTGACAGCTGCCATGTAGCTGGCGTC
20_MLST8._Seq_20	GGGATGTATTGAAGGAGGATCGTCAGATTCCAGACATAGCAGTTTCCGGT
21_MLST8._Seq_21	GGGATGTATTGAAGGAGGATGAGCTGGGTCACCTCGTCACCAATGCCCCC
22_MLST8._Seq_22	GGGATGTATTGAAGGAGGATCGTGTGGGCAGGGATCTTAGTCTTGGGGAT
23_MLST8._Seq_23	GGGATGTATTGAAGGAGGATGGGGCTGAAGCGACACTGCAGGGCGTAGCG
24_MLST8._Seq_24	GGGATGTATTGAAGGAGGATAGCCGAGCAGGTGGCGAGGAGCGTGGAGTC
25_MLST8._Seq_25	GGGATGTATTGAAGGAGGATGGACGTCCTCCAGATCTTGCACGTCTGATC
26_MLST8._Seq_26	GGGATGTATTGAAGGAGGATGATGCTCAGCTCCGTCATCAGGGAGAAGTT
27_MLST8._Seq_27	GGGATGTATTGAAGGAGGATGCGGGAGGACTCCCCGGGGTTGCCGCTCTT
28_MLST8._Seq_28	GGGATGTATTGAAGGAGGATCCCCGAGAAGGCGCAGCCCCACATCCAGCC

29_MLST8._Seq_29	GGGATGTATTGAAGGAGGATCGAGGAAGCAGTGACGATGTACTGGGAGTC
30_MLST8._Seq_30	GGGATGTATTGAAGGAGGATCTCCACACACCAGAGCCGGGCCAGGTTGTC
31_MLST8._Seq_31	GGGATGTATTGAAGGAGGATGCCGCCATACTCTCTCTTGATCTCTCCAGT
32_MLST8._Seq_32	GGGATGTATTGAAGGAGGATGAAGGCCAGGCAGACAACAGCCTTCTGGTG
33_MLST8._Seq_33	GGGATGTATTGAAGGAGGATGGTCACAGGCTAGCCCAGCACACTGTCATT
34_MLST8._Seq_34	GGGATGTATTGAAGGAGGATTGCCACCACCTGCACCAGGCAGTCCCGAGG
35_MLST8._Seq_35	GGGATGTATTGAAGGAGGATTGACCTGGGTGCTGCATGGGTCCCTCCAGC
36_MLST8._Seq_36	GGGATGTATTGAAGGAGGATTGGCGCAGGCCGGCAGGGGAGGGTCTGCTC
37_MLST8._Seq_37	GGGATGTATTGAAGGAGGATAAGGCGCCACAGGGGGCCATCAGGTCCAGC
38_MLST8._Seq_38	GGGATGTATTGAAGGAGGATGGCTGAGAGTCCCAGGGCAGCCTGGCCCAG
39_MLST8._Seq_39	GGGATGTATTGAAGGAGGATAGCTCTGTCACATCTGGATAAGCAACTGGG
40_MLST8._Seq_40	GGGATGTATTGAAGGAGGATGTCCAGGAGTGTGCAGCCTGGCTTGGGTCG
41_MLST8._Seq_41	GGGATGTATTGAAGGAGGATCGACTTTCCCAGGCAGTGCAGGCTAGCCCA
42_MLST8._Seq_42	GGGATGTATTGAAGGAGGATCAGACCCCTCAGCAGCTTTGGGCCCTCGGC
43_MLST8._Seq_43	GGGATGTATTGAAGGAGGATACACACTAGCTTGGGGGTGGGCACCAGCCT
44_MLST8._Seq_44	GGGATGTATTGAAGGAGGATCCCTGAAACGCGGGCAGGGAGGGGCAGAGA
45_MLST8._Seq_45	GGGATGTATTGAAGGAGGATCATGGTGGTGGTGTTCTCTATGGACCGAGG
1_MAP2K2 -_Seq_1	GGGATGTATTGAAGGAGGATCGGCAGCACCGGCTTCCTCCGGGCCAGCAT
2_MAP2K2 -_Seq_3	GGGATGTATTGAAGGAGGATGGAGGCGCCCTCGCTGGTAGGGGATGGGCC
3_MAP2K2 -_Seq_8	GGGATGTATTGAAGGAGGATCGCGCCCAGCTCTGAGATCCTTTCGAAGTC
4_MAP2K2 -_Seq_12	GGGATGTATTGAAGGAGGATCTGCAGCTCGCGGATGATCTGGTTCCGGAT
5_MAP2K2 -_Seq_13	GGGATGTATTGAAGGAGGATGATGTACGGCGAGTTGCATTCGTGCAGGAC
6_MAP2K2 -_Seq_14	GGGATGTATTGAAGGAGGATGTCACTGTAGAAGGCCCCGTAGAAGCCCAC
7_MAP2K2 -_Seq_15	GGGATGTATTGAAGGAGGATCATGTGTTCCATGCAAATGCTGATCTCCCC
8_MAP2K2 -_Seq_16	GGGATGTATTGAAGGAGGATTTTCAGCACCTGGTCCAGGGAGCCGCCGTC

9_MAP2K2 - _Seq_17	GGGATGTATTGAAGGAGGATCAGGATCTCCTCGGGAATCCTCTTGGCCTC
10_MAP2K2 - _Seq_18	GGGATGTATTGAAGGAGGATGCCCCGGAGAACCGCGATGCTGACTTTCCC
11_MAP2K2 - _Seq_20	GGGATGTATTGAAGGAGGATGATGTTGGAGGGCTTCACATCTCGGTGCAT
12_MAP2K2 - _Seq_25	GGGATGTATTGAAGGAGGATGATGTCCGACTGCACCGAGTAATGTGTGCC
13_MAP2K2 - _Seq_26	GGGATGTATTGAAGGAGGATCAGCTCCACCAGGGACAGGCCCATGCTCCA
14_MAP2K2 - _Seq_27	GGGATGTATTGAAGGAGGATGGCCTCCAGCTCTTTGGCGTCGGGCGGGGG
15_MAP2K2 - _Seq_28	GGGATGTATTGAAGGAGGATTTCCCCGTCGACCACGGGCCGGCCAAAGAT
16_MAP2K2 - _Seq_29	GGGATGTATTGAAGGAGGATCCGAGGCGAGATGCTGTGAGGCTCTCCTTC
17_MAP2K2 - _Seq_30	GGGATGTATTGAAGGAGGATCCATCCCGTGACCGCTGACGGGGCGCCCGG
18_MAP2K2 - _Seq_31	GGGATGTATTGAAGGAGGATGTTCAAAGATGGCCATGGCAGGCCGGCTAT
19_MAP2K2 - _Seq_32	GGGATGTATTGAAGGAGGATGAGGTGGCTCGTTCACAATATAGTCCAGGA
20_MAP2K2 - _Seq_35	GGGATGTATTGAAGGAGGATATCTTCAGGTCCGCCCGCTCCGCTGGGTTC
21_MAP2K2 - _Seq_36	GGGATGTATTGAAGGAGGATGACCGCTTGATGAAGGTGTGGTTTGTGAGC
22_MAP2K2 - _Seq_37	GGGATGTATTGAAGGAGGATCAGCCGGCAAAATCCACTTCTTCCACCTCG
23_MAP2K2 - _Seq_38	GGGATGTATTGAAGGAGGATGGCTGGTTCAGCCGCAGGGTTTTACACAAC
24_MAP2K2 - _Seq_39	GGGATGTATTGAAGGAGGATCACTGTCACACGGCGGTGCGCGTGGGTGTG
25_MAP2K2 - _Seq_40	GGGATGTATTGAAGGAGGATGACGGTGGGCAGGTCACCAGCGGGACGCAG
26_MAP2K2 - _Seq_41	GGGATGTATTGAAGGAGGATCCTCAGCTGGAAGGGCGGGGCATGGACAGG
27_MAP2K2 - _Seq_42	GGGATGTATTGAAGGAGGATGGTGAGGCAGGAGGGTGGGTGGAGGCGCCA
28_MAP2K2 - _Seq_43	GGGATGTATTGAAGGAGGATCATGCGCTGTCGCCCCGCCACGGTGCTCTC
29_MAP2K2 - _Seq_44	GGGATGTATTGAAGGAGGATGACGGGCAGGAGAGGAGACCCCCGTTCCTG
30_MAP2K2 - _Seq_45	GGGATGTATTGAAGGAGGATGTCGCCCGTCCCCAGAGGCACCCCGGCCAG
31_MAP2K2 - _Seq_46	GGGATGTATTGAAGGAGGATAGCAGAGCCTCTGAGACCACACACAGCAGC
32_MAP2K2 - _Seq_47	GGGATGTATTGAAGGAGGATCTCTCCCTGTTTTGTTTTGTAACCTAAGGA
5_IQGAP3 - _Seq_5	GGGATGTATTGAAGGAGGATCTCCTTCAGGCAGGCCTCCATCCAGCGCTT

9_IQGAP3 - _Seq_9	GGGATGTATTGAAGGAGGATCTGCTCCACATCGTAGATCTTCTTCAAGGG
13_IQGAP3 - _Seq_13	GGGATGTATTGAAGGAGGATATAGATGTCCGTGGTCTCTGGGAAGAAGGT
17_IQGAP3 - _Seq_17	GGGATGTATTGAAGGAGGATCTCAGCTGTGAATTTCACTTTCCCGTATAG
21_IQGAP3 - _Seq_21	GGGATGTATTGAAGGAGGATAGCTGCATGGACTGCAGCCTCATCCACCGA
25_IQGAP3 - _Seq_25	GGGATGTATTGAAGGAGGATCTCTTGGTAGACGGCTGCCAGAGGCTCTCG
29_IQGAP3 - _Seq_29	GGGATGTATTGAAGGAGGATATGGTTGATATTGCCCTGGATTTCAGCCTG
33_IQGAP3 - _Seq_33	GGGATGTATTGAAGGAGGATAAAGTCTCTCCTCACCCCTCGCAGGGCCAG
37_IQGAP3 - _Seq_37	GGGATGTATTGAAGGAGGATCTTTGTGTTGGCTGCAGCCACACCAGCCTG
42_IQGAP3 - _Seq_42	GGGATGTATTGAAGGAGGATCAGCTGGTACATAGACGATGCAACAGGGTA
46_IQGAP3 - _Seq_46	GGGATGTATTGAAGGAGGATACTGGCATCCCGGGCCTCCAGGGCCCGGTT
50_IQGAP3 - _Seq_50	GGGATGTATTGAAGGAGGATAGTCCTCACCCATCCCACGCTCCTGTCGCA
54_IQGAP3 - _Seq_54	GGGATGTATTGAAGGAGGATCAGGGCTGCCTTTGTCCAGAGCCTCATTGA
58_IQGAP3 - _Seq_58	GGGATGTATTGAAGGAGGATCTGTCACCTGGGCCTTCTGCCTTTTGGCTG
62_IQGAP3 - _Seq_62	GGGATGTATTGAAGGAGGATTGATGGCTTGATTGATGGCAGCCACACCAA
66_IQGAP3 - _Seq_66	GGGATGTATTGAAGGAGGATTCTTTGCCATGGCACTTTCCAGGGCTCGCT
70_IQGAP3 - _Seq_70	GGGATGTATTGAAGGAGGATTGAGGGGGCAGCCAGGAGGTTGCTCCCAGA
74_IQGAP3 - _Seq_74	GGGATGTATTGAAGGAGGATGGCGGGCCTGGAGCTGGATAACAAAGCCGA
78_IQGAP3 - _Seq_78	GGGATGTATTGAAGGAGGATGGTAAATCTTCCGCTGCCTATAACCCCGCC
83_IQGAP3 - _Seq_83	GGGATGTATTGAAGGAGGATAAAATGCCTGGATCTTCACAATGGAGTTAA
87_IQGAP3 - _Seq_87	GGGATGTATTGAAGGAGGATCAGCCAAGAAGTCTTGCTGGCTTTGATTCA
91_IQGAP3 - _Seq_91	GGGATGTATTGAAGGAGGATTGATCCGGTTCTTCACCAGCAGGCCAATCT
95_IQGAP3 - _Seq_95	GGGATGTATTGAAGGAGGATGCCGTTTCTCTTTGCTCAGCGACTTTAAAC
99_IQGAP3 - _Seq_99	GGGATGTATTGAAGGAGGATAAATCACTGCCTCCATGAACTTGGTGGTTT
103_IQGAP3 - _Seq_103	GGGATGTATTGAAGGAGGATCTGTCACCACGTCCTGGGGCTGCTCCACCT
107_IQGAP3 - _Seq_107	GGGATGTATTGAAGGAGGATCGCTGAGCACTTTGTCTTCTAGCACATCCT

111_IQGAP3 - _Seq_111	GGGATGTATTGAAGGAGGATCCTCGGGGTGGCTCAAGGCCTGCTCCG GGG
115_IQGAP3 - _Seq_115	GGGATGTATTGAAGGAGGATGGACTTTGGCCACATATCGCATCCCATA CG
120_IQGAP3 - _Seq_120	GGGATGTATTGAAGGAGGATGGGCTCCACCAGCTGCCATGGCCACAA TGT
124_IQGAP3 - _Seq_124	GGGATGTATTGAAGGAGGATGGTGTGTTTCCTCCAGATAGTCATTCAG GA
128_IQGAP3 - _Seq_128	GGGATGTATTGAAGGAGGATCCACGGTGATGTACACCATGGGTTTGGC CA
132_IQGAP3 - _Seq_132	GGGATGTATTGAAGGAGGATGGTCAGGGATGGTGGGCAGCTCCCCAA GAT
136_IQGAP3 - _Seq_136	GGGATGTATTGAAGGAGGATTACGGGTGTTGGAGTCATCAGCATCTGC CT
140_IQGAP3 - _Seq_140	GGGATGTATTGAAGGAGGATGCTGCTTGTGGGCTGCTTCTTGCTCTCT GG
144_IQGAP3 - _Seq_144	GGGATGTATTGAAGGAGGATTAGGTTCCGCAGGACGCGCCGCTGCTT CTC
148_IQGAP3 - _Seq_148	GGGATGTATTGAAGGAGGATCAGCTCTGCCTTCCGCCTGTGCCTGTGT CT
152_IQGAP3 - _Seq_152	GGGATGTATTGAAGGAGGATCTTGGAGTCGGGGGCCAGGTGGTCCAG GCA
156_IQGAP3 - _Seq_156	GGGATGTATTGAAGGAGGATAAAGATGACGTTTCTGAAGTGAGAGGCG GG
161_IQGAP3 - _Seq_161	GGGATGTATTGAAGGAGGATTTTGGCCTTGTTGAAGAGTTTCATGACA GC
165_IQGAP3 - _Seq_165	GGGATGTATTGAAGGAGGATGTGAGTTAGTGTTAAAGAAAGCATCCAG AG
169_IQGAP3 - _Seq_169	GGGATGTATTGAAGGAGGATCCAATTAGAAGATACACTGTCTGTGGCC AG
173_IQGAP3 - _Seq_173	GGGATGTATTGAAGGAGGATACACAAGAGTAATGGCTTTCCCAGGTCA AG
177_IQGAP3 - _Seq_177	GGGATGTATTGAAGGAGGATGGAGGTAGGGATGGGGAGCCTGGCCCT GGC
181_IQGAP3 - _Seq_181	GGGATGTATTGAAGGAGGATACATGGGCACTAACACACACTGCATCCC CC
185_IQGAP3 - _Seq_185	GGGATGTATTGAAGGAGGATAGAGTGTAAGGATGGGAGAAAGAATAAA TA
189_IQGAP3 - _Seq_189	GGGATGTATTGAAGGAGGATAACCTAAGGTGACTTTAAATCCAAGGTA AA
193_IQGAP3 - _Seq_193	GGGATGTATTGAAGGAGGATGAAGAGTCAGCTGTAAGGGATGAGAATC CT
197_IQGAP3 - _Seq_197	GGGATGTATTGAAGGAGGATTGGGAGTAACAGCTGCTTTTATTAACATC A
3_ALDH18A1 - _Seq_3	GGGATGTATTGAAGGAGGATATGAGATCTGAAGACGGTTGTACACTTG AC
5_ALDH18A1 - _Seq_5	GGGATGTATTGAAGGAGGATAGTGATAAACGGGATGTTGCTCCAAGAA CG
7_ALDH18A1 - _Seq_7	GGGATGTATTGAAGGAGGATGGCATGCTTCAGCTCACTGCGGTGGGC GAA

9_ALDH18A1 -_Seq_9	GGGATGTATTGAAGGAGGATCAGGCCACATTCATCCCCTCGGGTCACCAC
11_ALDH18A1 -_Seq_11	GGGATGTATTGAAGGAGGATTCTGCCCTGATTCTGCAGCACTGATACCTG
13_ALDH18A1 -_Seq_13	GGGATGTATTGAAGGAGGATCTCATGGCGCAAGCGTTGTTTGCCAAAGGC
15_ALDH18A1 -_Seq_15	GGGATGTATTGAAGGAGGATTTCTTTCAGCTGGTTCTGCCCCGAGTGGAG
17_ALDH18A1 -_Seq_17	GGGATGTATTGAAGGAGGATCATCAGCCCACTCTGTCCGGCAGCTGCACA
20_ALDH18A1 -_Seq_20	GGGATGTATTGAAGGAGGATGCGCTTCTGCTCATCATGGAAATCCAAATT
22_ALDH18A1 -_Seq_22	GGGATGTATTGAAGGAGGATGTTGACAATGGGGACAATGTTCATTCTAAG
24_ALDH18A1 -_Seq_24	GGGATGTATTGAAGGAGGATGCTATCATTATCTTTAACACTAATAACCCC
26_ALDH18A1 -_Seq_26	GGGATGTATTGAAGGAGGATTACATCTGAAAGAACAATCAAGAGATCAGT
28_ALDH18A1 -_Seq_28	GGGATGTATTGAAGGAGGATAGACTGCTGATCTCCGGGATAAAATATATC
30_ALDH18A1 -_Seq_30	GGGATGTATTGAAGGAGGATTGCTTTCACCTTGGCTTCCATGCCACCCAT
32_ALDH18A1 -_Seq_32	GGGATGTATTGAAGGAGGATCTTTGGGTGGGTTCCATTGGCAATAACAAC
34_ALDH18A1 -_Seq_34	GGGATGTATTGAAGGAGGATTGAAAAGAAGGTACCAACTTTCTTCCCCTC
37_ALDH18A1 -_Seq_37	GGGATGTATTGAAGGAGGATCTGCTCAGGTTCCAAGGTGGCCAACATCCT
39_ALDH18A1 -_Seq_39	GGGATGTATTGAAGGAGGATCAGGATCTCATCACGCTGGTCCGTCAACAG
41_ALDH18A1 -_Seq_41	GGGATGTATTGAAGGAGGATGGCTTAAACGTTTCAGCAGAGGAGCTGCAA
43_ALDH18A1 -_Seq_43	GGGATGTATTGAAGGAGGATGGGAGGAGGCTGCGATCTGTCGCAGACCGA
45_ALDH18A1 -_Seq_45	GGGATGTATTGAAGGAGGATGTTCCAGTTCCAAGTTTTTGGCGATTCGGG
47_ALDH18A1 -_Seq_47	GGGATGTATTGAAGGAGGATGTAGACAGTCAGGACGAGATTCAAAGATCA
49_ALDH18A1 -_Seq_49	GGGATGTATTGAAGGAGGATCCTTCCCTCCTTTGAGTAACAAGCCATTGC
51_ALDH18A1 -_Seq_51	GGGATGTATTGAAGGAGGATCATGGATTGAGAGAGCCTCCTGGGTCAGGA
54_ALDH18A1 -_Seq_54	GGGATGTATTGAAGGAGGATGTGGAATGATCAGATCTATCATTTTGTCTA
56_ALDH18A1 -_Seq_56	GGGATGTATTGAAGGAGGATCCATCACTGGAATCCCCTTAGCAGCTTTCT
58_ALDH18A1 -_Seq_58	GGGATGTATTGAAGGAGGATTGACCTTATCAACACTGGCCTCGGAATCCA
60_ALDH18A1 -_Seq_60	GGGATGTATTGAAGGAGGATAAGTCTCCAAAGCATTACAGGCAGCTGGAT

62_ALDH18A1 -_Seq_62	GGGATGTATTGAAGGAGGATTCAGCATATCAATGATCTGGTCAAATAATG
64_ALDH18A1 -_Seq_64	GGGATGTATTGAAGGAGGATGGCTGAAGGTCAGATAGGAGGCAAATTTGG
66_ALDH18A1 -_Seq_66	GGGATGTATTGAAGGAGGATCTACTTCAATGCATAATTCCAGGTCCCCAT
68_ALDH18A1 -_Seq_68	GGGATGTATTGAAGGAGGATCATCCGTGTGGGAGCTGCCATACTTGTGGA
71_ALDH18A1 -_Seq_71	GGGATGTATTGAAGGAGGATAAAAGCGAGTGCTGGCATTCCAGAACACAC
73_ALDH18A1 -_Seq_73	GGGATGTATTGAAGGAGGATCGTGGATTCTCGATGTACTGATTCCCACTT
75_ALDH18A1 -_Seq_75	GGGATGTATTGAAGGAGGATCCTTCCCTCGCAGCAGCCACTTAGTAGTAA
77_ALDH18A1 -_Seq_77	GGGATGTATTGAAGGAGGATGGAGGTTCTCATGAAGATATTTTAAACTTC
79_ALDH18A1 -_Seq_79	GGGATGTATTGAAGGAGGATCTTTTGGAAAATTCCCGGGTTTTCCTGGCT
81_ALDH18A1 -_Seq_81	GGGATGTATTGAAGGAGGATCAGGAACTGGGAGACAAGAGCGGGCTCTCT
83_ALDH18A1 -_Seq_83	GGGATGTATTGAAGGAGGATTGCTATTGCCAAACGGAGCCCAGAAGCATC
85_ALDH18A1 -_Seq_85	GGGATGTATTGAAGGAGGATCTATCGGTAGCAACTATTTTCTTACTTTAA
88_ALDH18A1 -_Seq_88	GGGATGTATTGAAGGAGGATAAGGGGGACTGTAAGTCACTGAGGTGACAC
90_ALDH18A1 -_Seq_90	GGGATGTATTGAAGGAGGATGATGACTACATGTGAAAGAAATAAAATGTG
92_ALDH18A1 -_Seq_92	GGGATGTATTGAAGGAGGATTCTGATGAGAATGCTAAAAAGAAGAGTTGC
94_ALDH18A1 -_Seq_94	GGGATGTATTGAAGGAGGATCAAATAAATACAAAAGGTCAATCTTCCCAG
96_ALDH18A1 -_Seq_96	GGGATGTATTGAAGGAGGATCACAGCATCTCCTGGATGCAGGAAGCTGCA
98_ALDH18A1 -_Seq_98	GGGATGTATTGAAGGAGGATGGAACATCCTGAAACTTGCATCTCCTGCTG
100_ALDH18A1 -_Seq_100	GGGATGTATTGAAGGAGGATGGTAGGACGACAAAATAATTCATACAAAAA
102_ALDH18A1 -_Seq_102	GGGATGTATTGAAGGAGGATAAAAGGGGGAAGAATCCAAAGTATTAAAAT
2_TES -_Seq_2	GGGATGTATTGAAGGAGGATGGCTCCAAATCCTTGCTCGTGACCTAAGCC
4_TES -_Seq_4	GGGATGTATTGAAGGAGGATTACGACATATTTTTCTCCAGAAGTGCAGTT
5_TES -_Seq_5	GGGATGTATTGAAGGAGGATCATCATGCTCTTCTTGGCCACACTTGCAGT
7_TES -_Seq_7	GGGATGTATTGAAGGAGGATTATACTTGGTGTCTTCAAAAAGTTTTCCCA
8_TES -_Seq_8	GGGATGTATTGAAGGAGGATCATCTGACTTTAGTTTTGCAATCAGAGTGG

10_TES - _Seq_10	GGGATGTATTGAAGGAGGATTCTTCTTGGCAGCAACTGGATTCGTCAATA
11_TES - _Seq_11	GGGATGTATTGAAGGAGGATACTCATAGGTAACTGTATTGATGGAGACAT
13_TES - _Seq_13	GGGATGTATTGAAGGAGGATCCTTGGGTAGCATCTGCATGTACTGCCTGG
14_TES - _Seq_14	GGGATGTATTGAAGGAGGATCCCCCTCTGAGCCTGCTACTGGCTGCTTTT
16_TES - _Seq_16	GGGATGTATTGAAGGAGGATTTGAAGGGTCCTGGTCATGTGCAGGGAGCT
17_TES - _Seq_17	GGGATGTATTGAAGGAGGATTCACCTCTCTGGGAGACAACTCATGGCACT
19_TES - _Seq_19	GGGATGTATTGAAGGAGGATTGACATCTCCTACTCCCAGAGCTTCGCTCT
20_TES - _Seq_20	GGGATGTATTGAAGGAGGATGGCCTTGGGCATCCATCTCACAGGGAAGTT
22_TES - _Seq_22	GGGATGTATTGAAGGAGGATCCATGGCCCCCACTGCTGCTGGGGTGCTTC
23_TES - _Seq_23	GGGATGTATTGAAGGAGGATGAGTTCTTTTGTGCTCAGCAGATTTGTCCT
25_TES - _Seq_25	GGGATGTATTGAAGGAGGATCGGCATAGATGGCTGGGTCACCTTCTTTCA
26_TES - _Seq_26	GGGATGTATTGAAGGAGGATGGTGCCACAGTTTATCATAGCCAGCCCTTT
28_TES - _Seq_28	GGGATGTATTGAAGGAGGATTCCAAAAATAAATCATGTCAACCAGGAGTT
29_TES - _Seq_29	GGGATGTATTGAAGGAGGATAATGTCTGCCACAGTATAGCTTCTCATTCT
31_TES - _Seq_31	GGGATGTATTGAAGGAGGATACTCATTGCTGAATATCAGCTCGTCACAGC
32_TES - _Seq_32	GGGATGTATTGAAGGAGGATGGTGCCAATTCTGGTTTTCTGCCTGGGTAT
34_TES - _Seq_34	GGGATGTATTGAAGGAGGATCCATCACGTATATCTCCCCAGCTAGAATGC
35_TES - _Seq_35	GGGATGTATTGAAGGAGGATAGCAGGGCTTGCACACGGGCTTGTCATTGA
37_TES - _Seq_37	GGGATGTATTGAAGGAGGATGCACTTCTGGGTCGATGGCATTGTGGCATC
39_TES - _Seq_39	GGGATGTATTGAAGGAGGATAAGAGCACAGAAAGCACTCTGTGGATGCAT
40_TES - _Seq_40	GGGATGTATTGAAGGAGGATACTTCTGCCCAATGAGGCATTTGCTGCAGC
42_TES - _Seq_42	GGGATGTATTGAAGGAGGATCCTAAGACATCCTCTTCTTACATTCCACTG
43_TES - _Seq_43	GGGATGTATTGAAGGAGGATCTATGGCTCGATACTTCTGGGTGCCCTCCT
45_TES - _Seq_45	GGGATGTATTGAAGGAGGATATCTCTTGGTTTCCTTTACAGTTTCTTTTT
46_TES - _Seq_46	GGGATGTATTGAAGGAGGATAAACCAAGTTTAAAAGTTGAGACCGAAAAA

48_TES - _Seq_48	GGGATGTATTGAAGGAGGATTAATGAGATCCAAGCTTCCAAAAATGATTT
49_TES - _Seq_49	GGGATGTATTGAAGGAGGATGTGGCACAAATGGAATAGAGACATGAAGTT
51_TES - _Seq_51	GGGATGTATTGAAGGAGGATAAAAGAAGTGTAGAACTAGGAATGCTCATC
52_TES - _Seq_52	GGGATGTATTGAAGGAGGATTTTTCTTTTCATTTTACACATGAGGGGGAA
54_TES - _Seq_54	GGGATGTATTGAAGGAGGATAAAGGTCAGTGAATAAGACGAGGCAATAAA
55_TES - _Seq_55	GGGATGTATTGAAGGAGGATTGTCAAAAAGAATTCACTGTGTATCATTAC
57_TES - _Seq_57	GGGATGTATTGAAGGAGGATGAAAGAGTAAATGCATAGGCATTAAAACAG
58_TES - _Seq_58	GGGATGTATTGAAGGAGGATTAAAGAAAATGCCACCTCTGCCTAAATCAG
60_TES - _Seq_60	GGGATGTATTGAAGGAGGATGGCCACAGATGCAAGTCACCAACTTACAAA
61_TES - _Seq_61	GGGATGTATTGAAGGAGGATGATACTGTTATGCCACATGTGATAATAAAA
63_TES - _Seq_65	GGGATGTATTGAAGGAGGATGGCTAACATGGTGAAAACCTGTCTCTACTA
64_TES - _Seq_68	GGGATGTATTGAAGGAGGATCAGGCATGGTGGCTCCCACACCTGTAATCC
66_TES - _Seq_70	GGGATGTATTGAAGGAGGATGGTGGCTTGGCTTTTATGTCCAAGCCAAAA
67_TES - _Seq_71	GGGATGTATTGAAGGAGGATGGTACAAAAACTATACATGTTCTTTGGATT
69_TES - _Seq_73	GGGATGTATTGAAGGAGGATCCATTAGGAAAGAATAAAAACCATGCAAAA
70_TES - _Seq_74	GGGATGTATTGAAGGAGGATGACAGGCTTGGAAGTATTATAAAACAGGAT
72_TES - _Seq_76	GGGATGTATTGAAGGAGGATGAATAAACATTAGAAATACCTAGCCATGAA
73_TES - _Seq_77	GGGATGTATTGAAGGAGGATGCATAGCTATGTGTAGAAGTACACAGGGAA

4E	No RBP vs TIA1-L1++	-2.9	4.3E-3
4E	TIS11B+/TIA1-L1++	-9.7	4.0E-22
4F	No RBP vs TIS11B+	-17.1	2.0E-65
4F	No RBP vs TIS11B+++/TIA1-L1+	-15.2	2.1E-52
4F	No RBP vs TIS11B++/TIA1-L1+++	-17.7	7.7E-70
4F	No RBP vs TIA1-L1++	-8.3	2.1E-16
4F	TIS11B+/TIA1-L1++	-4.5	8.5E-6
4G	No RBP vs TIS11B+	-3.1	0.002
4G	No RBP vs TIS11B+++/TIA1-L1+	-1.2	0.222
4G	No RBP vs TIS11B++/TIA1-L1+++	-9.7	4.2E-22
4G	No RBP vs TIA1-L1++	-9.0	2.8E-19
4G	TIS11B+/TIA1-L1++	-7.3	2.2E-13
4H	No RBP vs TIS11B+	-0.343	0.7
4H	No RBP vs TIS11B+++/TIA1-L1+	-2.0	0.043
4H	No RBP vs TIS11B++/TIA1-L1+++	-5.8	4.7E-9
4H	No RBP vs TIA1-L1++	-6.7	1.9E-11
4H	TIS11B+/TIA1-L1++	-5.8	7.4E-9
S2A	UB vs TGER	-20.6	5.9E-94
S2A	UB vs CRER	-2.6	0.008
S2A	UB vs CY	-13.2	1.1E-39
S2B	UB vs TGER	-2.7	0.007
S2B	UB vs CRER	-0.193	0.85
S2B	UB vs CY	-15.2	2.6E-52
S2C	UB vs TGER	-12.9	4.7E-38
S2C	UB vs CRER	-6.1	1.4E-9
S2C	UB vs CY	-20.0	5.3E-89
S2D	UB vs TGER	-7.3	2.9E-13
S2D	UB vs CRER	-3.6	3.5E-4
S2D	UB vs CY	-20.5	2.7E-93
S2E	UB vs TGER	-2.4	0.016
S2E	UB vs CRER	-20.3	1.1E-91
S2E	UB vs CY	-22.2	1.3E-109
S3D	No RBP vs Any RBP, TGER	-9.4	8.6E-21
S3D	No RBP vs Any RBP, CRER	-9.0	3.1E-19
S3D	No RBP vs Any RBP, CY	-12.2	4.4E-34
S3F	No RBP vs LARP4B	-10.3	5.6E-25
S3F	No RBP vs METAP2	-6.6	3.0E-11
S3F	No RBP vs LARP4B/METAP2	-8.3	1.0E-16
S3H	No RBP vs AU-RBP	-42.0	0
S3H	No RBP vs L/M-RBP	-10.0	1.8E-23
S3H	AU-RBP vs L/M-RBP	-27.2	2.9E-162
S3I	No RBP vs AU-RBP	-21.8	6.2E-105
S3I	No RBP vs L/M-RBP	-11.7	1.3E-31
S3I	AU-RBP vs L/M-RBP	-27.3	2.3E-164
S5A	No RBP vs TIS11B	-13.3	2.0E-40
S5A	No RBP vs HuR	-6.4	1.8E-10
S5A	No RBP vs PUM2	-4.8	1.0E-6
S5A	No RBP vs TIS11B/HuR/PUM2	-15.6	1.4E-54
S5C	No RBP vs TIS11B+	-28.2	6.7E-175

S5C	No RBP vs TIS11B+++/TIA1-L1+	-29.2	6.0E-187
S5C	No RBP vs TIS11B++/TIA1-L1+++	-28.0	8.8E-173
S5C	No RBP vs TIA1-L1++	-11.1	1.2E-28
S5C	TIS11B+/TIA1-L1++	-11.2	2.6E-29
S5D	No RBP vs TIS11B+	-17.9	1.2E-71
S5D	No RBP vs TIS11B+++/TIA1-L1+	-19.9	4.1E-88
S5D	No RBP vs TIS11B++/TIA1-L1+++	-19.1	4.2E-81
S5D	No RBP vs TIA1-L1++	-8.9	8.0E-19
S5D	TIS11B+/TIA1-L1++	-3.7	1.9E-4